University of Stavanger

FACULTY OF SCIENCE AND TECHNOLOGY

MASTER'S THESIS

Study programme/specialisation: Structural Engineering and Materials Science/ Civil Engineering Structures	Spring semester, 2020 Open
Author: Susanne Lien Fjeldstad	
Programme coordinator: Sudath C. Siriwardane Supervisor: Associated Professor, Yanyan Sha	
Title of master's thesis: Seismic Response of Floating Bridges	
Credits: 30	
Keywords: Floating bridge Time-domain analysis Nonlinearity Seismic analysis Finite element method Ground motion Time history	Number of pages: 72 + supplemental material/other: 1 Stavanger, 13.06.2020

Preface

This Master's Thesis is a result of work done by Student Susanne Lien Fjeldstad at the University of Stavanger during the spring semester of 2020. The scope of work was developed by Associated Professor Yanyan Sha.

The topic of the thesis is the Seismic Response of Floating Bridges. Performing time-domain simulations of floating bridges under seismic excitations have been the most important work during this project. The analyses are carried out using USFOS, a non-linear FEM-tool used to develop finite element models. The bridge model was prepared by Ida Osvoll, a student from NTNU, Trondheim.

Most of the time has been used on seismic analyses in USFOS, which was more challenging than initially expected. Due to no experience in either the program and topic, I feel that I have done and understood a lot.

I would like to thank my supervisor Yanyan Sha for flexible help during this master thesis with meetings over Skype and emails. He has contributed with help in USFOS and questions during the semester. This help has been essential for implementing this project.

It has been a challenging semester writing a thesis with no existing design guidelines for floating bridges against seismic.

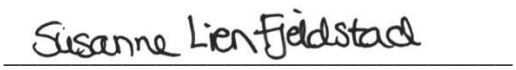

Susanne Lien Fjeldstad 15.06.2020

Summary

The object of this study is to collect the results of an end-anchored floating bridge when it is subjected to seismic excitations. The bridge is an end-anchored floating bridge, mounted on 46 separate pontoons, with an elevated cable-stayed part in the south end supported by a 230 m tall bridge tower. The cable-stayed part and the floating part constitutes a total length of 5.5 km. The bridge has a location in Bjørnafjorden and is a project purposed by the Norwegian Public Road Administration (NPRA). A powerful finite element analysis (FEA) software, USFOS, is used to perform nonlinear analyses on the bridge structure.

Due to no design guidelines for floating bridges, requirements, and analysis methods from Eurocode 8, AASTHO and NORSOK for general bridges and offshore structures are discussed to make a suitable solution for floating bridges against seismic excitations.

Time-domain analysis has been performed in USFOS and the behavior of the bridge is studied when subjected to seismic excitations. The seismic ground motions are generated by Dr. Kaiming Bi where the spatially correlated time histories are generated in accordance with the design spectra from Eurocode 8-2. A Sobczyk model is used to describe the coherency loss between the ground motions for the different fixed boundary locations and a shape function is applied to modulate the simulated time histories.

During the master, a bridge model made by Ida Osvoll is used to run numerical analyses on the bridge, subjected to seismic excitations. The model is carefully reviewed and understood before the analyses are completed. Motions are collected along the length of the bridge to see the global response for all load cases. Forces and stresses in the bridge girder are also collected from the simulations to see how the bridge reacts to the excitations.

Furthermore, numerical simulation of floating bridges shows that the floating bridge is reliable when subjected to seismic excitations of low to moderate seismicity. In other words, seismic excitations with PGA=0.08g do not have a significant impact on floating bridges.

Keywords: Floating bridge, time-domain analysis, nonlinearity, seismic analysis, finite element method, ground motion, time history

Norsk Sammendrag

Under denne masteroppgaven er målet å samle resultater fra en analyse kjørt på en endeforankret flytebro utsatt for seismiske eksitasjoner. Flytebroen er endeforankret, montert på 46 separate pongtonger med en forhøyet strekkstagbro i sørendene som er støttet opp av et 230 meter høyt tårn. Den totale broen utgjør en lengde på 5.5 km. Broen har beliggenhet i Bjørnafjorden utenfor Bergen og er et prosjekt planlagt av Statens Vegvesen. En kraftig programvare, USFOS, for benyttet i denne oppgaven for å utføre ikke-lineære analyser på broen.

Da det ikke finnes tidligere retningslinjer for flytende broer utsatt for seismisk last, diskuteres krav og analysemetoder fra Eurocode 8, AASTHO og NORSOK for generelle broer og offshore konstruksjoner. En passende løsning for flytebroer utsatt for seismiske eksitasjoner er ønskelig å finne.

En tidshistorieanalyse er utført i USFOS hvor broens oppførsel blir studert under påkjenning av jordskjelv. De seismiske grunnakselerasjonene er frembrakt av Dr. Kaiming Bi, der romlige korrelerte tidshistorier står i samsvar med designspektrene for Eurocode 8-2. En Sobczyk-modell er benyttet for å beskrive korrelasjonstapet mellom grunnbevegelsen for de forskjellige lokasjonene for fast innspenning og en «shape-function» blir benyttet til å modulere de simulerte tidshistoriene.

Modellen brukt for å kjøre numeriske analyser på broen under seismisk last er laget av Ida Osvoll. Modellen er nøye gjennomgått og forstått før analysene er fullført. Responsbevegelsene til broen er samlet inn langs broens lengde for å kunne se den totale globale responsen for alle lasttilfeller. Krefter og spenninger i brobjelken er også samlet inn fra simuleringene for å se hvordan broen reagerer.

Videre viser numerisk simulering av flytende broer at de er pålitelige når de utsettes for seismiske eksitasjoner av lav til moderat størrelse. Seismiske eksitasjoner gir med andre ord ikke betydelig innvirkning på flytebroer utsatt for en grunnakselerasjon på 0.83m/s^2.

Table of Contents

Preface ..... **i**

Summary ..... **ii**

Norsk Sammendrag ..... **iii**

List of Figures ..... **vii**

List of Tables ..... **ix**

List of Symbols ..... **xi**

Abbreviations ..... **xiii**

1. Introduction **1**

1.1. About the Project 1

1.2. Background 2

1.3. Objective 3

1.4. Scope and Limitations 3

1.5. Floating Bridges - Advantages and Challenges 4

1.6. Different Types of Floating Bridges 4

1.6.1. Continuous and Separated Pontoon Bridge 4

1.6.2. TLP-supporting Floating Bridge 5

1.6.3. Submerged Floating Tunnels (SFT) 5

1.7. Seismology 6

1.7.1. Plate Tectonics 6

1.7.2. Seismic Waves 6

2. Literature Review **7**

2.1. Existing Design Guidelines 7

2.2. Previous Research on Floating Bridge Design 11

2.3. Seismic Design and Analysis of Long, Flexible Bridges 12

2.3.1. Response Spectrum Analysis 12

2.3.2. Non-linear Time History Method 13

2.3.3. Summary and Discussion of Analysis Methods 14

3. Theory 15
3.1. Equation of Motion 15
3.2. Solution Algorithm 15
3.3. Eigenvalue Analysis 16
3.4. Rayleigh Damping 17
3.5. Earthquake Ground Motions 19
3.6. Load Combinations for Seismic Action 20
3.6.1. Combination of Seismic Action with Other Loads 21
4. Seismic Ground Motion Modelling 22
4.1. Defining Response Spectra According to Eurocode 8 22
4.2. Generation of Accelerograms 23
4.3. Results from Ground Motion Generation 25
5. Modelling of the Bridge in USFOS 29
5.1. USFOS as a Finite Element Tool 30
5.2. Bridge Design 30
5.3. Bridge Girder Design 32
5.4. Cable Tower 35
5.5. Stay-cables 37
5.6. Pontoon Design 38
5.7. Column Design 41
5.8. Modelling of the Earthquake Parameters 42
5.9. Eigenvalue Analysis 43
5.10. Structural Damping 43
6. Time Domain Simulation of the Bridge Response 44
6.1. Permitted Motion 44
6.2. Response of Stay-cables 45
6.3. Forces Along the Bridge Girder 50
6.3.1. Axial Forces 50
6.3.2. Strong Axis Bending Moment 52
6.3.3. Weak Axis Bending Moment 53

6.4. Motion Along the Bridge Girder 55
6.4.1. Accelerations 55
6.4.2. Displacements 57
6.5. Sensitivity Study 59
6.5.1. Forces and Stresses in the Stay-cables 59
6.5.2. Bridge Girder Response 62
6.5.3. Motions Along the Bridge Girder 65
7. Discussion 66
7.1. Seismic Scenario of 0.08g 66
7.2. Seismic Scenario of 0.4g and 0.8g 67
8. Concluding Remarks 68
9. Recommendations for Future Work 69
Bibliography 70
Appendix A I

List of Figures

Figure 1 - Illustration of Bjørnafjorden floating bridge (Statens Vegvesen, 2017b) 1
Figure 2 - USFOS model of Bjørnafjorden floating Bridge 3
Figure 3 - TLP-supported bridge (Statens Vegvesen, 2018) 5
Figure 4 - Submerged floating tunnel illustration (Statens Vegvesen, 2018) 5
Figure 5 - Illustration of seismogram (NORSAR, 2020) 6
Figure 6 - Importance class, target performance level and classification for floating bridges (Eiichi Watanabe & Utsunomiya, Tomoaki, 2003) 11
Figure 7 - Rayleigh Damping (Wai-Fah Chen & Duan, Lian, 2014) 18
Figure 8 - Example of accelerogram (Einar N. Strømmen, 2012) 19
Figure 9 - Generated base rock motions in horizontal x-direction for all three cases 25
Figure 10 - Generated base rock motions in horizontal y-direction for all three cases 26
Figure 11 - Generated base rock motions in vertical direction for all three cases 27
Figure 12 - Actual and target response spectra 28
Figure 13 - Comparison of coherency loss between the generated time histories for each site 28
Figure 14 - Bridge illustration from USFOS 29
Figure 15 - Orientation of the bridge in elevation and plan view (Norconsult AS, 2017a) 30
Figure 16 - The end anchored floating bridge concept 31
Figure 17 - General cross section of bridge girder (Norconsult AS, 2017a) 32
Figure 18 - Direction of forces on beam element (USFOS, 1999b) 32
Figure 19 - Cable tower (Norconsult AS, 2017a) 35
Figure 20 - Strong axis bending moment of bridge girder due to pretension in stay-cables 37
Figure 21 - Geometry of the pontoons (Norconsult AS, 2017a) 38
Figure 22 - Spring connection in pontoons 39
Figure 23 - Applied damping to the model (Ida Fagerli Osvoll, 2018) 43
Figure 24 - Loads working on stay-cables due to bridge girder deformations 45
Figure 25 - Location of maximum axial force in the stay-cables 46
Figure 26 - Location of maximum stress along the cables 47
Figure 27 - Maximum axial force in the girder for (a) longest cable and (b) shortest cable 47
Figure 28 - Maximum axial force in the girder for (a) longest cable and (b) shortest cable only considering seismic load 47
Figure 29 - Axial force due to seismic load along the cable-pairs for 0.08g 48
Figure 30 - Stresses along the cable-pairs for 0.08g 49
Figure 31 - Axial force along the bridge for (a) Only pre-stress load (b) Seismic and pre-stress for all cases (c) Mean seismic load 51
Figure 32 - Strong axis bending moment for (a) Total seismic and pre-stress load (b) Mean seismic load only 52
Figure 33 - Weak axis moment for (a) only pre-stress (b) seismic and pre-stress (c) mean seismic load 53

FIGURE 34 - LOCATIONS ON THE BRIDGE FOR CHECK OF ACCELERATION 55
FIGURE 35 - NODAL ACCELERATIONS FOR (A) NODE 1, (B) NODE 2 AND (C) NODE 3 55
FIGURE 36 - PEAK ACCELERATION ALONG THE BRIDGE LENGTH (A) ALL LOAD CASES (B) MEAN VALUE 56
FIGURE 37 - DISPLACEMENTS ALONG THE BRIDGE LENGTH (A) HORIZONTAL (B) TRANSVERSE AND (C) VERTICAL DIRECTION 57
FIGURE 38 - AXIAL FORCE ALONG THE CABLE-PAIRS FOR 0.08G, 0.4G, AND 0.8G ONLY 60
FIGURE 39 - LOCATION OF MAXIMUM AXIAL STRESS IN THE STAY-CABLES 60
FIGURE 40 - MAXIMUM AXIAL STRESS ON THE EAST SIDE OF CABLE-PAIRS FOR (A) 0.4G AND (B) 0.8G 61
FIGURE 41 - AXIAL FORCE IN BRIDGE DECK FOR (A) PRE-STRESS AND SEISMIC (B) SEISMIC EFFECT ONLY 62
FIGURE 42 - STRONG AXIS MOMENT FOR (A) PRE-STRESS AND SEISMIC LOAD (B) SEISMIC LOAD ONLY 63
FIGURE 43 - WEAK AXIS MOMENT FOR (A) SEISMIC AND PRE-STRESS LOAD (B) SEISMIC LOAD ONLY 64
FIGURE 44 - VERTICAL ACCELERATION FOR (A) CABLE-STAYED PART (B) MIDDLE BRIDGE (C) NORTH BRIDGE END 65

List of Tables

TABLE 1 - VALUE OF IMPORTANCE FACTOR ACCORDING TO (EUROPEAN STANDARD, 2005) 7
TABLE 2 - ACCELERATIONS COEFFICIENT (AASHTO, 2009) 8
TABLE 3 - ANALYSIS PROCEDURE (AASHTO, 2009) 9
TABLE 4 - REGULAR BRIDGE REQUIREMENT (AASHTO, 2009) 9
TABLE 5 - COMBINATION OF SEISMIC LOAD AT DIFFERENT LOCATIONS 13
TABLE 6 - ANALYSIS APPLICABILITY AND PERFORMANCE 14
TABLE 7 - COMBINATION OF ENVIRONMENTAL LOADS FOR ULS AND ALS (NORSOK STANDARD, 2007) 20
TABLE 8 - LOAD COMBINATIONS FOR ACCIDENTAL LIMIT STATE (STATENS VEGVESEN, 2017C) 21
TABLE 9 – VALUES OF PARAMETERS DESCRIBING TYPE 2 ELASTIC RESPONSE SPECTRA FOR GROUND TYPE A 22
TABLE 10 – VALUES DESCRIBING THE VERTICAL ELASTIC RESPONSE SPECTRA (TYPE 2) 22
TABLE 11 - EXPLANATION OF SITE LOCATIONS FOR FIGURES 9-11. 25
TABLE 12 - MAIN GIRDER CROSS-SECTION PROPERTIES (IDA FAGERLI OSVOLL, 2018) 32
TABLE 13 - BRIDGE GIRDER STEEL PROPERTIES (IDA FAGERLI OSVOLL, 2018) 33
TABLE 14 - EQUIVALENT DENSITIES FOR BRIDGE GIRDER (IDA FAGERLI OSVOLL, 2018) 33
TABLE 15 - CABLE ANCHOR MASSES (IDA FAGERLI OSVOLL, 2018) 34
TABLE 16 - GEOMETRY OF THE BRIDGE TOWER (IDA FAGERLI OSVOLL, 2018) 36
TABLE 17 - PROPERTIES OF THE TOWER TOP OF THE BRIDGE (IDA FAGERLI OSVOLL, 2018) 36
TABLE 18 - MATERIAL PROPERTIES OF BRIDGE TOWER (IDA FAGERLI OSVOLL, 2018) 36
TABLE 19 - PROPERTIES OF STAY-CABLES 37
TABLE 20 - GEOMETRY OF THE PONTOONS (IDA FAGERLI OSVOLL, 2018) 38
TABLE 21 - PONTOON MATERIAL PROPERTIES (IDA FAGERLI OSVOLL, 2018) 39
TABLE 22 - MATERIAL DENSITIES FOR THE PONTOONS (IDA FAGERLI OSVOLL, 2018) 39
TABLE 23 - RESULTING WATERPLANE STIFFNESS FOR THE PONTOONS (IDA FAGERLI OSVOLL, 2018) 39
TABLE 24 - ADDED MASS IN SURGE, SWAY, AND HEAVE (IDA FAGERLI OSVOLL, 2018) 40
TABLE 25 - DRAG COEFFICIENT AND DIAMETERS FOR THE PONTOONS (IDA FAGERLI OSVOLL, 2018) 40
TABLE 26 - COLUMN PROPERTIES (IDA FAGERLI OSVOLL, 2018) 41
TABLE 27 - ADDITION STEEL MASS TO COLUMN TOP(IDA FAGERLI OSVOLL, 2018) 41
TABLE 28 – NODAL LOCATIONS AT THE SOUTH END 42
TABLE 29 – NODAL LOCATIONS AT BRIDGE TOWER 42
TABLE 30 – NODAL LOCATIONS AT THE NORTH END 42
TABLE 31 - MAXIMUM ALLOWABLE RESPONSE ACCORDING TO (STATENS VEGVESEN, 2017C) AND (STATENS VEGVESEN, 2009) 44
TABLE 32 – MAXIMUM FORCE AND STRESS FOR THE LONGEST AND SHORTEST STAY CABLE 46
TABLE 33 - AXIAL FORCES IN THE EASTERN STAY-CABLES (SEISMIC, PRE-STRESS AND TOTAL FORCES) 48
TABLE 34 - AXIAL FORCES IN THE WESTERN STAY-CABLES (SEISMIC, PRE-STRESS AND TOTAL FORCES) 48
TABLE 35 - MAXIMUM, MINIMUM AND VARIATION OF FORCE FOR THE SHORTEST CABLE 59

TABLE 36 - MAXIMUM, MINIMUM AND VARIATION OF FORCE FOR THE LONGEST CABLE 59
TABLE 37 - MAXIMUM AXIAL FORCE ALONG CABLE-PAIRS FOR 0.08G, 0.4G, AND 0.8G ONLY 60
TABLE 38 - DISPLACEMENTS OF BRIDGE DECK FOR 0.08, 0.4G AND 0.8G 65
TABLE 39 - MAXIMUM BRIDGE RESPONSE FOR THE SEISMIC LOAD OF 0.08G 66
TABLE 40 - MAXIMUM BRIDGE RESPONSE FOR SEISMIC LOADS OF 0.4G AND 0.8G 67
TABLE 41 - STAY-CABLE PROPERTIES (IDA FAGERLI OSVOLL, 2018) I

List of Symbols

Latin Symbols

A	Cross-sectional area
C	Damping matrix
C_{33}	Waterplane stiffness (Heave)
C_{44}	Waterplane stiffness (Roll)
C_{55}	Waterplane stiffness (Pitch)
E	Elastic modulus
E_{Edi}	Component of ground motion in direction *i*
I_y	Moment of inertia (y-axis)
I_z	Moment of inertia (z-axis)
K	Stiffness matrix
L_{lim}	Limited length of the continuous bridge deck
L_g	Distance between which the ground motions may be considered as completely correlated NS-EN 1998-2:2005
M	Mass matrix
M_s	Earthquake surface-wave magnitude
R(t)	External excitation force
S	Soil factor for ground types defined in NS-EN 1998-1:2004, Cl 3.2.2.2
S_{D1}	Design earthquake response spectral accelerations coefficient
$S_e(T)$	Horizontal elastic response spectrum
$S_{ve}(T)$	Vertical elastic response spectrum
T_1	Fundamental period of vibration
T_B	Lower limit of the period of the constant spectral acceleration branch NS-EN 1998-1:2004
T_C	Upper limit of the period of the constant spectral acceleration branch NS-EN 1998-1:2004
T_D	Value defining the beginning of the constant displacement response range of the spectrum; NS-EN 1998-1:2004
W_{pi}	Plastic section modulus about *i* axis
a_g	Design ground acceleration for ground type A NS-EN 1998-1:2004
a_{gR}	Reference peak ground acceleration for ground type A
c	Damping coefficient
c_c	Critical damping coefficient
d_{jk}	Distance between j' and k'

g	Acceleration of gravity (9.81m/s^2)
m	Mass
t	Time
r	Structural response vector for displacement
$\dot{r}$	Structural response vector for velocity
$\ddot{u},\ddot{r}$	Structural response vector for acceleration
x	Horizontal longitudinal axis of the bridge
y	Horizontal transverse axis of the bridge
z	Vertical axis of the bridge

Greek Symbols

α,β	Parameters for Rayleigh damping
γ_I	Importance factor for the bridge
$\gamma_{j\acute{k}}$	Lagged coherency loss between j' and k'
ξ	Damping ratio
ξ_n	Damping ratio for n^{th} node
ω_n	Natural frequency for n^{th} node
φ_n	Shape matrix

Abbreviations

ALS	Accidental Limit State
ULS	Ultimate Limit State
NPRA	Norwegian Public Roads Administration
TDA	Time Domain Analysis
DOF	Degree of Freedom
USFOS	Ultimate Strength
TLP	Tension Leg Platform
SFT	Submerged Floating Tunnels
SRSS	Square root of sum Squares
SDC	Seismic Design Category
ESA	Equivalent Static Analysis
EDA	Equivalent Dynamic Analysis
TH	Time History
PGA	Peak Ground Acceleration
SDOF	Single Degree of Freedom
MDOF	Multiple Degree of Freedom
FEA	Finite Element Analysis
FEM	Finite Element Method
HHT-α	Hilber Hughes Taylor-α Method

Chapter 1

1. Introduction

Floating bridges are structures that can be built over fjords and rivers, supported by pontoons instead of fixed supports. These types of bridges are widely used in the world because of its ability to be built over a wide and long waterway. With deep water and soft seabed, floating bridges might be a good choice. (Eiichi Watanabe, 2003) Floating bridges might have complex geometry which leaves the calculations of the response very comprehensive. Norway has numerous fjords along the coast, and some are too wide for building suspension-bridge and too deep for building underwater tunnels. The use of floating bridges is an opportunity, and knowledge in how the bridge structure will respond to conditions like extreme environmental loads is of importance when designing for safer bridges.

1.1. About the Project

E39 is a route that goes from Kristiansand in the south to Trondheim in the north and crosses seven fjords. This is an ongoing ferry-free project, directed by National Public Road Administration (NPRA). To make the route ferry-free, bridges and underwater tunnels will be built within 2029. (Statens Vegvesen, 2017a) Floating bridges are an alternative for crossing several of these fjords.

Bjørnarfjord is one of the challenging straits along E39 with about five kilometers long and 550 meters deep waterway. (Statens Vegvesen, 2017b) With this dimension, it is impossible to build and solve for a conventional bridge solution. There are two options for the floating bridge: side-anchored floating bridge and end-anchored floating bridge. This thesis will focus on the end-anchored floating bridge, illustrated in Figure 1. The end-anchored floating bridge is fixed at the ends with a c-curved bridge girder in the horizontal plane which can be seen in the figure. (Norconsult AS, 2017a)

Floating bridges have earlier been analyzed against wind, wave, and current loadings, but not against seismic excitations. To predict the response of the structure under various excitation loads and soil conditions, simulations of the bridge will be necessary.

Figure 1 - Illustration of Bjørnafjorden floating bridge (Statens Vegvesen, 2017b)

1.2. Background

The accidental limit state (ALS) evaluation is one of the key aspects in the design of floating bridges. Common loads to floating bridges include ship collision, vehicle impact, explosions, and earthquakes. The earthquake-induced seismic excitation and tsunami loads can pose a significant threat to the bridge structure. Unfortunately, there are no existing design guidelines for floating bridges against seismic excitations. With the advance of computer techniques today, dynamic analysis of complex structures such as floating bridges is practically possible. The most used analysis approaches for seismic analysis is time-history analysis and response spectra analysis. For the time-history analysis, earthquake recordings are applied to the idealized structure model as dynamic loading, either as acceleration/displacement time-histories on the bridge supports or by uniform acceleration to the whole structure. Response spectrum analysis is based on the natural modes of vibration and is a linear-dynamic analysis for elastic structures. Pseudo-Spectral acceleration, velocity, and displacement as a function of structural periods can be determined by analyzing the natural modes. As a result of this, the peak ground acceleration can be established. This is a good way of describing and understanding the seismic action and dynamic behavior of the structure. The response spectrum analysis is the most used analysis method in practice due to its simplicity and shorter duration than for time-history analysis. Simplifications to small and fixed structures do not cause any major differences and problems in the analysis. However, for long and large, complex floating bridges, simplifications may cause significant differences in the results. In this thesis, earthquake-induced seismic excitation is going to be studied on the floating bridge.

A floating bridge is not an onshore or an offshore structure, but a combination. Due to the difference between the structural characteristics for offshore and onshore, a specific design procedure needs to be specified for use on a floating bridge. Earthquakes are by their nature a dynamic event that can cause significant damage. Due to the dynamic loading, size, and complexity of the bridge, a nonlinear dynamic time-history analysis is intended to use on the floating bridge.

1.3. Objective

The main objective of this study is to conduct a nonlinear finite element analysis of floating bridges under seismic excitations. A requirement for a structure subjected to seismic excitation is to have a certain amount of safety due to strength, ductility, and energy absorption in addition to withstand the dynamic loading. Since the response of this action is unknown, we need to carry out nonlinear dynamic analyses of the bridge. This thesis aims to use USFOS to study how the bridge will respond during excitations from earthquakes.

A model of the floating bridge is created in USFOS by Ida Osvoll. (Ida Fagerli Osvoll, 2018) Before using the model to perform analyses of seismic excitation, a good understanding of the model and program are necessary. This program is used to investigate how the floating bridge will respond to several generated ground motions. An illustration of the model in USFOS is shown in Figure 2. During the work with the floating bridge, seismic analysis procedure for general bridges and offshore structures will be discussed.

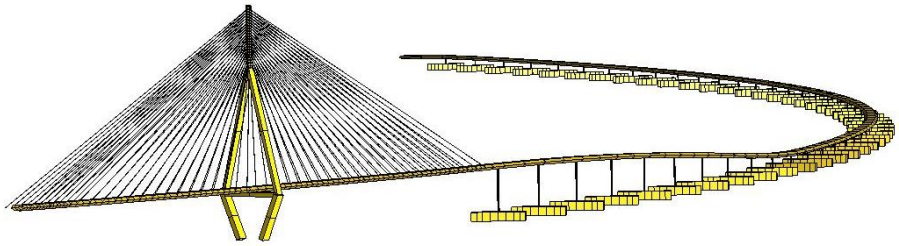

Figure 2 - USFOS model of Bjørnafjorden floating Bridge

1.4. Scope and Limitations

The scope of work in this thesis is to get familiar with structural dynamics and hydrodynamics on the bridge. To develop proficiency in using USFOS and to develop a finite element model of floating bridges is an important part. As explained in section 1.3, the model used is developed by Ida Osvoll due to the limited time of only one semester. The main focus in USFOS has been to understand the modelling of the structure and to collect responses from the simulations to see the global response.

Time-domain simulations of floating bridges under seismic excitations are the main task in the thesis for conducting the unknown responses. An evaluation of the bridge response considering various ground motions is important, and discussion of design guidelines for general bridges according to different design codes is essential. The response due to seismic excitations are unknown for floating bridges and there are no existing design guidelines.

Since the details for the cable properties are not available, the values for yield stress are set to a very high value in the model. As the yield stress for the stay-cables and bridge tower is unknown, the utilization of the cables cannot be assessed, but a limit and a minimum requirement can be set. The response of the bridge tower and pontoons are not completed.

1.5. Floating Bridges - Advantages and Challenges

Bridges today is used to connect islands or island to the mainland. Floating bridges are often used when traditional bridges are not possible to use. These traditional bridges may not be feasible due to wide fjords, deep water, and too soft seabed for the tower legs to support the structure. In places like Bjørnafjorden, where traditional bridges are not possible to use, floating bridges are an opportunity for the fjord to be ferry-free and the people to save time and money.

Traditional bridges have a lot of fixed supports that leave the bridge quite rigid. In this case, the bridge will not be able to move so much under earthquake loadings due to the stiff parts. But, in floating bridges, small seismic excitations may have a big influence because of the flexibility in the bridge. There are no constraints along the bridge length which leaves the bridge to move in quite a flexible manner.

There are not only positive things by choosing a floating bridge as a crossing of the waterway. There are a couple of associated challenges such as the waterborne traffic where an elevation of a part on the bridge will be necessary. This again will give a more unstable bridge and higher maintenance cost.

Bad weather with lots of wind generates waves and current, which will give the bridge movement and may cause bad comfort and safety for bridge users. Floating bridges are also very susceptibility to damage from environmental loads. Tidal variations affect the bridge ends as well, since the floating part moves along with the tide.

1.6. Different Types of Floating Bridges

There are many ways on how a floating bridge can be designed. Some of the alternatives are described below, but there are only continuous pontoon bridges and separated pontoon bridges that are used in the common time. TLP-supported bridge and submerged floating tunnels have not yet been used as a crossing of waterway but are under development. From the early morning, bridges were built for military use and operations. From the military bridge, designers studied and made changes to the bridge. Elevation on parts of the bridge for passing of boats, movable spans for large ship passage, and so on, are examples. Different types of floating bridges and structures are described in the following sections.

1.6.1. Continuous and Separated Pontoon Bridge

Continuous and separated pontoon bridges are of the most used bridges for civilian crossings. These are the modern floating bridges with concrete pontoons, either reinforced or prestressed. This type of bridge can have an elevated part for boat passage.

A continuous pontoon bridge consists of many pontoons that are joint together at the ends to form one long girder. Pontoons can either be identical or with different lengths. It can be used by building a structure on top of the pontoons or use it straight on the pontoon surface. (M. Myint Lwin, 2000) Ribbon floating bridges are a type of continuous pontoon floating bridge.

Separated pontoon bridges are a superstructure supported by floating pontoons that are not directly connected, as the name implies. The superstructure needs to be stiff and strong to maintain the position of pontoons. The two floating bridges built in Norway are separated pontoon bridges.

1.6.2. TLP-supporting Floating Bridge

Another floating bridge concept is the suspension bridge with tension leg platform (TLP) foundations, illustrated in Figure 3. The tension leg platform is connected to the seabed with long pre-tensioned steel pipes which gives the platform added stiffness and a reduction in motions. The tension cables shall be designed to withstand longitudinal and transverse loads such as wind, waves, etc. (M. Myint Lwin, 2000) By using this type of bridge system, a reduction of pontoon quantity is possible, this without increasing dynamic effects. This bridge concept is an alternative for the crossing of Bjørnafjorden.

Figure 3 - TLP-supported bridge (Statens Vegvesen, 2018)

1.6.3. Submerged Floating Tunnels (SFT)

Submerged floating tunnels are a novel structural solution for waterway crossing which is floating between the seabed and the sea surface. (J. Mirzapour, Shahmardani, M., & Tariverdilo, S., 2017) The structure is either placed in the water and held fixed at a position through mooring tethers which is anchored to the seabed or it is held afloat by pontoons on the surface. The solution with pontoons is illustrated in Figure 4. SFT can be a good solution when the water is deep and environmental restrictions make it impossible for a traditional crossing to take place. So submerged tunnels can be used when there are deep water crossings. This type of crossing is not commonly called a bridge but has the same service as a bridge. This type of crossing has not been used before.

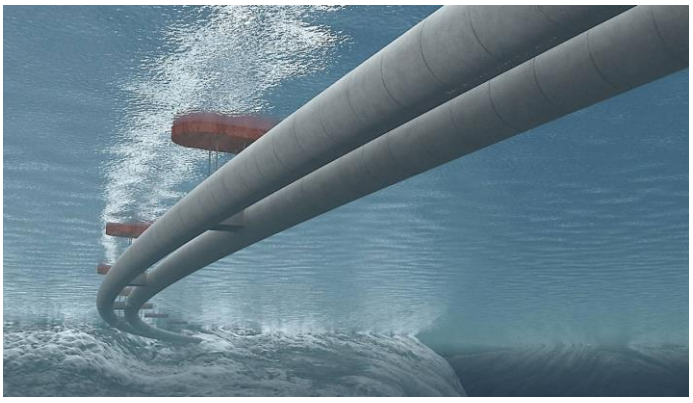

Figure 4 - Submerged floating tunnel illustration (Statens Vegvesen, 2018)

1.7. Seismology

The duration of earthquakes is short - from seconds to maximum a few minutes. Shaking of the ground and/or ground failure are the most dominant damage when it comes to earthquakes. There are different types of earthquakes which lead to shaking of the ground besides tectonic earthquakes: Explosions, blasting of mines or tunnels, and landslides. (NORSAR, 2020)

1.7.1. Plate Tectonics

Tectonic earthquakes occur because of plate tectonic boundaries in the earth's crust or lithosphere. As the plates are constantly moving, some of the plates lock together because of friction and are unable to move. The other plates will keep moving which leads to increased pressure and strain energy on the locked plates. After a while, the strain energy will exceed its resistance and high pressure will lead to a rapid slip of the plates which causes a tectonic earthquake. (Wai-Fah Chen & Duan, Lian, 2014) The convective motion of the material in the earth's mantle, which is generated by the heat in the earth's core, gives this constant movement of tectonic plates. The energy from a tectonic earthquake is released by seismic waves.

1.7.2. Seismic Waves

Seismic waves are energy waves that go through the earth in a broad spectrum of frequencies. The two main types of seismic waves are body waves and surface waves. Body waves are divided into P (primary) waves and S (secondary) waves, which move through the earth's interior while surface waves are divided into Rayleigh waves and Love waves, which move on the surface of the curst. (Wai-Fah Chen & Duan, Lian, 2014)

P-waves transmit the energy via push-pull motion and are the fastest wave. These waves can travel through all types of mediums (solids, fluids, and gas). (NORSAR, 2020) S-waves transmit the energy via shear action perpendicular to the direction of motion and are slower than P-waves. These waves do not travel through fluids or water on the outer core. ("Seismic waves,") Rayleigh waves are moving in the direction of propagation and perpendicular (vertical) direction. These waves motions are similar to water waves by its form. Love waves are analogous to S body waves and oscillate horizontally and are generally parallel to the earth's surface. These waves are largest at the earth's surface and decrease in amplitude with depth.

When recording an earthquake motion, P-waves is the first arriving energy on the seismogram, where the intensity of ground motion is increasing. The next wave arriving at the seismogram is the S-waves where the intensity of ground motion remains the strongest. After this, the ground motion will die down in the last phase of the seismogram. A complete seismic motion, as illustrated in Figure 5, is called a *nonstationary random process*. (Wai-Fah Chen & Duan, Lian, 2014)

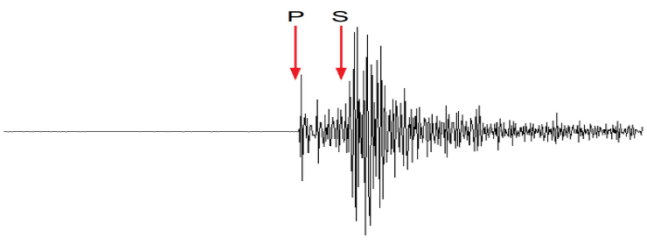

Figure 5 - Illustration of seismogram (NORSAR, 2020)

Chapter 2

2. Literature Review

This part will summarize information from Eurocode 8, AASHTO, and NORSOK from the design codes based on the seismic zones, etc. Design code information from general bridges is a very important part of this thesis due to no guidelines for floating bridges.

2.1. Existing Design Guidelines

Concerning the seismic analysis types, existing design guidelines for bridge design is available. The European Standard EN 1998-1:2004 (European Standard, 2004) is used for the design of structures against earthquakes. Part 2, EN 1998-2:2005 (European Standard, 2005), for bridges, is used as a design code for traditional bridges against seismic actions. AASHTO has published two codes for designing highway bridges in the United States: Standard Specifications for Highway Bridges and LRFD Bridge Design Specifications. In this thesis, the design code from AASTHO Guide Specifications for LRFD Seismic Bridge Design will be studied. (AASHTO, 2009) NORSOK is used for offshore structure design and will also be studied in this thesis to find the best matching values for the bridge against seismic excitations. (NORSOK standard, 2007) Since the analysis of floating bridges against seismic motion never has been completed, comparison and combination of these standards and design codes will be used to get the most realistic preparation of the response from seismic excitations.

EN 1998-2:2005 contains particular Performance Requirements, Compliance Criteria, and Application Rules applicable to the design of earthquake resistance on traditional bridges. Design of floating bridges is not included in the scope of EN 1998-2:2005, according to clause 1.1.1(4). The goal of the design code is that the bridge remains operational after an earthquake event or allows significant damage on the bridge without collapse. That human lives are protected is an important factor when designing a bridge against seismic loadings. In the case of low seismicity, simplified criteria may be established. Low seismicity are considered if $a_g < 0.04g$ (0.39 m/s^2) or if $a_g S < 0.05g$ (0.49 m/s^2) according to clause 3.2.1(5)P in EN 1998-1:2004. (European Standard, 2004)

Bridges are classified into importance classes in EN 1998-2:2005, depending on the consequence of collapse if an earthquake event should arise. There are three different importance classes with corresponding importance factor, given in Table 1. The value for importance factor is further used to determine the design ground acceleration, a_g.

Importance class	**Importance factor, γ_I**
I	1.0
II	1.0
III	1.3

Table 1 - Value of importance factor according to (European Standard, 2005)

There are two recommended types of shapes for the elastic spectrum of bridges: Type 1 and Type 2, depending on the magnitude of an earthquake event. Type 2 yields for earthquakes with surface-wave magnitude (M_s) lower than 5.5. (European Standard,

2004) The soil types are divided into five different types from A to E with individual soil factors. These parameters together with the ground acceleration for a referent return period (a_{gR}) gives the value of the design ground acceleration – a_g ($a_g = \gamma_I a_{gR} S$).

In EN 1998-2:2005, it is stated that the seismic action is represented by three translational components and that the earthquake motion shall be quantified in terms of response spectrum or time-history representation. By using the response spectrum, each of the three components will be analyzed separately as one-component actions. The horizontal and vertical components are given by clause 3.2.2, which refers to the application of clause 3.2.2.2 and 3.2.2.3 of EN 1998-1:2004.

EN 1998-2:2005 states that spatial variability shall be considered in ground motions at different locations if the bridge deck exceeds a limit length $L_{lim} = L_g/1.5$, where L_g for soil type A is 600m, or if the soil properties along the length are different. Long span bridges have challenges with the spatial effects in the context of an earthquake. There are several reasons for spatial variability in seismic ground motions. When spatial effects shall be accounted for, EN 1998-2:2005 states that wave passage effect, caused by different arrival times of the seismic wave at various supports; loss of coherency due to distance between the supports and to seismic wave scattering in the heterogeneous medium of the ground; site response effect, caused by the local soil properties at the supports; should be regarded, even in a simplified way. (Kaiming Bi & Hao, Hong, 2012) Ground motion spatial variations influence and have a large effect on the structural responses.

Time-history representation is done according to EN 1998-2:2005 clause 3.2.3 by representing the elastic response spectra, with 5% damping: $S_e(T)$. The seismic action for bridges is dependent on the natural period of vibration – T_1, where T_1 is the natural period of the fundamental mode of the structure in case of a ductile bridge. Clause 3.2.3(3)P needs to be fully satisfied to achieve consistency of the time domain with the spectrum. This means that for periods between $0.2T_1$ and $1.5T_1$, the SRSS (square root of sum squares) of the spectra of each component of the accelerogram, should be higher than $1.3S_e(T)$. (European Standard, 2005)

There are four analysis methods described and the selection of analysis is according to chapter 4 in (European Standard, 2005). Response Spectrum Method (Linear), Fundamental Mode Method, non-linear dynamic time-history analysis, and static non-linear analysis (Pushover Analysis) are the analysis methods described to conduct the response of an earthquake event.

Value of $S_{D1} = F_v S_1$	SDC
$S_{D1} < 0.15$	A
$0.15 \leq S_{D1} < 0.30$	B
$0.30 \leq S_{D1} < 0.50$	C
$0.50 \leq S_{D1}$	D

Table 2 - Accelerations coefficient (AASHTO, 2009)

AASHTO LRFD (AASHTO, 2009) specifies detailed seismic analysis and design of traditional bridges. These provisions should be taken as minimum requirements. The importance of bridges is classified as Critical bridges and essential bridges. The selection of which procedure to be used, are based on the seismic design categories,

similar to the seismic zone used in AASHTO LRFD Bridge Design Specifications. There are four Seismic Design Categories (SDCs) that the bridge shall be assigned into SDC A, SDC B, SDC C, and SDC D, with individual requirements. These categories are based on 1-sec period design spectral acceleration for the life safety design earthquake. (AASHTO, 2009) The code states that for single-span bridges and bridges in SDC A, detailed seismic analysis is not required. For the rest of the bridge types, one of the analysis methods described in AASTHO needs to be used. Table 2 shows the design earthquake response spectral accelerations coefficient, S_{D1}, at 1.0-sec period for the different Design Categories.

The selection of an analysis procedure is according to section 4.2 in AASTHO. Table 3 and Table 4 show the requirements of the analysis procedure. If all requirements in Table 4 are met, the bridge is considered as regular.

Seismic Design Category	Regular Bridges with 2 through 6 Spans	Not Regular Bridges with 2 or More Spans
A	Not required	Not required
B, C, or D	Use Procedure 1 or 2	Use Procedure 2

Table 3 - Analysis procedure (AASHTO, 2009)

Parameter	Value				
Number of Spans	2	3	4	5	6
Maximum subtended angle (curved bridge)	30°	30°	30°	30°	30°
Maximum span length ratio from span-to-span	3	2	2	1.5	1.5
Maximum bent/pier stiffness ratio from span-to-span excluding abutments)	—	4	4	3	2

Table 4 - Regular bridge requirement (AASHTO, 2009)

As mentioned earlier, single-span bridges do not require seismic analysis, but for multi-span bridges, there are three different analysis procedures for analyzing the bridge. These analyses are Equivalent static analysis (ESA), Elastic dynamic analysis (EDA), and Nonlinear time history (TH). Table 3 shows only 2 procedures, but the third procedure is used for geometrically complex bridges and bridges that are near active earthquake faults and/or are critical or essential structures.

For irregular or complex bridges, non-linear time-history analysis is required to use, which is named as procedure 3 in AASTHO. This method is used to bridges of critical manner and if a more accurate representation of the dynamic analysis is needed. This analysis requires a minimum of three selected ground motion time histories, one vertical and two horizontal components. (AASHTO, 2009)

According to NORSOK clause 10.3.2.3, seismic actions may be described by ground response spectra or time-domain motion histories. (NORSOK standard, 2007) For time histories, the peak ground acceleration (PGA) should be used to characterize the maximum motion.

The motion of earthquake according to (NORSOK standard, 2007) can be described by two orthogonally horizontal and one vertical motion acting simultaneously. It prefers that the major horizontal component shall be in the main axis of the bridge and that the orthogonal horizontal and vertical component should be scaled with 2/3 of the major horizontal component. NORSOK, clause 6.5.1, informs that the load effect should be calculated based on at least three different sets of time histories. It is stated that the mean of maximum values from the time history analysis should be taken as a basis for the design.

NORSOK requires ULS (strength) check with an annual probability of occurrence of 10^{-2} and ALS (collapse) check with an annual probability of occurrence of 10^{-4}. Annual probability of occurrence of 10^{-2} during ALS check can be disregarded. Peak ground acceleration (PGA) can be determined based on the seismic zonation map form NFR/NORSAR (1998). (NORSOK standard, 2007)

Response spectra for a single degree of freedom system are used as the first procedure to check whether the structure needs to be checked further for the seismic response. If a further check is necessary, strength check of soil-structure and ductility check according to 10.3.7.1 and 10.3.7.2 will be carried out. If these checks are not fulfilled, more accurate analysis of the site-specific seismic hazard may be carried out. (NORSOK standard, 2007)

2.2. Previous Research on Floating Bridge Design

Damages due to earthquakes are of rare occurrence. The seismic behavior in some cases has not been studied thoroughly. Some people have studied and researched the seismic response of floating bridges, like Abrahams (Michael J Abrahams, 2007). He states that a floating bridge is a big floating mass, connected at the ends to the landmass and are not able to respond to seismic motions. He also states that the approach that can be used on general bridges might not be appropriate for evaluating floating bridges. (V. Abbasian M. Hossein, 2012) analyzed a kind of floating bridge subjected to earthquake and found that in some cases, for low-frequency earthquakes, the end supports of the deck may get damaged due to the bridge tendency to extensive lateral motions. (Eiichi Watanabe, Maruyama, Tadaaki, Tanaka, Hiroshi, & Takeda, Sumio, 2000) states that floating bridges are considered not to be affected by earthquakes, but that seismic safety has to be verified and the displacements need to be considered in the design for earthquakes.

As mentioned in section 2.1, floating bridges do not have any specific design guidelines. (Eiichi Watanabe & Utsunomiya, Tomoaki, 2003) states that the design of floating bridges should comply with the general rule of design practice, but also with special criteria inherent to floating bridges.

Floating bridges have long natural periods. Due to the investigation of the bridge, long-period waves from seismic load should be used. Floating bridges are base-isolated except the end connections where the bridge is directly connected with the ground. The environmental loads on a floating bridge shall be taken into consideration when designing the bridge. In case of an earthquake, the bridge shall be designed to secure the target performance level depending on the importance class. According to (Eiichi Watanabe & Utsunomiya, Tomoaki, 2003), the tables in Figure 6 below explain which importance class, target performance level and classification the floating bridge are in.

Table 5 Classification of floating bridges according to coefficient of importance

Coefficient of importance	Classification
A	Floating bridges other than those described below
B	High-speed roadway, urban high-speed roadway, designated city roadway, general national road, double cross-sections, over-bridges, over-railroad bridges and especially important bridges of prefectural and municipal roads

Table 6 Target performance levels for floating bridges

Performance level	Description on damage
0	No damage to bridge stability
1	No damage to soundness of bridge function
2	Damages may limit bridge function but the function soon recovered
3	Damages may cause loss of bridge function, but limited so that the safety against collapse, sinking and drifting secured

Table 7 Relationships of load level, coefficient of importance and performance level

Load and load level	Coefficient of importance	Performance level required
For ordinary loads and at the service wave conditions	A or B	0
Against level 1 earthquakes	A or B	1
Against stormy waves	B	1
	A	2
Against tsunamis and level 2 earthquake	B	2
	A	3

Figure 6 - Importance class, target performance level and classification for floating bridges (Eiichi Watanabe & Utsunomiya, Tomoaki, 2003)

Based on the tables; a bridge exposed to earthquake level 1 will not get damaged due to bridge function, independent of floating bridge type. Special types of floating bridges exposed for earthquake level 2 and tsunamis may cause loss of bridge function, but total collapse will not occur. Earthquake loading goes under secondary loads (S), where the principal loads (P) are dead loads, live loads, impact loads, etc.

Since floating bridges undergo finite displacements, the horizontal- and vertical displacements and inclination are among the most important factors in the design of floating bridges. The stability, serviceability, and bridge safety depend on these factors mentioned. (Eiichi Watanabe & Utsunomiya, Tomoaki, 2003)

2.3. Seismic Design and Analysis of Long, Flexible Bridges

Dynamic analysis of the bridge structure will be used in this thesis due to the time-dependent earthquake load. The earthquake load depends on the magnitude, direction, and position, where all of them vary with time. There are several methods for analyzing a bridge against this earthquake loads. The different analysis procedures are found from AASHTO (AASHTO, 2009), Eurocode 8 ((European Standard, 2004) & (European Standard, 2005)) and Bridge Handbook (Wai-Fah Chen & Duan, Lian, 2014). Multiple degree of freedom (MDOF) analysis will be used since Single degree of freedom (SDOF) are not applicable for a complex bridge as Bjørnafjorden floating bridge. Finding the right analysis method depends on the seismic zone, geometry, and importance class of the bridge structure. (Wai-Fah Chen & Duan, Lian, 2014) A brief description of the different methods for analyzing long, flexible bridges will be described in this section. It is important to mention that the methods are intended for general bridges.

2.3.1. Response Spectrum Analysis

The response spectrum method is a method that gives the maximum response of an SDOF structure. The analysis uses the same damping ratios but different natural frequencies. For a structure with *n* DOF, the structure can be divided into *n* SDOF-systems such that the principles of response spectra can be applied to the many DOF-system. It is important to know that the response spectrum method is used for the estimation of peak values and must be used carefully. It is strictly limited to linear elastic analysis. (Wai-Fah Chen & Duan, Lian, 2014)

2.3.1.1. Equivalent Static Analysis (ESA)

According to AASHTO, equivalent static analysis can be used to establish the displacement demand for bridges with regularity, i.e. where a single-degree-of-freedom model is sufficient to represent the seismic response. Both the *uniform load method* and *single-mode spectral analysis method* are acceptable equivalent static analysis procedures, where the method assumes that the seismic load can be applied as an equivalent static force in either longitudinal or transverse direction. (AASHTO, 2009)

The Uniform load method is used to analyze simple bridges that respond principally in their fundamental mode of vibrations (bridges with relatively straight alignment, small skew, balanced stiffness, etc). The method is not suitable for bridges with a stiff superstructure. (Wai-Fah Chen & Duan, Lian, 2014) The earthquake load is distributed over the whole structure (to all elements) and assumes continuity. This method of analysis may be used for either transverse or longitudinal earthquake motions. *Uniform Load Method* can give an unrealistic distribution of seismic forces due to an overestimation of transverse shears at the abutments. (AASHTO, 2009) The stiffness used to calculate the equivalent static earthquake load uses the maximum lateral displacement that occurs when an arbitrary uniform lateral load is applied to the bridge.

To avoid unrealistic distributions of seismic forces on the bridge, a *single-mode spectral analysis* may be used instead of the uniform load method. This method assumes that the seismic force for structures responds predominantly in the first mode of vibration. (Wai-Fah Chen & Duan, Lian, 2014) Irregular bridges have often higher modes of vibrations that affect the response, i.e. force distributions and deformations,

significantly. The single-mode spectral analysis is not a suitable method for the analysis of irregular bridges.

This method is often used to frames and buildings with well-balanced spans and equally distributed stiffness and is based on the natural period of a single degree of freedom (SDOF) response spectra. It assumes that the seismic load can be applied as an equivalent static horizontal force in either the longitudinal or transverse direction to find the mode shape. The deformed shape is then calculated. A detailed procedure description of analysis can be found in chapter 3.4.1 in the Bridge Handbook (Wai-Fah Chen & Duan, Lian, 2014).

2.3.1.2. Elastic Dynamic Analysis (EDA)

If a more complex linear elastic structure subjected to earthquake excitation is being studied, *multi-mode spectral analysis* is more suitable then a single-mode spectral analysis, i.e. structures with irregular geometry, stiffness, or mass. Member forces, displacements, and mode shapes due to seismic loads can be computed using the cross-correlation combination (CQC) method and the square root of the sum of the squares (SRSS) method. (Wai-Fah Chen & Duan, Lian, 2014) The percentage rule (100/30) shown in Table 5 is recommended by AASHTO to use. (AASHTO, 2009)

Seismic Load case	Transverse [%]	Longitudinal [%]	Vertical [%]
1	100	30	30
2	30	100	30
3	30	30	100

Table 5 - Combination of seismic load at different locations

Multiple support response spectrum (MSRS) method accounts for spatial variability of ground motions due to multiple supports. The three important effects of ground motion spatial variability are accounted for in this method, i.e. incoherence, wave passage, and site response effect. These components can influence the response. (Wai-Fah Chen & Duan, Lian, 2014) The superposition of response can be used to calculate the total response due to independent support input. This method is suitable for long multiple support bridges.

2.3.2. Non-linear Time History Method

According to clause 4.1.9.(2) in EN 1998-2:2005 (European Standard, 2005), the realistic response of irregular bridges can be estimated with means of dynamic non-linear time-history analysis. By using the time-history method, direct numerical integration of its non-linear equation of motion shall be used to find the response of the bridge. Accelerogram shall be used as ground motion time-histories. The nonlinear time-domain analysis is the most rigorous analyzing method, utilizing the combination of ground motion records with a structural model. (Junbo Jia, 2012)

There are some limitations by using the analysis. It takes more computational effort than for any other type of analysis. This method often needs several records of ground motion because the calculated response is very dependent on ground motion characteristics. EN 1998-2:2005 requires three sets of horizontal ground motion records for new bridges when designing against earthquake motion in the time-

domain. (European Standard, 2005) The response of the bridge is also very sensitive when a change in the numerical parameter occurs during time integrations. (Junbo Jia, 2012)

Load steps can be large if the structure behaves "linearly". Due to the non-linearity of the bridge structure, the time steps should be small of size. The more nonlinear, the smaller the load steps should be. (USFOS, 1999a)

2.3.3. Summary and Discussion of Analysis Methods

Table 6 illustrate the applicability and performance of the main analysis methods. Dynamic effects, spatial variation of the ground, computation cost, and geometric nonlinearity are the effects in this method of analysis.

Analysis method	Dynamic effects	Spatial variation	Computation cost	Geometric nonlinearity	Use for SDOF	Use for MDOF
Response spectrum analysis	YES	YES	Low	NO	YES	NO
Nonlinear dynamic time-domain analysis	YES	YES	Very high	YES	NO	YES

Table 6 - Analysis applicability and performance

Due to the complexity of the Bjørnafjorden bridge, equivalent static analysis (ESA) will not be suitable methods for analyzing the response during earthquake loading. Elastic dynamic analysis (EDA) is for linear, but more complex bridges. Due to the complexities of a bridge, simplifying the structure with one degree of freedom is not possible. Finite element analysis can then be used to model the structure and finding the vibration modes. (Junbo Jia, 2012) Nonlinear time history analysis is the best suitable analysis method for complex bridges with non-regularities.

Nonlinear dynamic time-domain analysis and response spectrum analysis shall generally give a similar calculated response, but the response spectrum method will give a more conservative evaluation. (Junbo Jia, 2012) For flexible structures, such as Bjørnafjorden floating bridge, the result begins to differ.

For offshore structures, among all the analyses, the most used method is the response spectrum method. Today, the trend has led to more use of the nonlinear dynamic time-domain analysis. (Junbo Jia, 2012)

Chapter 3

3. Theory

3.1. Equation of Motion

Since the bridge cannot be expressed as SDOF but as an MDOF system, the equation of motion is expressed by matrices. The bridge has multiple supports with a long distance between them. Three of them are close to each other, but the support in the North end is approximately 5 km away from the others. We cannot assume that the supports undergo the same excitations due to the distance. That assumption is valid for supports near each other according to EN 1998-2:2005. (European Standard, 2005) The distance from the epicenter and localized soil layer decides the earth's motion at a location. (Wai-Fah Chen & Duan, Lian, 2014) (p.118) Bridges with supports laying far from each other will experience different seismic ground motions. To evaluate the response of a long bridge with multiple supports, different ground excitations are recommended. According to (Wai-Fah Chen & Duan, Lian, 2014) the equation of motion for an N-DOF bridge with multiple supports with different ground excitations becomes:

$$[\boldsymbol{M}]\{\ddot{r}\} + [\boldsymbol{C}]\{\dot{r}\} + [\boldsymbol{K}]\{r\} = -[\boldsymbol{M}]\{\ddot{u_g}\} \quad (1)$$

Where **M** is the mass matrix, **C** is the damping matrix and **K** is the stiffness matrix. All the matrices are n x n square matrices. $\{\ddot{u_g}\}$ is a displacement array with accelerations at each support location and zero value for non-supports.

3.2. Solution Algorithm

Time-domain analyses will be used in this thesis and are the only suitable analysis method due to the non-linear response of the structure. All time-domain analyses have in common that the analysis of the structure is performed in the time domain by stepwise integration of the dynamic equation of motion, Equation 2:

$$[\boldsymbol{M}]\ddot{r}(t) + [\boldsymbol{C}]\dot{r}(t) + [\boldsymbol{K}]r(t) = \boldsymbol{R(t)} \quad (2)$$

The acceleration, velocity, and displacement vectors, $\{\ddot{r}\}, \{\dot{r}\}$ and $\{r\}$, are the unknowns. R(t) is the external excitation force. The mass, damping, and stiffness matrices consist of constants and are symmetric if linearly structures are modelled. The solution of the system is then straight forward. Nonlinearities are often to be found in bridge models which gives no guarantees for the mass, damping, and stiffness matrices to be symmetric. This system cannot be solved directly. One of the most commonly used algorithms to solve this problem is the Newmark-β method with full newton iteration at each time step. (Wai-Fah Chen & Duan, Lian, 2014) Wilson-θ method can also be used to solve the equation of motion.

The USFOS software used to analyze the bridge uses Hilber-Hughes-Taylor-α method (HHT-α). HHT-α method is based on Newmark's-β method and uses the following equations to calculate the response at time step k+1:

$$\dot{r}_{k+1} = \dot{r}_k + (1-\gamma)\cdot\Delta t\cdot\ddot{r}_k + \gamma\cdot\Delta t\cdot\ddot{r}_{k+1} \quad (3)$$

$$r_{k+1} = r_k + \Delta t \cdot \dot{r}_k + \left(\frac{1}{2} - \beta\right) \cdot \Delta t^2 \cdot \ddot{r}_k + \beta \cdot \Delta t^2 \cdot \ddot{r}_{k+1} \quad (4)$$

Where γ and β are weight parameters that can be chosen according to requirements regarding numerical stability and accuracy. (Einar N. Strømmen, 2012)(page 241) The current iteration step is denoted as *k* and the next iteration step is denoted *k*+1.

The Newmark-β method is unconditionally stable if Equation 5 is fulfilled:

$$\gamma \geq \gamma_0 = \frac{1}{2} \quad , \quad \beta \geq \beta_0 = \frac{1}{4}(\gamma + \frac{1}{2})^2 \quad (5)$$

Constants, $\gamma = \frac{1}{2}$ and $\beta = \frac{1}{4}$ gives the Newmark's method identical properties to constant average acceleration (Average Acceleration Method), which is conditionally stable.

HHT-α method has suggested an extension of the Newmark-β method by introducing a coefficient $\alpha \leq 0$ which increases the amount of numerical damping without a change in the accuracy in the method. The method uses Equation (6) and (7) to formulate displacement and velocity at t_{k+1}:

$$\boldsymbol{M}\ddot{r}_{k+1} + (1+\alpha)\boldsymbol{C}\dot{r}_{k+1} - \alpha\boldsymbol{C}\dot{r}_k + (1+\alpha)\boldsymbol{K}r_{k+1} - \alpha\boldsymbol{K}r_k = \boldsymbol{R_\alpha} \quad (6)$$

Introducing this to the dynamic equation of motion at t_{k+1}:

$$[\boldsymbol{M}]\ddot{r}_{k+1} + [\boldsymbol{C}]\dot{r}_{k+1} + [\boldsymbol{K}]r_{k+1} = \boldsymbol{F_{k+1}} \quad (7)$$

3.3. Eigenvalue Analysis

To get the eigenfrequencies (natural frequency) of the bridge, an eigenvalue analysis needs to be performed. There are no external loads during an eigenvalue analysis, i.e. only the systems self-weight is included. This analysis gives the mode shapes and natural frequencies of the bridge system. By setting [C] and $\{\ddot{u_g}\}$ to zero, Equation 1 becomes the equation of motion for undamped free vibrations and are given by (Wai-Fah Chen & Duan, Lian, 2014):

$$[\boldsymbol{M}]\{\ddot{r}\} + [\boldsymbol{K}]\{r\} = 0 \quad (8)$$

Which can be rearranged as follows:

$$\left[[\boldsymbol{K}] - \omega_n^2[\boldsymbol{M}]\right]\{\varphi_n\} = 0 \quad (9)$$

Here, φ_n is the shape matrix and ω_n is the natural frequency for mode n. The solution of Equation 9 can be made by setting:

$$\left[[\boldsymbol{K}] - \omega_n^2[\boldsymbol{M}]\right] = 0 \quad (10)$$

The natural frequencies (ω_n) of the dynamic equation are the roots and eigenvalues of Equation 10. (Wai-Fah Chen & Duan, Lian, 2014) The eigenvectors (φ_n), can then be determined by Equation 9. The eigenvalues and eigenvectors can be found simultaneously by iterations. Eigenvectors are also called mode shapes of the system.

3.4. Rayleigh Damping

Damping is related to the energy dissipation during a motion. A dynamic structure will always be subjected to damping in the physical world, otherwise, the response/oscillation will never decrease. Without damping, the response of the structure will be very large. Damping can be inherent or deliberately added. (Robert D. Cook, Malkus, David S., Plesha, Michael E., & Witt, Robert J., 2002) There are several types of damping that influence structural dynamics, such as viscous damping, hysteresis damping, coulomb damping, and radiation damping. To represent viscous damping, two devices are commonly used: Proportional and modal damping. The damping ratio is a term that is often used when damping is the subject. The damping ratio is the fraction of critical damping and is termed in Equation 11:

$$\xi = \frac{c}{c_c} = \frac{c}{2m\omega} \tag{11}$$

Where c is the damping coefficient, c_c is the critical damping coefficient, m is the mass and ω is the natural frequency. Damping of structures are often small, typical $\xi < 0.15$. (Robert D. Cook et al., 2002)

Rayleigh damping is the traditional damping model used for step-by-step or time-history programs. Rayleigh damping is also called proportional damping and describes the damping matrix of the structure as a linear combination of global mass (mass proportional) and stiffness matrix (stiffness proportional) shown in Equation 12:

$$[\boldsymbol{C}] = \alpha[\boldsymbol{M}] + \beta[\boldsymbol{K}] \tag{12}$$

Where $[\boldsymbol{C}]$, $[\boldsymbol{M}]$ and $[\boldsymbol{K}]$ are the damping, mass, and stiffness matrices, respectively. α and β are constants with numerical values that limit the modal damping ratio and can also be expressed as weight factors that can be determined from specified damping ratios at two different and independent dominant modes. (Wai-Fah Chen & Duan, Lian, 2014)(p.114) This type of damping can be considered as viscous damping of structural elements.

The damping ration for the n^{th} mode (ξ_n) can be computed as

$$\xi_n = \frac{\alpha}{2}\frac{1}{\omega_n} + \frac{\beta}{2}\omega_n \tag{13}$$

where ω_n are the frequency of n^{th} mode. To calculate the values of α and β, a damping ratio of ξ_i and ξ_j to the i^{th} and j^{th} modes with the frequencies ω_i and ω_j needs to be prescribed. By assuming that the damping ratio (ξ) for the i^{th} and j^{th} mode are equal, α and β can be computed as:

$$\alpha = \xi\frac{2\omega_i\omega_j}{\omega_i+\omega_j} \qquad \beta = \xi\frac{2}{\omega_i+\omega_j} \tag{14}$$

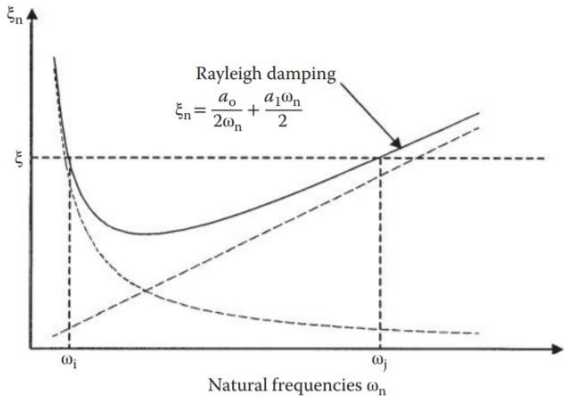

Figure 7 - Rayleigh Damping (Wai-Fah Chen & Duan, Lian, 2014)

As Figure 7 shows, damping value at a location between ω_i and ω_j can be less than ξ. (Wai-Fah Chen & Duan, Lian, 2014) For the $\alpha[\boldsymbol{M}]$, low natural frequencies are hard to damp and for $\beta[\boldsymbol{K}]$, high natural frequencies are hard to damp. For both, the damping ratio is defined only at one frequency. It is important to identify the most important frequencies in the response problem to specify the damping ratios, such that the values are reasonable in all mode shapes.

3.5. Earthquake Ground Motions

This section gives a brief description of ground motion input for seismic bridge analysis. The earthquake ground motion is termed seismogram or time histories where the time-histories contains recorded accelerations called accelerogram. A typical accelerogram containing earthquake excitations is shown in Figure 8. This is called a time-domain analysis. Earthquake excitation is a non-periodic transient process, also known as a stochastic process. (Einar N. Strømmen, 2012) The time histories theoretically contain all information about the motion at a location with orthogonal records (two horizontal and one vertical). Time histories or earthquake motion can differ drastically in duration, frequency content, and amplitude. As the ground motion contains random vibrations, the behavior is not possible to predict. The Peak Ground Acceleration (PGA) is the maximum recorded amplitude and is often the most important factor during seismic analysis. The acceleration is the recorded parameter where velocity and displacements can be determined by direct integration. For design purposes, only the maximum amplitude of the response time history is enough to know, i.e. PGA.

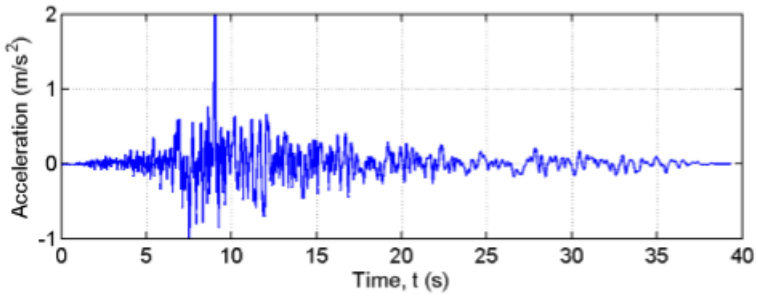

Figure 8 - Example of accelerogram (Einar N. Strømmen, 2012)

(Junbo Jia, 2012) states that there are three ways to obtain the ground motion time-histories:

- Measured data, e.g. on the seabed
- Site response analysis
- Artificial time history from a predefined design spectrum

To measure the structure response, a generated time history with suitable ground motions needs to be implemented. The ground motion generated for this thesis is described in Chapter 4.

3.6. Load Combinations for Seismic Action

The NORSOK standard "Actions and action effects" shows an overview of combinations of environmental loads in the modelling of 100-years and 10 000-years, shown in Table 7. (NORSOK standard, 2007) The table shows that for an accidental limit state (10 000-years), the only environmental load that needs to be combined is the earthquake load for a mean water level. Characteristic load for abnormal environmental load shall be calculated with a 10.000-years return period according to (Statens Vegvesen, 2017c).

Limit state	Wind	Waves	Current	Ice	Snow	Earthquake	Sea level [a]
Ultimate Limit State	10^{-2}	10^{-2}	10^{-1}	-	-	-	10^{-2}
	10^{-1}	10^{-1}	10^{-2}	-	-	-	10^{-2}
	10^{-1}	10^{-1}	10^{-1}	10^{-2}	-	-	m
	-	-	-	-	10^{-2}	-	m
	-	-	-	-	-	10^{-2}	m
Accidental Limit State	10^{-4}	10^{-2}	10^{-1}	-	-	-	m*
	10^{-2}	10^{-4}	10^{-1}	-	-	-	m*
	10^{-1}	10^{-1}	10^{-4}	-	-	-	m*
	-	-	-	10^{-4}	-	-	m
	-	-	-	-	-	10^{-4}	m

[a] m - mean water level
m* - mean water level, including the effect of possible storm surge
Seismic response analysis should be carried out for the most critical water level.

Table 7 - Combination of environmental loads for ULS and ALS (NORSOK standard, 2007)

As mentioned earlier, modelling the seismic actions provides three different directions of the earthquake action. There are two horizontal directions and one vertical direction. According to NS-EN 1998-2:2005 (European Standard, 2005) clause 4.2.1.4, the maximum action effect due to seismic action can be estimated according to the following combination formulas (4.20) - (4.22) in NS-EN 1998-1:2004 (European Standard, 2004):

$$E_{Edx} + 0{,}30E_{Edy} + 0{,}30E_{Edz} \tag{15}$$

$$0{,}30E_{Edx} + E_{Edy} + 0{,}30E_{Edz} \tag{16}$$

$$0{,}30E_{Edx} + 0{,}30E_{Edy} + E_{Edz} \tag{17}$$

Where E_{Edx} and E_{Edy} are the horizontal components and E_{Edz} are the vertical. The maximum action effect will be the most adverse combination of Equation 15 – 17. AASHTO (AASHTO, 2009) describes the seismic action in the same way as NS-EN 1998-2:2005 (European Standard, 2005).

3.6.1. Combination of Seismic Action with Other Loads

The seismic action shall be combined with other loads according to NS-EN 1998-2:2005 (European Standard, 2005), cl.5.5(1).

According to (Statens Vegvesen, 2017c), earthquake load shall be combined with permanent load and traffic load in the accidental limit state, which is given in Table 8. ψ_2 is the combination factor according to Table NA. A2.1 in NS-EN 1990:2002+ +NA:2008. (Standard Norge, 2008)

Load combinations with accident loads		**Stage a**			**Stage b (damaged condition)**		
		Earthquake	Abnormal environmental loads	Ship impact	Pontoon filled with water	Lost anchorage	Lost cable stay
		Ψ_2	Ψ_2	Ψ_2	Ψ_2	Ψ_2	Ψ_2
Permanent loads							
Permanent loads	G- EQ_K	1.0	1.0	1.0	1.0	1.0	1.0
Variable loads							
Traffic loads	Q_Trf_K	0.2	0	0.2	0.2	0.2	0.2
Temperature loads	$Q\text{-}Temp_K$	0	0	0	0	0	0
Other loads	Q_K	0	0	0	0	0	0
Environmental loads in event of damage	$Q\text{-}E_{K(100\ year)}$	0	0	0	1.0	1.0	1.0
Accident loads							
Earthquake	A-EarthQ	1.0	0	0	0	0	0
Abnormal environmental loads	$Q\text{-}E_{K(*)}$	0	1.0	0	0	0	0
Ship impact	A-Coll	0	0	1.0	0	0	0
Pontoon filled with water	A-Flood	0	0	0	1.0	0	0
Lost mooring cables	A-Morfail	0	0	0	0	1.0	0
Lost cable stay	A-SCab	0	0	0	0	0	1.0

Table 8 - Load combinations for accidental limit state (Statens Vegvesen, 2017c)

According to N400 (Statens Vegvesen, 2009) section 6.3.6, traffic load can be neglected if the bridge is assumed closed under damaged conditions.

Chapter 4

4. Seismic Ground Motion Modelling

This chapter will explain the method used for generating the seismic ground motions used to simulate the bridge response in USFOS. First, the response spectrum method in NS-EN 1998-2:2005 (European Standard, 2005) is used to define the response spectrum, and then a synthetic accelerogram is generated which closely matches the design response spectrum. This accelerogram will then be applied to the floating bridge as time history input in USFOS.

4.1. Defining Response Spectra According to Eurocode 8

The components of ground motions will be treated separately when using the response spectrum method of the bridge. The code also states that only the translational components of the seismic action are sufficient for the design of bridges. The seismic action is represented by three one-component actions according to clause 3.1.2(1)P in (European Standard, 2005).

The horizontal component during the response spectrum method shall be according to NS-EN 1998-1:2004 (European Standard, 2004), clause 3.2.2.2. Clause 3.3 in NS-EN 1998-2:2005 will be used when the soil type changes along with the bridge support or if the continuous deck exceeds a limited length, L_{lim}. The horizontal elastic response spectra, $S_e(T)$, is defined by equation 3.2 - 3.5 in NS-EN 1998-1:2004, where T_B, T_C and T_D represents the value of periods and S is the soil factor. The values can be found when the ground type is determined. Bjørnafjorden has ground type A according to (Statens Vegvesen, 2017d) which represents rock foundation. Since the bridge is placed where the surface-wave magnitude of an earthquake is not greater than 5.5, type 2 spectrum will be adopted and Table 9 gives the values for periods and soil factors applicable for ground type A.

Ground-type	**S**	T_B (s)	T_C (s)	T_D (s)
A	1.0	0.05	0.25	1.2

Table 9 – Values of parameters describing Type 2 elastic response spectra for ground type A

The vertical component will be determined according to clause 3.2.2.3 and represented by a vertical elastic response spectrum, $S_{ve}(T)$, found from equation 3.8 - 3.11 in NS-EN 1998-1:2004. (European Standard, 2004) The values for T_B, T_C and T_D and the a_{vg} are given in Table 10.

Spectrum	a_{vg}	T_B (s)	T_C (s)	T_D (s)
Type 2	0.45	0.05	0.15	1.0

Table 10 – Values describing the vertical elastic response spectra (Type 2)

Response spectrum method is widely used for bridge structure resistance against earthquakes. (Xiuyun Gao & Jiang, Yitan, 2014) By using the values from Table 9 and Table 10, the acceleration response spectra can be made. The seismic action in horizontal directions can then be found by Equation 18:

$$a_g = \gamma_I \cdot a_{gR} \tag{18}$$

where a_{gR} is the peak ground acceleration and γ_I is the importance factor.

4.2. Generation of Accelerograms

When using dynamic analysis method, NS-EN 1998-2:2005 requires that at least three sets of horizontal ground motion time-history components shall be used on each site, applied simultaneously. (European Standard, 2005) When these sets of ground motions are not available, simulated/generated accelerograms can replace them. In our case, with complex structural systems, generation of artificial seismic ground motion is required. Long span bridges with large dimensions need to consider different ground motions at different stations (supports), also known as spatial variability effect.

To get a reliable analysis of the bridge, properly defining the ground motion is crucial. The ground motions used to analyze the bridge against seismic excitations are made by Dr. Kaiming Bi, Senior Lecturer, Curtin University in Australia. The motions generated are displacement and acceleration time histories according to the response spectrum for the code (chapter 4.1) and the location of the supports, including the spatially varying ground motions. The ground motion shall be applied to three different locations.

Different methods are suitable to generate time histories for ground motions. In our case, the spatial varying ground motions on the surface of an uneven site are modelled in two steps. First, the base rock motions are modelled by a filtered Tajimi-Kanai power spectral density function. The spatial variation of the base rock ground motion is modelled by an empirical coherency loss function. The power spectral density functions are derived based on the 1D wave propagation theory. Secondly, a stochastic method to generate the spatially varying time histories and a coherency function is made to generate the ground motions of an uneven site. (Kaiming Bi & Hao, Hong, 2012)

Spatially correlated time histories are generated to be compatible with the design spectra specified in (European Standard, 2005) and the considerations from the design basis (Statens Vegvesen, 2017e). The design response spectra from Eurocode 8 and the response spectra for the different sites will be compared in the next sub-chapter. The soil-class at the three sites are class A. The peak ground acceleration is $0.83\frac{m}{s^2}$ according to (Statens Vegvesen, 2017e). To describe the coherency loss between the ground motions at points j and $\acute{k}$ ($j \neq k$), the Sobczyk model is used (Kaiming Bi & Hao, Hong, 2012):

$$\begin{aligned} \boldsymbol{\gamma_{j\acute{k}}(i\omega)} &= \left|\boldsymbol{\gamma_{j\acute{k}}(iw)}\right| \boldsymbol{exp}\left(-\boldsymbol{i\omega d_{j\acute{k}} cos\alpha / v_{app}}\right) \\ &= \boldsymbol{exp}(-\beta\omega d_{j\acute{k}}^2 / v_{app}) \cdot \boldsymbol{exp}(-i\omega d_{j\acute{k}} cos\alpha / v_{app}) \end{aligned} \tag{19}$$

Where $\left|\boldsymbol{\gamma}_{j\acute{k}}(iw)\right|$ represents the lagged coherency loss, β is a coefficient (reflects the level of coherency loss), $\boldsymbol{d_{j\acute{k}}}$ is the distance between j' and k', α is the incident angle of the incoming wave to the site, and $\boldsymbol{v_{app}}$ is the apparent wave velocity at the base rock.

Jennings envelope function is multiplicated with the simulated time histories to include the variation of ground motions. This is a shape function and is given in Equation 20:

$$\xi(t) = \begin{cases} (t/t_0) & 0 \le t \le t_0 \\ 1 & t_0 < t \le t_n \\ exp[-0.155(t - t_n)] & t_n < t \le T \end{cases} \quad (20)$$

Where T is the duration time. The generated time histories for the three locations, in form of accelerations and displacements, are given in Figure 9-11 in Chapter 4.3. These generated time histories are used as input for analyzing the bridge in USFOS.

4.3. Results from Ground Motion Generation

The accelerations and displacements obtained by the generation method from chapter 4.2 are given here. There are three different load cases including displacements which are combined in the plots to compare if huge variations occur during the time. The theoretical peak ground acceleration (PGA) defined in the response spectra is 0.83 m/s^2.

Site 1	South end
Site 2	Bridge tower
Site 3	North end

Table 11 - Explanation of site locations for figures 9-11.

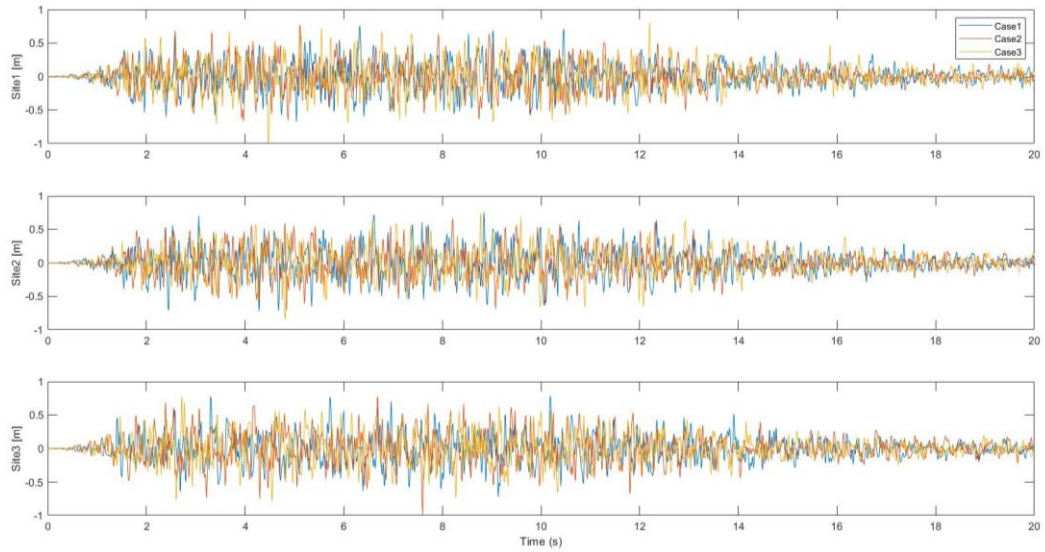

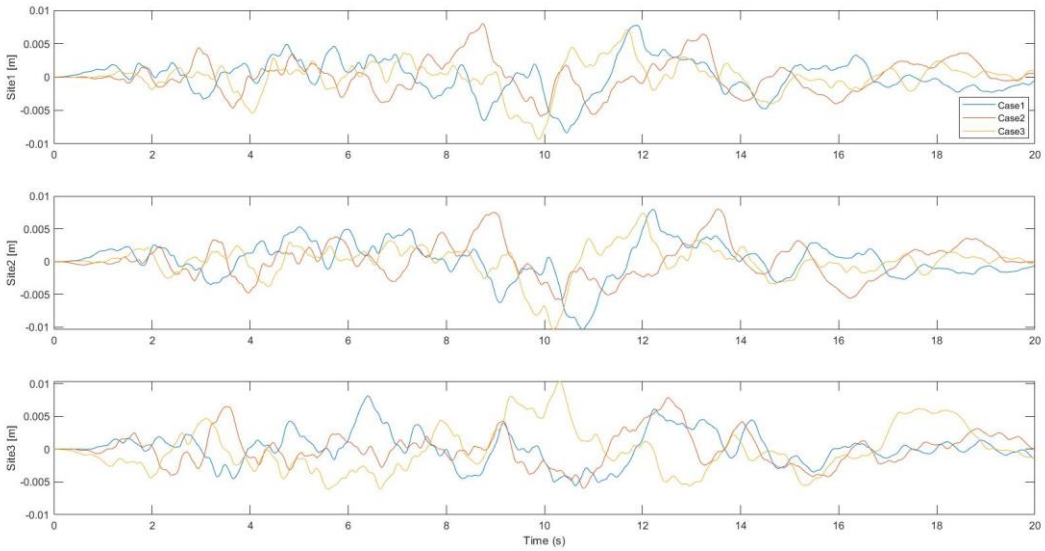

Figure 9 - Generated base rock motions in horizontal x-direction for all three cases

The three generated horizontal (x-direction) motions are shown in Figure 9 (a) and (b) for acceleration and displacement, respectively. The PGA's and PGD's of the simulated motions are 0.80766, 0.75367, 0.7859 m/s^2 and 0.00802, 0.00798, 0.01037 m. The peak ground accelerations are relatively close to the theoretical value of 0.83 m/s^2. These values are the maximum of the three cases in the time histories.

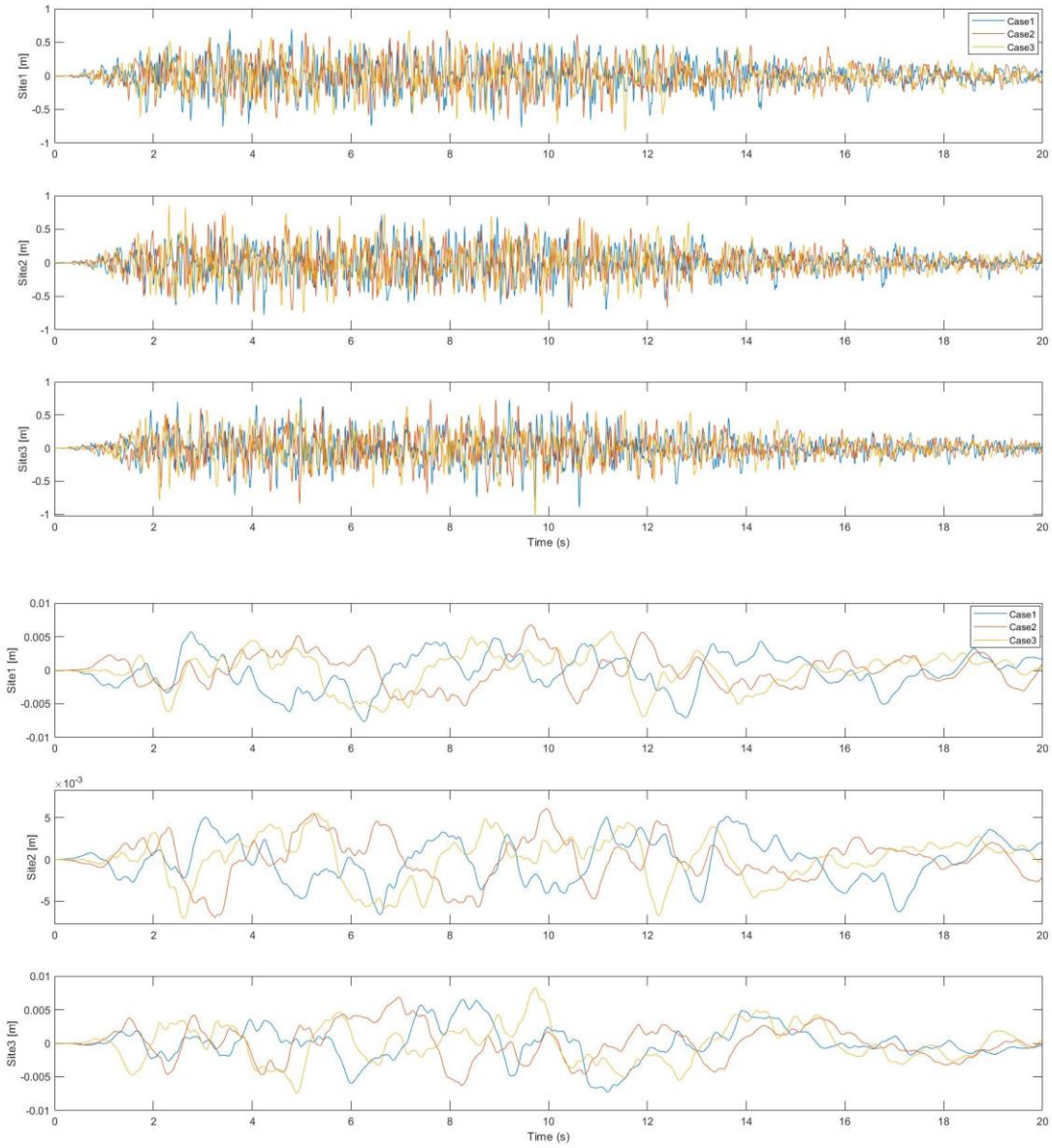

Figure 10 - Generated base rock motions in horizontal y-direction for all three cases

The three generated horizontal (y-direction) motions are shown in Figure 10 (a) and (b). The PGA's of the simulated motions are 0.69782, 0.86129, 0.76171 m/s^2 and 0.00675, 0.00611, 0.00827 m, respectively. These values are also close to the theoretical peak ground acceleration.

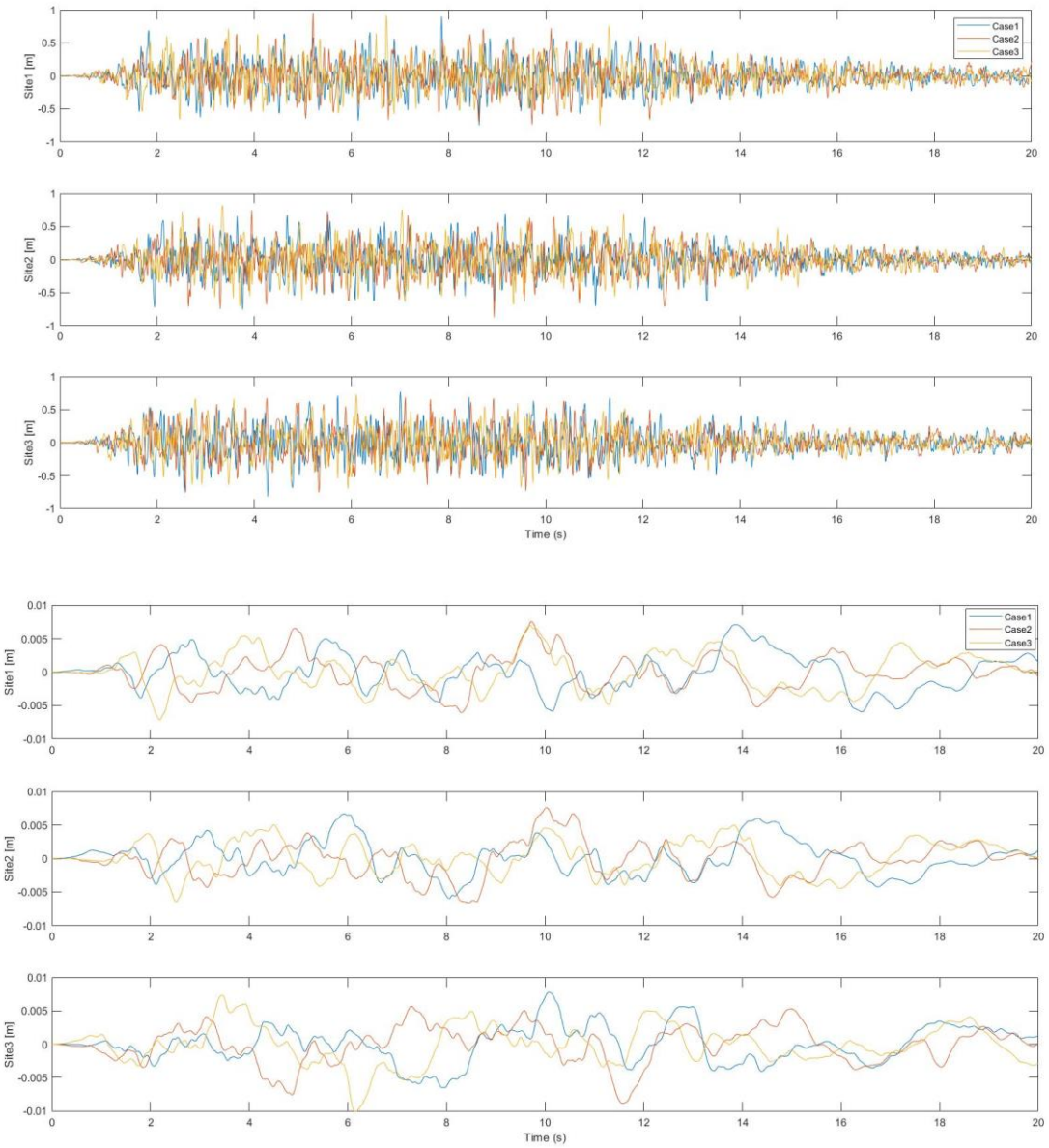

Figure 11 - Generated base rock motions in vertical direction for all three cases

The three generated vertical (z-direction) motions are shown in Figure 11 (a) and (b). The PGA's and PGD's of the simulated motions are 0.95878, 0.82134, 0.77161 m/s^2 and 0.00751, 0.00761, 0.00777 m for the three different sites. These values are also similar to the theoretical PGA. In agreement with the supervisor, Yanyan Sha, the input value in vertical direction shall be multiplicated with a factor of 0.5 as input in USFOS since the vertical vibrations in real life will not be the same as for the horizontal directions.

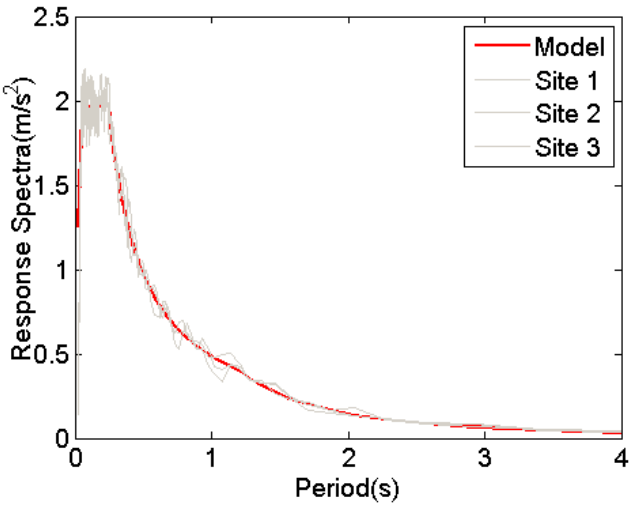

Figure 12 - Actual and target response spectra

Figure 12 shows good matching with the actual site spectra's and the target response spectra used to generate the ground motions. The light plot is from the calculated synthetic accelerograms.

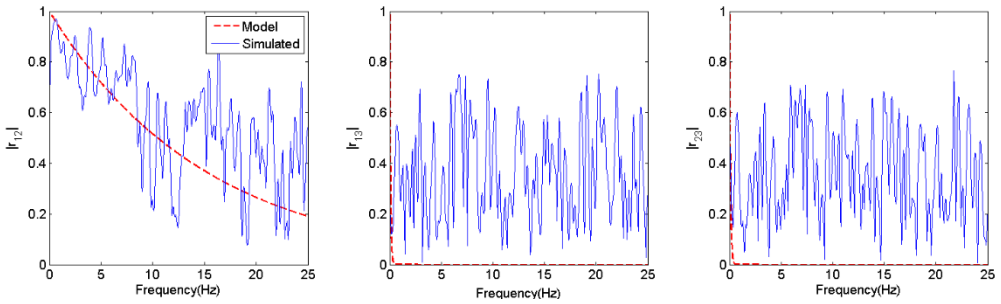

Figure 13 - Comparison of coherency loss between the generated time histories for each site

The coherence in Figure 13 illustrates the relevance of the seismic time histories between two locations. In our case, the bridge tower (r_2) and the south end (r_1) is far from the north end (r_3), which result in a very low coherence (~0.4). If the factor is 1, it means they are completely related which can be illustrated for r_{12}, which is between the south end and the bridge tower. The results for r_{13} and r_{23} indicate incoherency with the sites as explained in Chapter 2. Since the bridge tower is very close to the south end, the results for r_{13} and r_{23} shows a good match with each other.

Chapter 5

5. Modelling of the Bridge in USFOS

This chapter will inform us about the design of the floating bridge used to analyze for seismic excitations in USFOS. There will be a short description of how the bridge girder, pontoons, columns, and cables are modelled and how the bridge is designed. The end-anchored floating bridge is described with different structural elements (sub-elements) in the following subchapters. The model is based on the bridge described in "K7 Bjørnarfjord End-anchored floating bridge – Summary report" (Norconsult AS, 2017c) by Norconsult. The structural drawings are taken from the "K7 Bjørnarfjord End-anchored floating bridge, Appendix A – Drawing binder".(Norconsult AS, 2017a) Figure 14 shows an illustration of the bridge model in USFOS.

The model described in this section is made by Ida Osvoll (Ida Fagerli Osvoll, 2018). Values in the tables and formulas used in this chapter are derived from her model and the Summary report. For more details about how the bridge is modelled, read chapter 4 in (Ida Fagerli Osvoll, 2018).

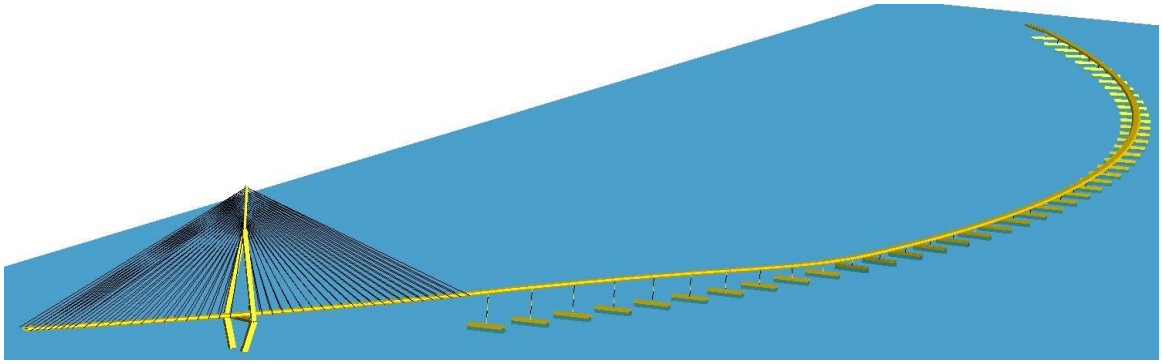

Figure 14 - Bridge illustration from USFOS

5.1. USFOS as a Finite Element Tool

USFOS (Ultimate Strength for Framed Offshore Structures) is a powerful finite element analysis (FEA) program which is developed for nonlinear analysis of space frame structures. This software is widely used in the offshore branch and can perform a wide range of analyses on progressive collapse and in ultimate strength. (USFOS, 2020)

USFOS is used to analyze the floating bridge of Bjørnafjorden. For accidental load analysis, USFOS is the world-leading computer program for fixed offshore structures. USFOS gives a better insight into how the structure behaves and the safety of the structure. (USFOS, 2020)

Dynamic analysis can be done in USFOS by using predefined load histories. This is a numerical analysis based on a mass matrix that can be set to either a consistent or lumped mass matrix. The response of dynamic analysis is highly dependent on the duration and intensity of the load history applied.

Each node in a finite element model has 6 degrees of freedom, 3 translations, and 3 rotations, illustrated in Figure 18. (USFOS, 1999b) The bridge girders are modelled in USFOS with GENBEAM, the columns and cables are modelled as PIPE and the cables are modelled as BOX [RHS-sections].

5.2. Bridge Design

The bridge is an end-anchored floating bridge with a cable-stayed part in the south end and the rest is floating on supporting pontoons. It is a single-girder bridge and has a total length of 5.5 km with a c-curvature between the south and north abutment. The orientation and elevation view of the floating bridge is shown in Figure 15 with axis numbering and lengths.

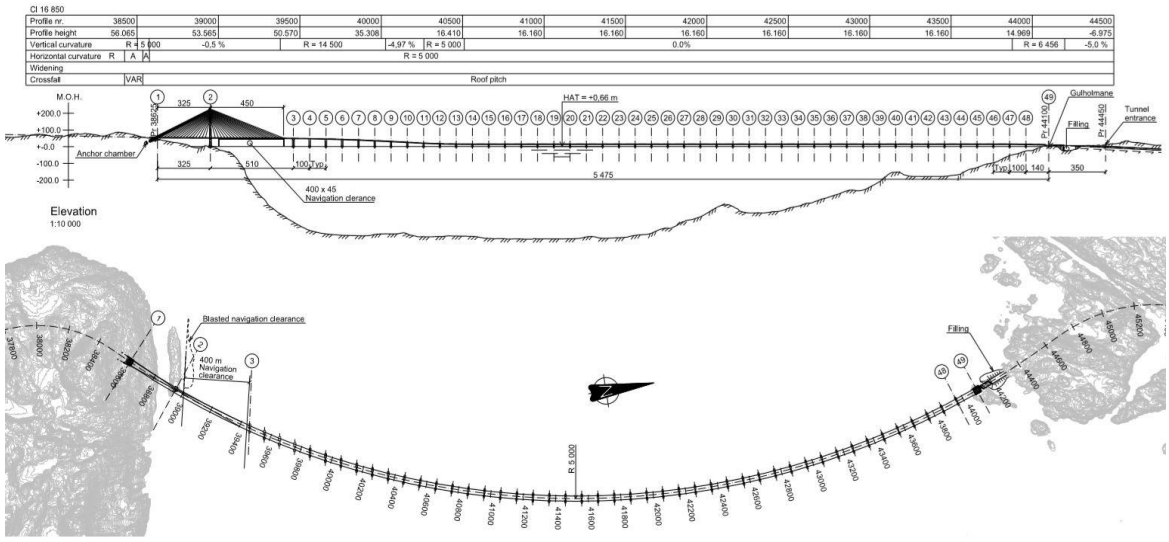

Figure 15 - Orientation of the bridge in elevation and plan view (Norconsult AS, 2017a)

The bridge is divided into three different parts according to the drawings: Cable-stayed bridge, High bridge, and Low bridge. Start and end of the cable pairs define the cable-stayed bridge, the floating high bridge includes the last 4 cable pairs at the north end and ends after the 12th column. The remaining part of the bridge is defined as the low bridge (axis 13 to axis 48), as illustrated in Figure 16. These definitions of the bridge

sections will be used further. The length of the cable-stayed part is 769 meters and the total length of the floating bridge is 4670 meters.

The bridge tower is 232 m tall and has 44 cable pairs to connect to the bridge girder. There are 22 cable pairs on each side of the tower. All the cables are modelled with pre-tension. The usage of the cable-stayed part is for ship passage and is elevated at the maximum to about 55 m.

The main part of the bridge is a floating bridge, having a total length of 4670 meters, a free span of approximately 100 meters, and a deck width of 27.6 m mounted on 46 pontoons with dimension shown in Chapter 5.6. Each pontoon is supported by a single column. From the start of the high bridge to the end, the elevation decreases from 55m until it reaches a height of 14.4m, where it continues with constant column height. The columns are numbered from south to north – First columns after the cable-stayed part is number 1 and the last column is number 46, which has a location at the north end.

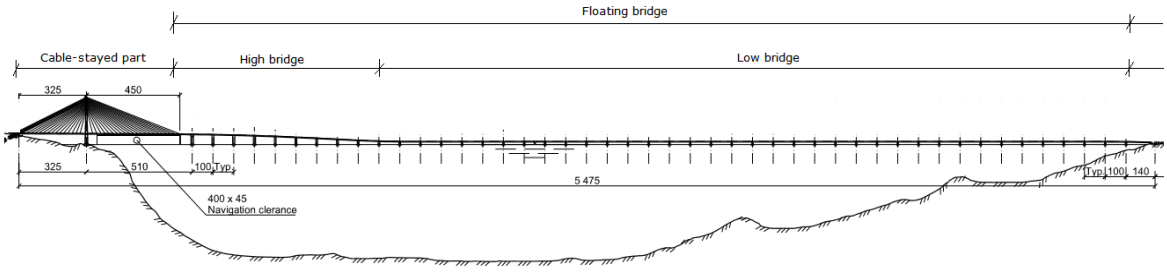

Figure 16 - The end anchored floating bridge concept

5.3. Bridge Girder Design

A beam with two nodes, one on each side, is used for developing the bridge girder in USFOS. Each node of the beam has six degrees of freedom as illustrated in Figure 18. The software uses a general beam element (GENBEAM) to model the bridge girder described above due to its complexity. A typical girder cross-section is shown in Figure 17. In USFOS, a single beam element with constant height and length are applied between each column. The beam gets the parameter values such as area, the moment of inertia, plastic section modulus, and shear area.

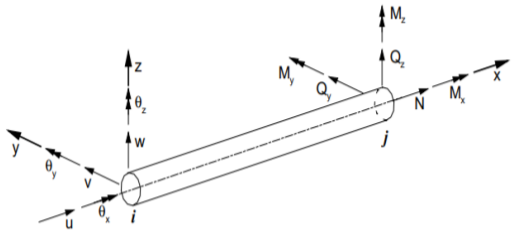

Figure 18 - Direction of forces on beam element (USFOS, 1999b)

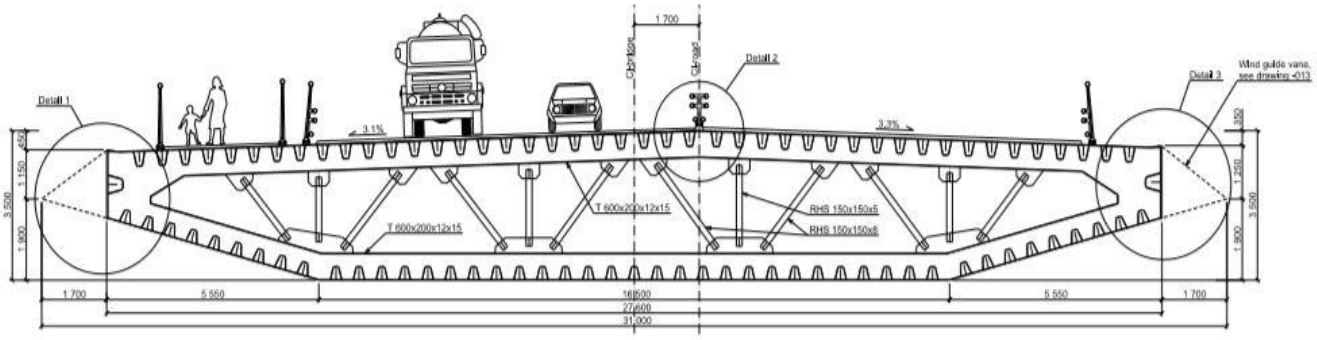

Figure 17 - General cross section of bridge girder (Norconsult AS, 2017a)

The length of the bridge is divided into sections with different bridge girder types. There are three types of cross-section and they are divided as follows: cable-stayed part and the lower-floating bridge has Type 1, the higher-floating bridge has Type 2 and the ends of the bridge have Type 3. In USFOS, the girder type is not changed at the exact location of transition, but at the nodes for simplicity. These simplicities will affect transitional areas. Ida Osvoll (Ida Fagerli Osvoll, 2018) checked this and found that the plastic utilization at the north end was high in static analysis. Due to this, the values for yield strength in type 3 cross-section was increased. Table 12 shows the girder cross-section properties used in USFOS.

Cross Section	Position [m]	Area [m^2]	I_t [m^4]	I_y [m^4]	I_z [m^4]	W_{px} [m^3]	W_{py} [m^3]	W_{pz} [m^3]	Sh_y [m^2]	Sh_z [m^2]
Type 1	110-750 1827.5-5475	1.43	6.10	2.680	115.62	2.30	1.647	7.815	0.624	0.245
Type 2	750-1827.5	1.68	7.32	3.200	132.47	2.76	1.938	8.824	0.624	0.245
Type 3	0-110 5475-5515	1.68	10.86	5.049	181.10	3.61	1.938	8.824	0.624	0.245

Table 12 - Main girder cross-section properties (Ida Fagerli Osvoll, 2018)

The second moment of inertia values is obtained from (Norconsult AS, 2017c). Simplified hand-calculations were computed by (Ida Fagerli Osvoll, 2018) to find the remaining values for the second moment of inertia for use in USFOS. These hand-calculations are based on the simplified cross-section which is a rectangular box with a height of 3.5 m and a width of 24 m. The second moment of inertia in y- and z-direction from Table 12 are calculated according to the standard formulas for hollow rectangular box-sections and gave approximately the same order of magnitude as the model description. (Norconsult AS, 2017c)

The shear area in the z-direction is taken as a cross-sectional area of vertical plates, and y-direction as a cross-sectional area of the horizontal plates where the original plate thickness is used in the calculations. The shear area is assumed to be sufficiently accurate for the bridge girder, due to the slender girder where bending stresses will govern over the shear area.

Due to little information about girder cross-section Type 3 in the bridge drawings (Norconsult AS, 2017a), section moduli and shear areas for Type 2 cross-section are used due to similar cross-section area for Type 2 and Type 3.

The bridge girder has steel quality S420 and is earlier modelled as elastic during the whole analysis. This was done by increasing the yield strength by a factor of 1000 as can be seen in Table 13 with the material properties of the bridge girder used in USFOS. By increasing the yield capacity in the bridge girder, the girder material will not yield during the analysis. Therefore, forces will not get limited by yielding and high load-levels will be reached. If stresses in the girder are of importance, this needs to be checked. When the general beam element is used in USFOS, plasticity model has an uncertain accuracy. However, buckling of the bridge girder cross-section is not predicted and therefore the girder may get overestimated in the analysis. This will be checked during the simulations of seismic motion.

Yield strength [MPa]	Elastic Modulus [MPa]	Poisson ratio [-]
420*1000	210 000	0.3

Table 13 - Bridge girder steel properties (Ida Fagerli Osvoll, 2018)

Increased material density is applied to the model due to the extra weight of the bridge girder in addition to self-weight. Therefore, the weight effect of plates, stiffeners, asphalt, railings, diaphragms, and anchor will be considered. It is only the distributed loads such as asphalt, railings, and diaphragms that will increase the material density. Table 14 shows how the girder gets the equivalent density.

Girder cross section type	1	2	3
Unit mass [kg/m]	17836	19798	27287
Cross-sectional area [m^2]	1.43	1.68	1.68
Equivalent density [kg/m^3]	12472.7	11784.5	16242.3

Table 14 - Equivalent densities for bridge girder (Ida Fagerli Osvoll, 2018)

Thus, the anchor weight, which is not a distributed load, will be applied to the model as point masses. The masses of the anchor-pairs are given in Table 15.

	Cable-stayed bridge	**Floating high bridge**
Total mass [kg]	60 000	8000
Number of anchor couples	33	4
Mass of anchor couple [kg]	1818.18	2000

Table 15 - Cable anchor masses (Ida Fagerli Osvoll, 2018)

5.4. Cable Tower

There is only one bridge tower since we only have the cable-stayed part at one end. Normally a cable-stayed bridge consists of two cable-stayed towers. The tower consists of two feet, one on each side of the bridge girder. The two feet meet at around 168 m over the water level, where the tower top starts. The tower is fixed to the seabed at the lowest points on the tower feet.

The cable-bridge tower is made of concrete. It has different properties with the elevation, it is divided into 4 parts as shown in Figure 19. The tower top is the connection point for all the cables on the bridge and is 59 m long. The legs of the tower have a varying cross-section in the drawings (Norconsult AS, 2017a), but in this thesis, it is simplified to a constant cross-section with the mean value of the leg width and height from the real tower legs. These simplifications should be acceptable since the bridge tower is expected to be rigid with high capacity. The properties assigned to the tower components are given in Table 16.

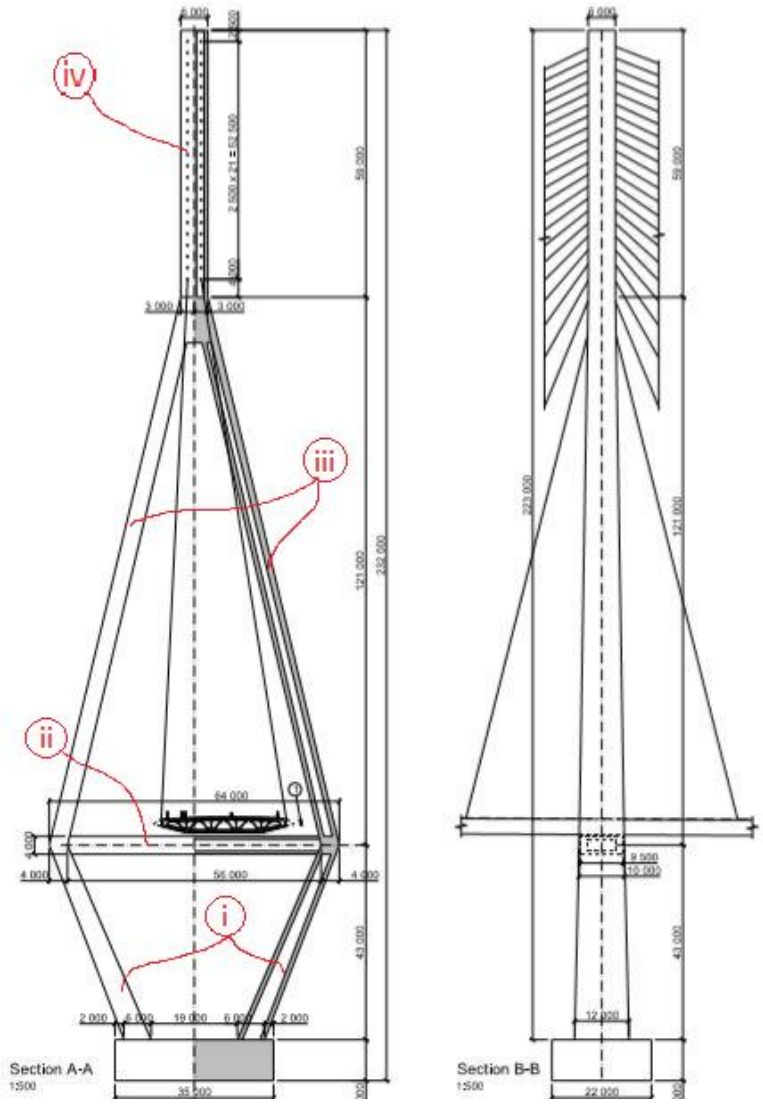

Figure 19 - Cable tower (Norconsult AS, 2017a)

Tower components	i	ii	iii
External height [m]	4.5	4	3
Thickness of side [m]	1.2	1.5	1.2
Thickness of bottom flange [m]	1	0.7	1
Thickness of top flange [m]	1	0.7	1
External height [m]	11	9.5	8.5

Table 16 - Geometry of the bridge tower (Ida Fagerli Osvoll, 2018)

The general beam element is used at the tower top and will then need information about the same properties as for the bridge girder. The properties from the drawings (Norconsult AS, 2017a) are not possible to predict due to unclear geometry. The shear area and section moduli are then given very high values, see Table 17.

Tower component	Area [m^2]	I_t [m^4]	I_y [m^4]	I_z [m^4]	W_{px} [m^3]	W_{py} [m^3]	W_{pz} [m^3]	Sh_y [m^2]	Sh_z [m^2]
iv	21.6	181.2	92.4	88.8	10e+03	10e+03	10e+03	10e+03	10e+03

Table 17 - Properties of the tower top of the bridge (Ida Fagerli Osvoll, 2018)

The density of the bridge tower is set to the regular density of concrete, 2500 kg/m^3, which excludes the steel contribution due to unknown reinforcement. This will underestimate Young's modulus. Yield strength and Poisson ratio are found from the model description of the bridge (Norconsult AS, 2017c) and are given in Table 18. A high value for yield strength is chosen since the stresses in the tower are not expected to reach the yield capacity and the tower is not expected to be subjected to yielding. 55 MPa is the characteristic compressive strength of the concrete, so this has been used multiplied with 1000. If the tower is of interest, it might be necessary to revise the yield strength.

Yield strength [MPa]	Elastic modulus [MPa]	Poisson ratio [-]	Density [kg/m^3]
55*1000	36 000	0.2	2 500

Table 18 - Material properties of bridge tower (Ida Fagerli Osvoll, 2018)

All properties are rough estimates due to the limited description of the tower.

5.5. Stay-cables

The stay-cables are connected parallel between the tower top and the bridge girder to support the bridge deck. Due to nodes at the deck center only, the cables are modelled with eccentricities such that they are connected at a distance off-center. All the cables occur in pairs, which gives one cable on each side of the bridge girder with the same cross-section area. USFOS uses a pipe element with a very small inner diameter, i.e. 0.0002 m when modelling the cables. The external diameter is calculated based on the area, i.e. $D = \sqrt{\frac{4A}{\pi}}$. (Ida Fagerli Osvoll, 2018) All the cables are defined in one group in USFOS.

The cables will function as tensile members and are formed in bunts of strands. Therefore, EA is the most important factor to know when designing the cables. Young's modulus and cross-section used to model the cables are known from the bridge modelling rapport from NRPA. (Norconsult AS, 2017c) Some properties for the cables are given in Table 19. The yield strength is not known from the papers, but a very high value was set since the cables were not expected to yield, i.e. 500*1000 MPa. Thus, this value is used to another analysis of the bridge where the cable response was of less interest. In general, the yield stress for stay-cables is set to 1600-1800 MPa due to large tension forces. All properties of each cable-pair are attached in appendix A.

Density [kg/m^3]	**Internal diameter [m]**	**external diameter [m]**	**Yield Stress [MPa]**	**Poisson's ratio [-]**
7850	0.0002	VAR	500*1000	0.3

Table 19 - Properties of stay-cables

The stay-cables are very slender and will not cope with compression loads. To avoid numerical issues due to this slenderness, a riser element in USFOS is been used to model the cables. Pre-tension of the cables is necessary to avoid compression forces in the stay-cables. The Cables are designed with a pretension of 520.8 MPa, but since USFOS does not have any pretension function, a temperature field is introduced. A reduction of temperature will strive the material strive to contract which causes tensile stresses in the cable. The temperatures used in the different cables can be found in Appendix A. The temperature differs from the west and east side of the tower due to torsion in the bridge girder if the same temperature field is applied.

This pretension in the cables causes large moments in the bridge girder which causes a utilization of 62% in unloaded conditions at the cable-stayed part. This is troublesome since yielding in the girder will occur at low load levels which is unrealistic. The moments in the bridge girder due to pretension are illustrated in Figure 20.

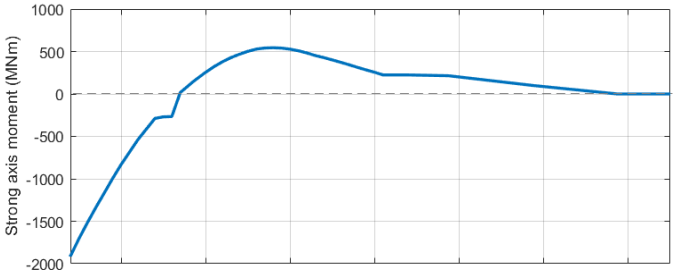

Figure 20 - Strong axis bending moment of bridge girder due to pretension in stay-cables

5.6. Pontoon Design

The pontoons are made of concrete and have varying geometry along the bridge, in alignment with the column geometry, i.e. four different pontoon geometries. The smallest and biggest size of the pontoons is illustrated in Figure 21. The width of the pontoon is varying from 10-16m and the diameter of the outer form varies from 5-8m. The pontoons are modelled with springs and beam elements in this model. This is due to the deficient buoyance element in USFOS. There are 46 pontoons over the bridge length and hydrodynamic properties need to be considered due to connection with waterplane.

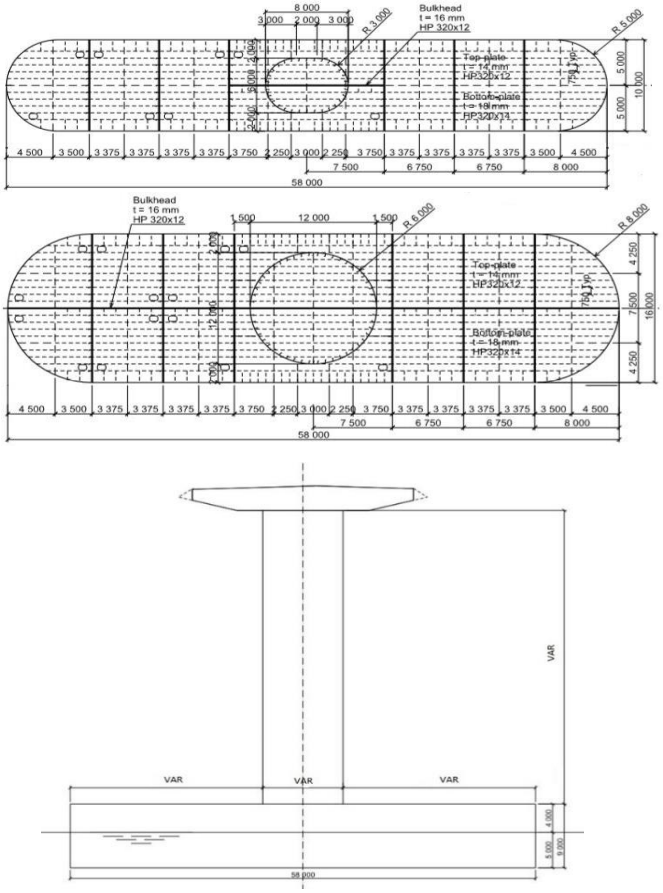

Figure 21 - Geometry of the pontoons (Norconsult AS, 2017a)

For simplicity, the pontoons are modelled with rectangular cross-sections, i.e. with sharp corners. The same values for height and width found from the bridge drawings (Norconsult, 2017a) are used to model the pontoons. To get the right waterplane area, the length of the different pontoons is changed, and an arbitrary thickness of pontoon walls is set to 1 cm. Table 20 gives the dimensions of the pontoons.

Pontoon type	**Symbol**	**1**	**2-4**	**5-10**	**11-46**
Length [m]	L_p	54.57	55.00	55.43	55.86
Width [m]	B_p	16.00	14.00	12.00	14.00
Height [m]	H_p	9.00	9.00	9.00	9.00
Thickness of flange and webs [m]	t	0.01	0.01	0.01	0.01

Table 20 - Geometry of the pontoons (Ida Fagerli Osvoll, 2018)

The yield modulus and yield strength are set to 1000 times larger value than expected since the pontoons are assumed to not be subjected to yielding and large deformations. Table 21 gives the values which are applied to the model as material properties.

Young's modulus [GPa]	Poisson's ratio [-]	Yield strength [MPa]
210*1000	0.3	420*1000

Table 21 - Pontoon material properties (Ida Fagerli Osvoll, 2018)

The pontoons will have extra added mass due to ballast and steel. To find the correct mass for the pontoons, the density of the material is found, see Table 22. It is seen from the table that the density is about 6 times the density of steel, which is sensible.

Pontoon number	1-11	12-42	43-44	45	46
Density [kg/m]	7850*7.00	7850*6.00	7850*6.20	7850*4.40	7850*1.30

Table 22 - Material densities for the pontoons (Ida Fagerli Osvoll, 2018)

Four springs to ground elements are used on each pontoon as illustrated in Figure 22, where 25% of the total waterplane stiffness in heave is used on each spring. The stiffness in roll and pitch will account for yaw motions of the pontoons.

HJHANSEN is used to keep the bridge shape to avoid nodal coordinate change due to the bridge self-weight in the static analysis (the first second), deformations due to gravity are then disregarded.

HYDMASS is used to specify the hydrodynamic added mass in surge, sway, and heave in USFOS. The added mass is distributed over the four nodes for spring connections in the pontoons. Constant values for added mass needs to be used since the added mass cannot be modelled as frequency-dependent.

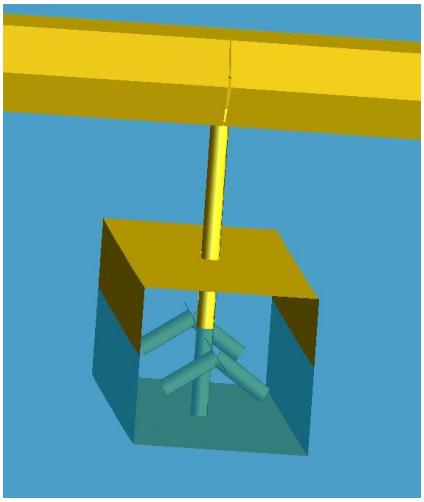

Figure 22 - Spring connection in pontoons

Stiffness in heave, roll, and pitch are determined by using Equation 21-23 and the result for the different pontoon stiffness is given in Table 23.

$$C_{33} = \rho g A_{WP} \tag{21}$$

$$C_{44} = \rho g \nabla G\, M_T = \rho g \frac{L_p B_p^3}{12} \tag{22}$$

$$C_{55} = \rho g \nabla G\, M_L = \rho g \frac{B_p L_p^3}{12} \tag{23}$$

Where A_{WP} is the waterplane area, ∇ is the displaced volume, GM_T and GM_L are the metacentric height in the transverse and longitudinal direction, L_p is the length of the pontoon and B_p is the width. (Ida Fagerli Osvoll, 2018)

Pontoon type	Symbol	1	2-4	5-10	11-46
Total pontoon stiffness in heave [MN/m]	C_{33}	8.78	7.74	6.69	5.62
Total pontoon stiffness in roll [MN/m]	C_{44}	187.3	126.4	80.3	46.8
Total pontoon stiffness in pitch [MN/m]	C_{55}	2179	1951	1712	1460

Table 23 - Resulting waterplane stiffness for the pontoons (Ida Fagerli Osvoll, 2018)

Oscillation Period	Motion	1 [kg]	2-4 [kg]	5-10 [kg]	11-46 [kg]
t > 40s	Surge	$5.6 \cdot 10^5$	$4.7 \cdot 10^5$	$3.7 \cdot 10^5$	$2.9 \cdot 10^5$
	Sway	$3.1 \cdot 10^6$	$3.1 \cdot 10^6$	$3.1 \cdot 10^6$	$3.0 \cdot 10^6$
	Heave	$10.6 \cdot 10^6$	$8.6 \cdot 10^6$	$6.7 \cdot 10^6$	$4.9 \cdot 10^6$
5s < t < 10s	Surge	$7.1 \cdot 10^5$	$5.8 \cdot 10^5$	$4.6 \cdot 10^5$	$3.5 \cdot 10^5$
	Sway	$4.6 \cdot 10^6$	$4.6 \cdot 10^6$	$4.6 \cdot 10^6$	$4.6 \cdot 10^6$
	Heave	$5.0 \cdot 10^6$	$4.0 \cdot 10^6$	$3.1 \cdot 10^6$	$2.2 \cdot 10^6$

Table 24 - Added mass in surge, sway, and heave (Ida Fagerli Osvoll, 2018)

The drag forces in the pontoons need to be included and are given in Equation 24:

$$dF_D = \frac{1}{2}\rho C_D D|u|u \tag{24}$$

where dF_D is the drag force, C_D is the drag coefficient, ρ is the water density, D is the characteristic diameter, and u is the water particle velocity. (O. M. Faltinsen, 1990) The values for drag coefficient and characteristic diameter are given in Table 25.

Pontoon Number	1	2-4	5-10	11-46
Characteristic diameter in surge [m]	16	14	12	10
Drag coefficient in surge [-]	0.8	0.8	0.8	0.8
Characteristic diameter in sway [m]	58	58	58	58
Drag coefficient in sway [-]	1.0	1.0	1.0	1.0

Table 25 - Drag coefficient and diameters for the pontoons (Ida Fagerli Osvoll, 2018)

The drag forces are included in the model by using vertical pipe elements inside the pontoon center since USFOS only account for drag forces in these elements. An illustration of the pipe element inside the pontoons can be seen in Figure 22 where the pipe element is extending from the top of the pontoon to the bottom. The pipe element is modelled with high stiffness and low density.

5.7. Column Design

The column is modelled with a general beam element instead of pipe-element in USFOS to account for the stiffeners. Due to this, the same properties parameters need to be known as for the girder. The columns are connected on the bottom of the bridge girders to the top of the pontoons. As mentioned earlier, the bridge girder only has center-nodes. Eccentricities need to be included in the top of the column to connect with the bottom of the bridge girder. Instabilities due to large eccentricities are not a problem.

There are four different cross-sections for the columns over the entire bridge length which can be seen in Table 26. The columns with geometry ID 30 and 31 have a circular cylinder with stiffeners and transverse frames. The columns with ID 32 and 33 are modelled with an elongated cross-section in the transverse direction of bridge girder and are circular with equivalent diameters. All cross-sections are constant over the column height where the transverse frames are included as additional weight. Simplifications with constant geometry at the ends are considered acceptable due to expected low utilization.

Column number	**1**	**2-4**	**5-10**	**11-46**
Geometry ID	30	31	32	33
Area [m^2]	2.101	1.158	0.977	0.872
External diameter [m]	12	10	9.185	0.872
I_t [m^4]	74.94	28.738	20.46	11.06
I_y [m^4]	37.47	14.369	10.23	5.53
I_z [m^4]	37.47	14.369	10.23	5.53
W_{px} [m^3]	15.984	7.348	5.696	3.955
W_{py}[m^3]	7.992	3.674	2.847	1.978
W_{pz} [m^3]	7.992	3.674	2.947	1.978
Sh_y [m^2]	0.736	0.406	0.342	0.306
Sh_z [m^2]	0.736	0.406	0.342	0.306
E-modul [GPa]	210	210	210	210
Poisson's ratio [-]	0.3	0.3	0.3	0.3
Yield strength [MPa]	420*1000	420*1000	420*1000	420*1000
Equivalent density [kg/m^3]	8242.3	8142.5	8143.3	8256.9
Mass per unit length [kg/m]	17 317	9 429	7 956	7 200

Table 26 - Column properties (Ida Fagerli Osvoll, 2018)

Some parameters are not known from the model description. Wall thickness and dimension of stiffeners were found based on their area and diameters. Plastic section moduli about y- and z-axis are obtained using Equation 25 and torsional section moduli (W_{px}) are twice of this size. Half the cross-sectional area is used as the shear area.

$$W_p = 4r^2t \tag{25}$$

The columns, which the bridge girder is resting on, will get additional weight from the girder. The weight is added as point load to the column, see Table 27.

Column number	**1**	**2-4**	**5-10**	**11-45**	**46**
Additional steel mass [kg]	101 000	71 400	59 000	55 000	71 400

Table 27 - Addition steel mass to column top(Ida Fagerli Osvoll, 2018)

5.8. Modelling of the Earthquake Parameters

The seismic ground motion is attached to the supports (fixed boundary conditions) in the USFOS bridge model. These locations will be affected if an earthquake occurs and the motions will propagate through the bridge. The soil condition or seismic ground motions is applied to 3 different locations in USFOS. The first node connects the north side to the ground, the south side has 7 nodes that are connected to the ground, and two nodes on the bridge-tower which are connected to the seabed. The excitations will be applied to these nodes since the floating part of the bridge is not vulnerable for seismic loadings due to no connections with the ground. By performing this in USFOS, concentrated (nodal) loads are applied as time histories. Table 28-30 gives the different node ID with the following coordinates for which the time histories are applied.

Node ID	**X-direction** [m]	**Y-direction** [m]	**Z-direction** [m]
10 000	0	0	54.560
10 004	8.5174	-5.2397	54.510
10 008	17.045	-10.462	54.460
10 012	25.584	-15.668	54.410
10 016	34.132	-20.856	54.361
10 020	42.691	-26.028	54.311
10 024	51.261	-31.182	54.261

Table 28 – Nodal locations at the south end

Node ID	**X-direction** [m]	**Y-direction** [m]	**Z-direction** [m]
20 000	324.99	-198.06	4.7912
20 050	336.46	-175.85	4.7912

Table 29 – Nodal locations at bridge tower

Node ID	**X-direction** [m]	**Y-direction** [m]	**Z-direction** [m]
14 900	5248.2	0	10.641

Table 30 – Nodal locations at the north end

The ground motions applied to the nodes are artificial recordings that are made by Dr. Kaiming Bi. Different simulation cases on the bridge will be tested and the response will be analyzed. Since there is a big distance between the fixed boundaries, assuming the same ground motion on every node will be wrong, as discussed in Chapter 4.3.

There are three different load cases for where the ground motion is applied to the bridge as TIMEHIST described by discrete nodal points. LOADHIST is used to define history by connecting a load vector to the time history. This function can scale the actual time history. As mentioned in Chapter 4.3, the vertical ground motion (z) is scaled by a factor of 0.5 since the vertical motion is smaller than for the horizontal planes (x- and y-directions).

A time-step of 0.05 seconds and an earthquake duration of 20 seconds are used during this dynamic analysis. The total duration of the analysis is 50 s which gives 30 s after the earthquake is finished, to see the response.

5.9. Eigenvalue Analysis

It is important to do an eigenvalue analysis of the bridge to get an indication of the response to different types of loading. Since the initial bridge model has not been changed, a new eigenvalue analysis is not necessary. The eigenvalue analysis done by Ida will account for this thesis as well. The mode shapes and results from the eigenvalue analysis can be found in (Ida Fagerli Osvoll, 2018).

5.10. Structural Damping

Rayleigh damping is the structural damping used in USFOS to analyze the bridge. Structural damping is necessary to include since the analysis may be unstable if it is neglected. The damping ratio is defined by two constants, α and β, discussed in Chapter 3.4. The best solution for a stable structure was found and is given in Figure 23 with the constants α=0.006 and β=00039. This gives a damping ratio of about 6% for the fundamental eigenperiod, which is on the non-conservative side where the energies might be damped out too early. For periods lower than 2 seconds, the damping ratio increases violently which causes the energies to be damped out immediately. The first 50 eigenmodes have periods higher than 2 seconds. (Ida Fagerli Osvoll, 2018)

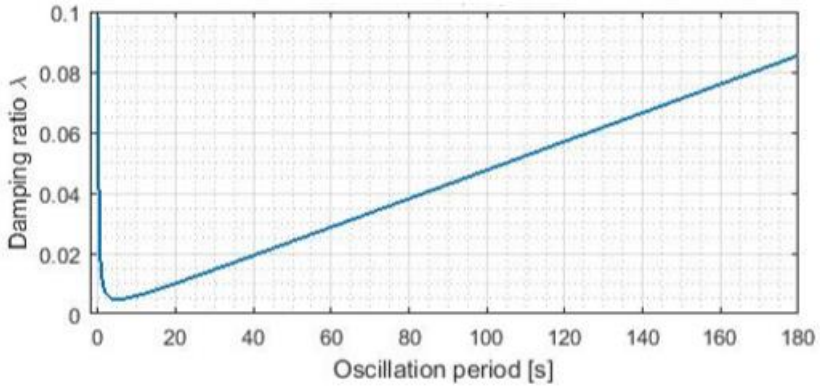

Figure 23 - Applied damping to the model (Ida Fagerli Osvoll, 2018)

Chapter 6

6. Time Domain Simulation of the Bridge Response

The analysis is studied under 3-dimensional earthquake excitations. For this purpose, USFOS has been used to model and study the response. The selected input records used in this thesis are made by Dr. Kaiming Bi, which covers a wide range of frequencies. How the ground motions are generated can be found in chapter 4.3, where Figure 9-11 shows the seismic input used to simulate the bridge. USFOS has no way of treating the spatial variability directly, so this effect has been considered under the generation of ground motions.

6.1. Permitted Motion

Bridges shall be designed to ensure comfort and safety for the users of the bridge. The permitted response in the floating bridge to seismic excitations is not specified, but motion limitations for a 1-year storm scenario are established and represented in (Statens Vegvesen, 2017c). The motion limitations for vertical displacement and acceleration are given in Table 31.

NRPA's handbook for bridges, N400, also provides additional requirements. (Statens Vegvesen, 2009) It is stated that the maximum displacement of the bridge deck should be limited to L/350 for traffic load alone, where L is the length of the bridge span. Cl. 5.1.3.1, states that the maximum allowable acceleration for bridges with pedestrian traffic is 0.6 m/s^2 and 1 m/s^2 for bridges without. These requirements yields for wind- or traffic loads, or a combination of them. (Statens Vegvesen, 2009)

Motion	Load	Maximum response
Vertical deformation from traffic loads	$0.7 \cdot$ traffic load	$u_z \leq 1.5\ m$
Vertical acceleration (Design basis, rev C)	1-year storm	$\ddot{u}_z \leq 0.5\ \frac{m}{s^2}$
Vertical acceleration (N400)	Wind and traffic load	$\ddot{u}_z \leq 0.6\ \frac{m}{s^2}$ (pedestrian) $\ddot{u}_z \leq 1\ \frac{m}{s^2}$ (without pedestrian)

Table 31 - Maximum allowable response according to (Statens Vegvesen, 2017c) and (Statens Vegvesen, 2009)

Seif and Inoue also state that the maximum vertical acceleration of the bridge shall not exceed 0.6 m/s^2 to ensure safe traffic for the users. (Mohammed Saeed Seif & Inoue, Yoshiyuki, 1998) To ensure safe traffic on the bridge, the most stringent requirement for acceleration will be used in this analysis, i.e. 0.5 m/s^2.

6.2. Response of Stay-cables

The bridge girder and stay-cables must be studied closer because the vertical vibrations of the bridge deck will give forces in the bridge which may result in yielding of stay-cables. As mentioned in Chapter 5; since the yield strength of the stay-cables are unknown and the cables are not expected to yield, the value of yield strength is unrealistically high to avoid plastic yielding during the analysis, i.e. 500*1000 MPa. The capacity of the bridge is therefore very high and high values for stresses in the cables can occur without notice.

The weight of the bridge girder works downwards which causes tension in the cables as it is being stretched. The tension members will further transfer the load to the tower top as compression. When the bridge is then subjected to earthquake loading, the vertical response of the girder gives extra forces in the cable members as illustrated in Figure 24. This figure demonstrates an extreme scenario where the slacking of the cables occurs in the rising side of the deck and large tension forces occur where the deck lowers. (Wai-Fah Chen & Duan, Lian, 2014)(p.226) The forces and stresses in the bridge tower will not be analyzed in this thesis.

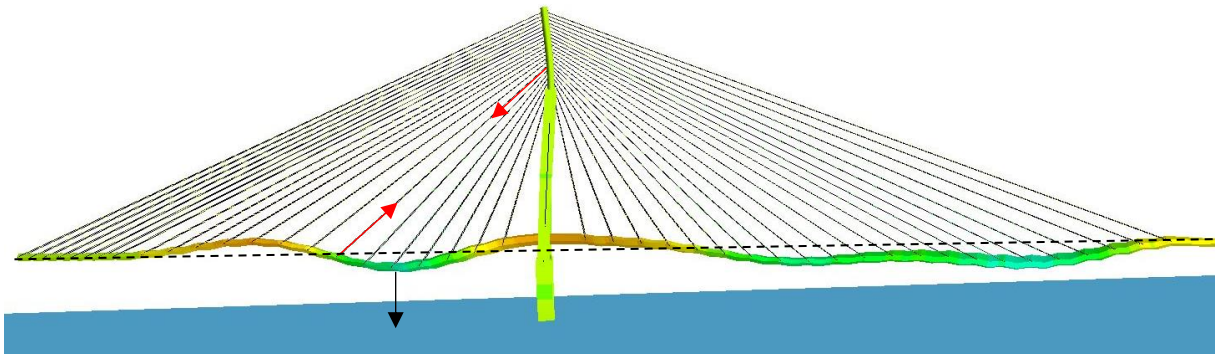

Figure 24 - Loads working on stay-cables due to bridge girder deformations

The largest axial cable force induced by seismic excitations occur in the longest stay-cable on the south end and will be investigated further. One of the shortest cables will also be investigated, i.e. the short cable on the east side (north span). Figure 25 shows the location of the maximum axial forces in the stay-cables. As the figure shows, the south (left) side has the highest values for tension force in the longest cables. These cables have the seismic ground motion applied on one end and are attached to the tower top on the other. The maximum axial stresses and forces for the two cables are given in Table 32, where the absolute maximum force is 6.5 MN. With a cross-section area of 0.011656m^2, the axial stress becomes 558MPa for the longest cable.

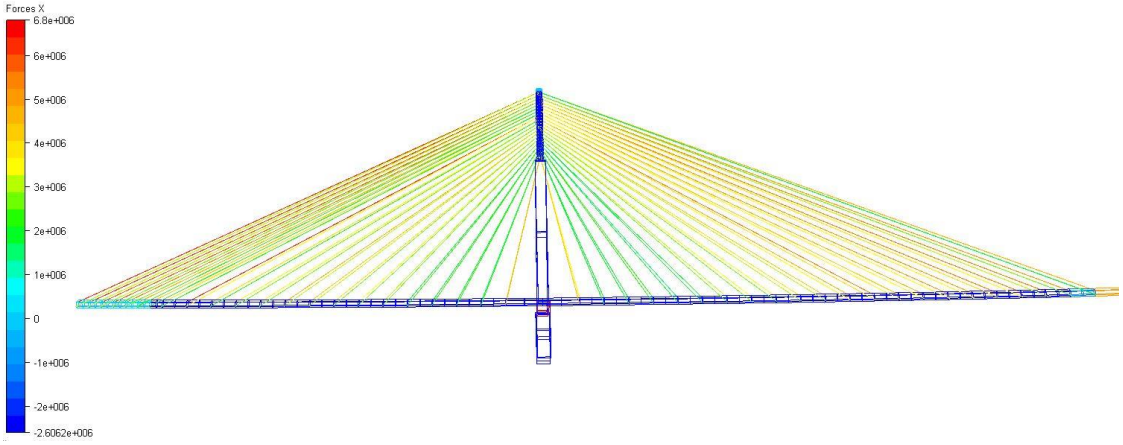

Figure 25 - Location of maximum axial force in the stay-cables

Response Component	Max and Min force [MN]	Axial Stress [MPa]	Location
Longest cable	6.503 6.102	558.0 523.5	Longest, south side of the bridge tower
Shortest cable	4.975 4.147	707.2 598.3	Shortest, north side of the bridge tower

Table 32 – Maximum force and stress for the longest and shortest stay cable

It is important to know that the values for cable forces and stresses are increase and decrease of the values as the bridge deck deforms, i.e. the cables do not have any compression force. The highest stress values occur mainly in the mid-section and closest to the bridge tower, and the smallest values are located on the longest cables.

The cross-section of the stay-cables varies, and the values are given in Appendix A, Table 41. The cable with the highest tension force will then necessarily not give the highest cable stress. The overall largest axial stress in the cables is 750 MPa which is much higher than the estimated value for yield strength in USFOS, i.e. 500 MPa. The maximum stress occurs in the middle of the north side of the bridge tower, as illustrated in Figure 26. If the cables are modelled with a yield capacity of 500 MPa, the utilization would be up to 1.4, which is too high. Plastic yielding would then occur. The value of yield strength should be set to about 1600-1800 MPa for stay-cables, as mentioned in Chapter 5. Since the input values for yield strength is very high, the bridge will have the same response (elastic) as if the value were changed to the monitored strength in USFOS. The stresses in the cables should then be checked against this modified yield strength to ensure that the capacity is not exceeded. For yield strengths of 1800 MPa and 1600 MPa, the maximum utilization will be 39.3% and 44.2%, respectively. Wind, wave, and current loadings are not included in this thesis and will contribute to an increase in the bridge motion and response.

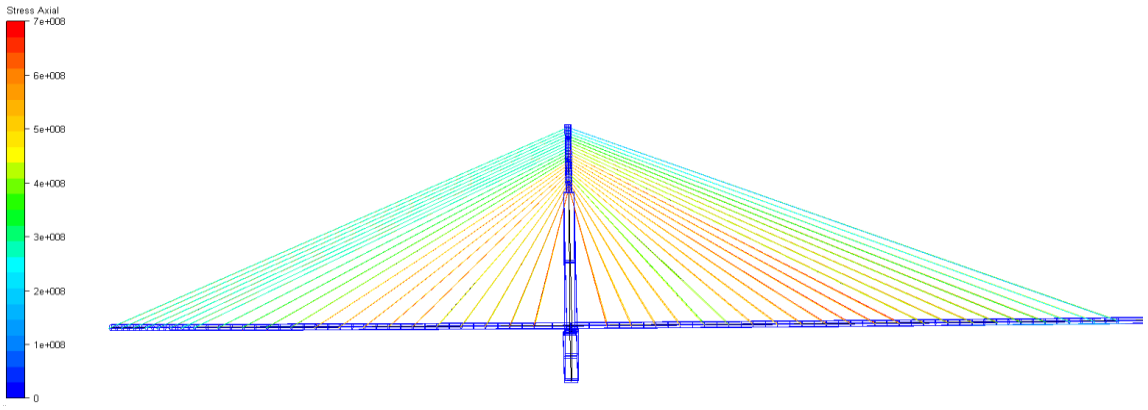

Figure 26 - Location of maximum stress along the cables

The axial force time series of the cables are shown in Figure 27 (a) and (b), for the longest and shortest cable, respectively. In the first second of the simulation, the axial force goes from zero to a relatively large value. This is due to the added pre-tension in the cables which can be found in Appendix A, modelled as temperatures. To see the effect of seismic load better, the pretension force is removed from the plot, illustrated in Figure 28 (a) and (b). The variation of axial force as the seismic load is applied is about 0.4 MN for the longest cable and about 0.83 MN for the shortest cable. As seen in Figure 28 (a), seismic case 1 gives the biggest variation of force in the longest cable. The axial response in the shortest cable is somewhat similar for cases 1 and 3, but

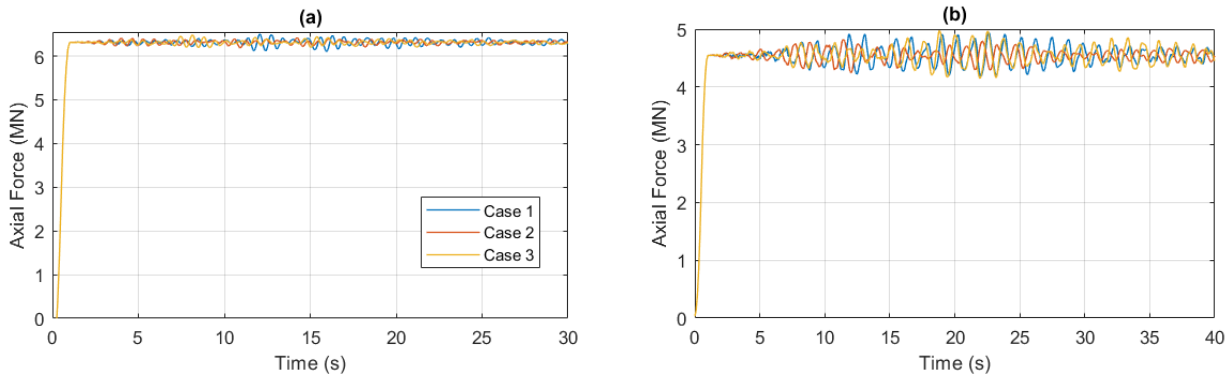

Figure 27 - Maximum axial force in the girder for (a) longest cable and (b) shortest cable

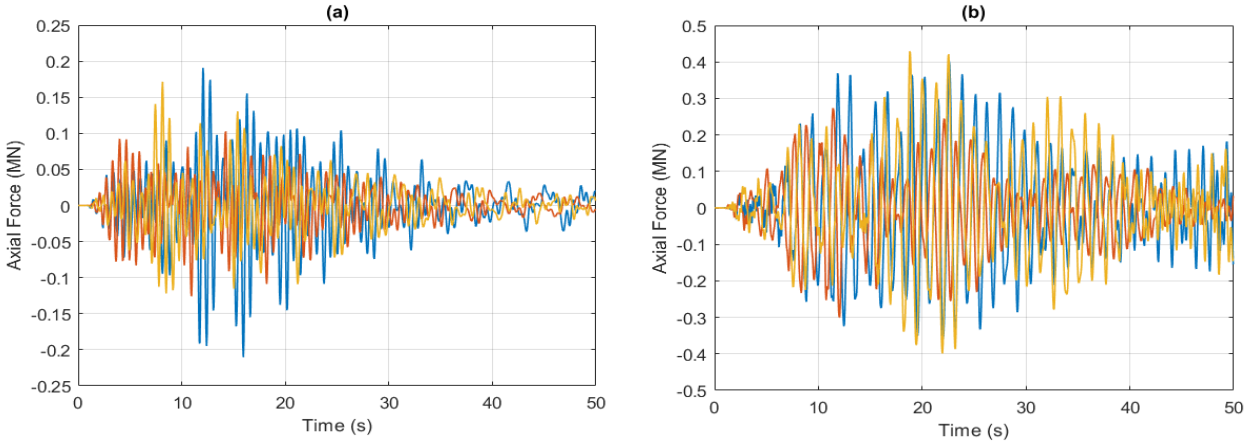

Figure 28 - Maximum axial force in the girder for (a) longest cable and (b) shortest cable only considering seismic load

case 2 gives a significantly lower response. Due to these random responses, the use of three load cases is necessary to find high and random peak values.

The longest cable stabilizes faster than the shortest cable. This is due to the vibration of the bridge deck when the seismic load is applied. The longest cable is connected to the north end which has small vibrations due to the fixed boundaries and will therefore stabilize faster after the earthquake is finished, i.e. drops regularly after 20 seconds. The shortest cable is located at the cable-stayed span where the vibrations of the bridge deck give longer response time for the cables.

Cable Number (East)	**1**	**9**	**16**	**22**	**23**	**29**	**36**	**44**
Case 1 [MN]	3.27	3.73	2.78	4.86	4.95	2.71	3.48	2.18
Case 2 [MN]	3.20	3.68	2.74	4.82	4.82	2.66	3.39	2.13
Case 3 [MN]	3.25	3.71	2.79	4.83	4.98	2.71	3.47	2.18
Only pre-stress [MN]	3.09	3.59	2.63	4.47	4.55	2.57	3.34	2.03
Seismic case 1 [MN]	0.18	0.14	0.15	0.39	0.40	0.14	0.15	0.15
Seismic case 2 [MN]	0.11	0.09	0.11	0.35	0.27	0.09	0.05	0.10
Seismic case 3 [MN]	0.16	0.12	0.16	0.36	0.43	0.14	0.13	0.15

Table 33 - Axial forces in the eastern stay-cables (seismic, pre-stress and total forces)

Cable Number (West)	**1**	**9**	**16**	**22**	**23**	**29**	**36**	**44**
Case 1 [MN]	6.50	6.21	3.41	3.41	4.07	3.16	4.40	4.65
Case 2 [MN]	6.42	6.16	3.37	3.36	3.96	3.12	4.30	4.59
Case 3 [MN]	6.48	6.20	3.42	3.38	4.10	3.17	4.36	4.63
Only pre-stress [MN]	6.31	6.07	3.27	3.02	3.69	3.03	4.25	4.50
Seismic, case 1 [MN]	0.19	0.14	0.15	0.39	0.38	0.13	0.15	0.15
Seismic, case 2 [MN]	0.10	0.09	0.11	0.34	0.27	0.09	0.06	0.09
Seismic, case 3 [MN]	0.17	0.12	0.16	0.36	0.42	0.14	0.11	0.13

Table 34 - Axial forces in the western stay-cables (seismic, pre-stress and total forces)

Since the pre-stresses in the cables contribute much to the forces and stresses in the stay cables, it is useful to remove the pre-stress to see how the seismic load alone affects the cable response along the length. Table 33 and Table 34 give the values for maximum cable force with and without pre-stress for all cases in the east and west cables. To see the variation of seismic load along the length, the maximum axial force for a set of cables are plotted, illustrated in Figure 29. As the results show, the seismic load has a small contribution to the total cable response, i.e. 2.9% for the longest cable and 8.6% for the shortest cable, respectively. This indicates that the seismic load contributes 3 times more to forces in the shortest cables than for the longest cables, which is the opposite of the forces due to pre-stresses. This small contribution from the seismic load is considered as acceptable when the stability of the stay-cables is the topic of interest.

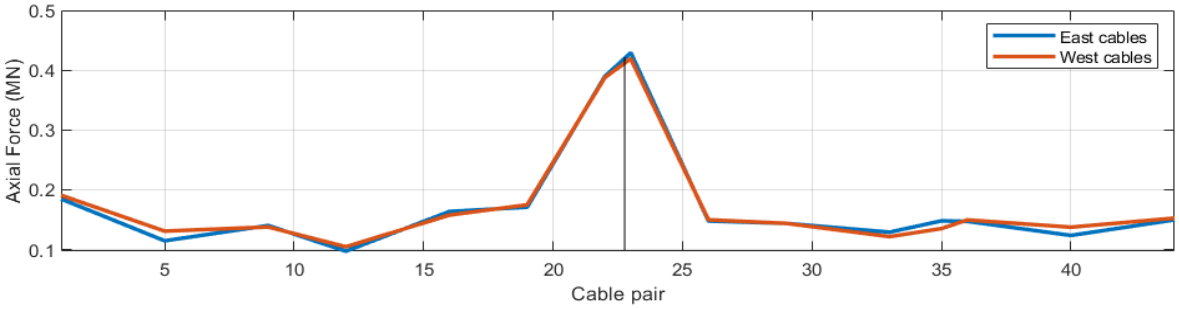

Figure 29 - Axial force due to seismic load along the cable-pairs for 0.08g

Stresses in the cables due to seismic load can be checked with the given forces and cross-sections for each cable. Cable-pair 22 and 23 have cross-sections 7004 mm^2 and 6996 mm^2, which yields to stresses of 55.7 MPa and 61.4 MPa, respectively. By setting the capacity of the cables to 1600 MPa, the cables give utilizations up to 3.84% which is a low utilization due to seismic effect only.

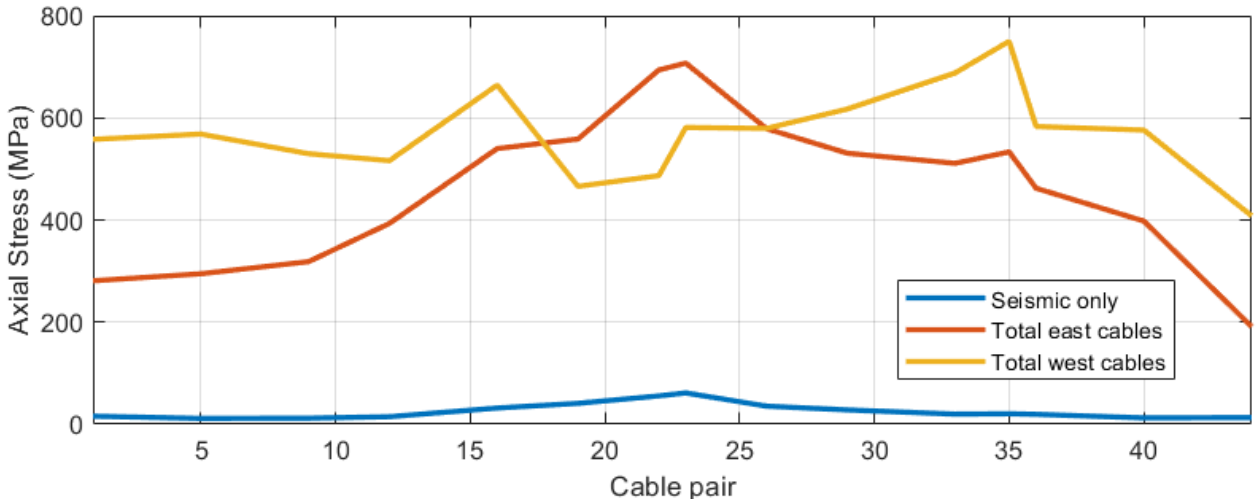

Figure 30 - Stresses along the cable-pairs for 0.08g

Figure 30 shows that the contribution from pre-stress to the total load is much higher than it is for seismic load alone. The east and west cables have a different distribution of maximum stress along the length, where the overall maximum stress is located at cable pair 35 with a magnitude of 750 MPa. This is due to the applied pre-stress in the stay-cables and gives utilization of 46.9% of the capacity. The maximum seismic load will therefore only contribute with 8.2% of the maximum total cable stress. This indicates that seismic loadings have a small contribution to forces and stresses in the cables during the numerical analysis of the bridge when subjected to earthquakes of PGA=0.08g.

6.3. Forces Along the Bridge Girder

In this part, global forces in the bridge girder from the numerical analysis are presented, i.e. axial forces, strong axis bending moment and weak axis bending moment. Torsional bending moments are not included in this thesis. To best represent the global force response in the bridge, peak values along the bridge length are plotted.

The bridge girder needs to be checked against the capacity, which cannot be exceeded. According to (Norconsult AS, 2017b), the bending moment capacity of the bridge girder strong axis is 3069 MNm and the girder capacity about the weak axis is 574 MNm. It is also stated that the buckling capacity for axial loads in the girder is 418 MN.

6.3.1. Axial Forces

The axial forces in the girder are due to the pre-stressing of the stay-cables and seismic loading. Peak axial force in the bridge due to pre-stress and seismic loading, static maximum due to pre-stressing only, and maximum force due to seismic effect alone is presented in this subchapter. The axial force in the floating and cable-stayed part differs a lot from each other, which can be seen in Figure 31 (b). This is due to the prestressing in the stay-cables, which causes compression forces in the bridge girder. The axial load increases from zero to about 120 MN within the floating high bridge part. Regarding the floating part of the bridge, the axial force is significantly lower than in the cable-stayed part, i.e. varies around 8-13 MN for the case with pre-stress and seismic loading. The utilization of the axial buckling capacity to self-weight is 28.7%.

By removing the static pre-stress load from Figure 31 (b), the effect of mean seismic load alone can be studied easier. Figure 31 (c) shows that the axial load in the cable-stayed part is in compression and for the floating part the girder is in tension. The maximum load for the girder is 7.42 MN and is located at the end of the high bridge where the low bridge starts, i.e. after 1600 m. The other peak value is located at 820 m which is the end of the cable-stayed bridge. Floating low bridge has small changes in axial load since the seismic load is only applied to the boundary conditions, i.e. tower legs and abutments.

Comparison with the capacity for axial load in the girder, the max utilization along the bridge length becomes up to 1.7% for seismic load alone, which indicates a small contribution from the seismic load. Since the utilization for the total load is 28.7%, the utilization for seismic load alone compared to the utilization for pre-stress alone, indicates that the seismic load has almost no contribution to the axial load in the girder.

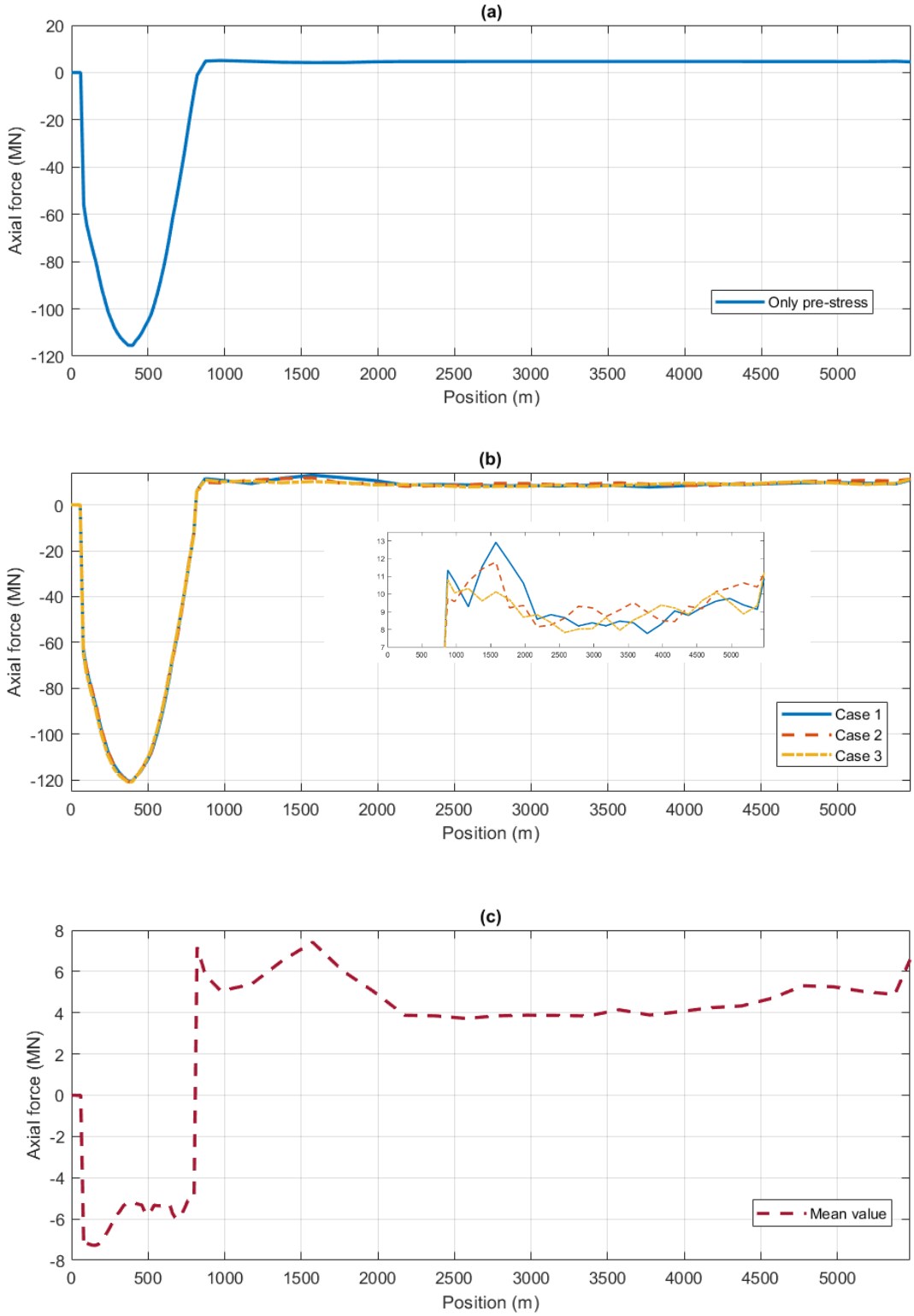

Figure 31 - Axial force along the bridge for (a) Only pre-stress load (b) Seismic and pre-stress for all cases (c) Mean seismic load

6.3.2. Strong Axis Bending Moment

Figure 20 in Chapter 5 shows the bending moment in the unloaded condition, where only pre-stressing of the stay-cables are included. By removing the moments due to pre-stressing, it is easier to study the response to the seismic effect only. Figure 32 (b) depicts the strong axis bending moment along the bridge length by only considering the seismic effect. Figure 32 (a) shows the total moment from the analysis, including pre-stress. It can be seen that the maximum response occurs at the start of the cable-stayed bridge which is due to the pre-stressing of the cables. The zero moments at the beginning of the plot is because of the fixed boundaries at the abutment.

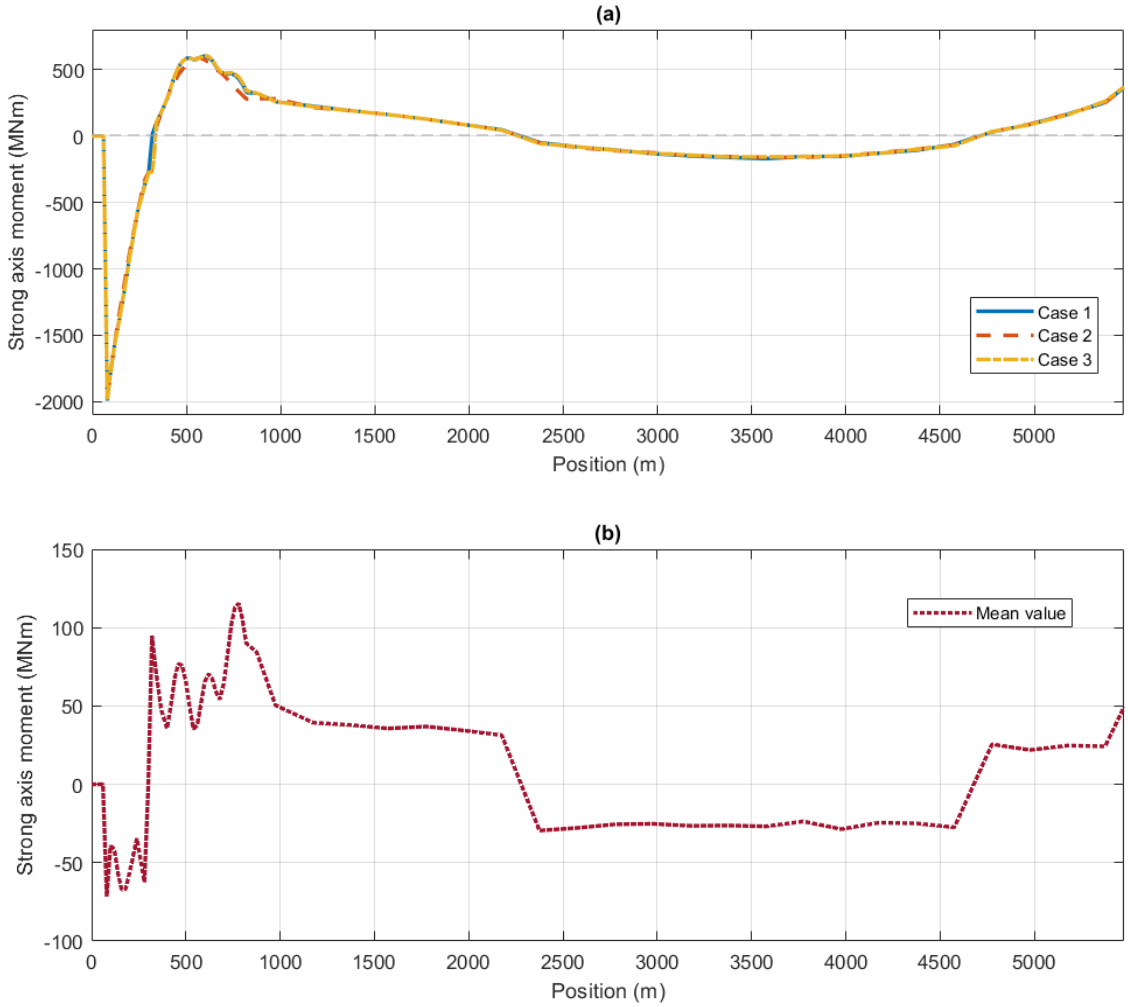

Figure 32 - Strong axis bending moment for (a) Total seismic and pre-stress load (b) Mean seismic load only

The maximum strong axis moment due to seismic effect only is 115.5 MN which gives utilization of 3.8% when the capacity of 3069 MN is used. Considering both pre-stressing and seismic load, the utilization becomes 65% which might be too high since other environmental loads are not considered in this analysis and will act on the bridge as well.

6.3.3. Weak Axis Bending Moment

Weak axis moment due to pre-stressing is higher in the floating bridge compared to the capacity. There is a small contribution of pre-stress in the start of the cable-stayed part but gives a rapid response in the north cable-stayed end. By comparing the figures, the seismic load does not contribute much to the weak axis bending moment relative to the effect of pre-stressing in the floating bridge. However, in the cable-stayed bridge, the seismic load contributes much to the total load, i.e. about 36%. The maximum dynamic weak axis moment is found to be 566.5 MNm for the north abutment and 356.5 MNm for the end of the cable-stayed part. Maximum moments for static and dynamic seismic load only have not the same locations.

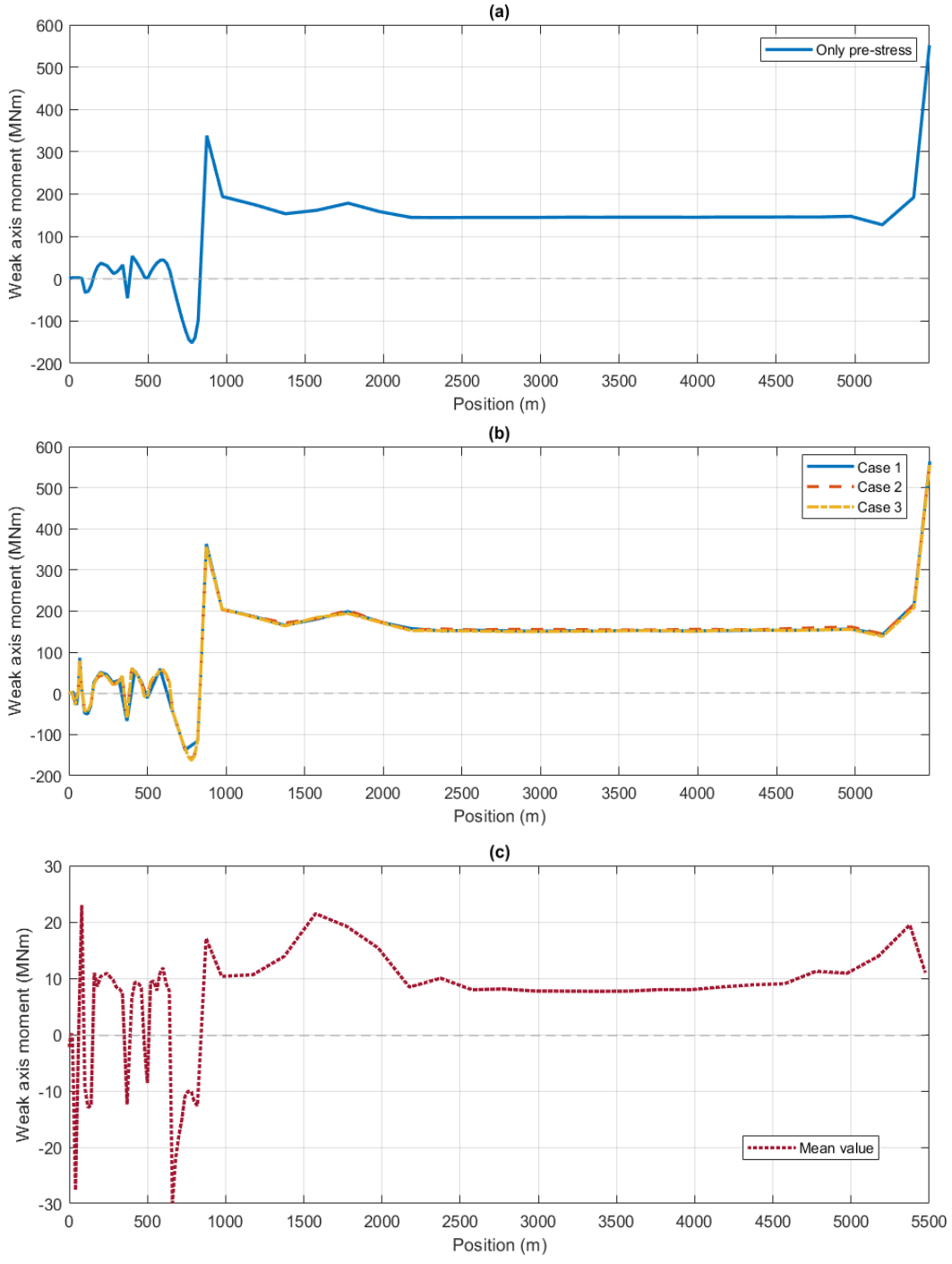

Figure 33 - Weak axis moment for (a) only pre-stress (b) seismic and pre-stress (c) mean seismic load

The bending moment about the weak axis is high compared to the bridge capacity of 574 MNm. In the north abutment, the moment in the girder becomes 566.5 MN. Thus, the utilization becomes 98.7%, which is too high due to only self-weight and seismic load. However, the dynamic seismic response gives only a utilization of 5.2%, which indicates that the seismic load has little effect on the floating bridge response, i.e. 29.9 MNm. This can also be found in Figure 33 (c).

6.4. Motion Along the Bridge Girder

To ensure safe traffic, bridge motions are important to investigate. Accelerations and displacements of the bridge girder are going to be studied in this subchapter. Peak displacements are necessary to find along the bridge to ensure structural safety.

6.4.1. Accelerations

The nodal accelerations will be compared from different locations: cable-stayed part (Node 1), Mid-bridge (Node 2), and Low bridge (Node 3) illustrated in Figure 34. This is done to capture the difference in acceleration time histories for different locations. To confirm safe traffic on the bridge, a maximum vertical acceleration of 0.5 m/s^2 must not be exceeded, as discussed in Chapter 6.1. This is one of the most important considerations in the design of floating bridges. (Mohammed Saeed Seif & Inoue, Yoshiyuki, 1998)

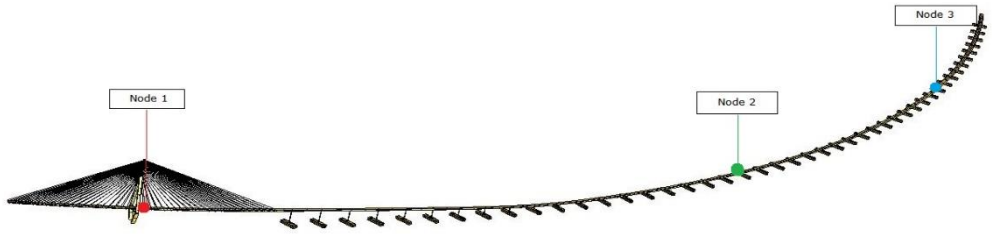

Figure 34 - Locations on the bridge for check of acceleration

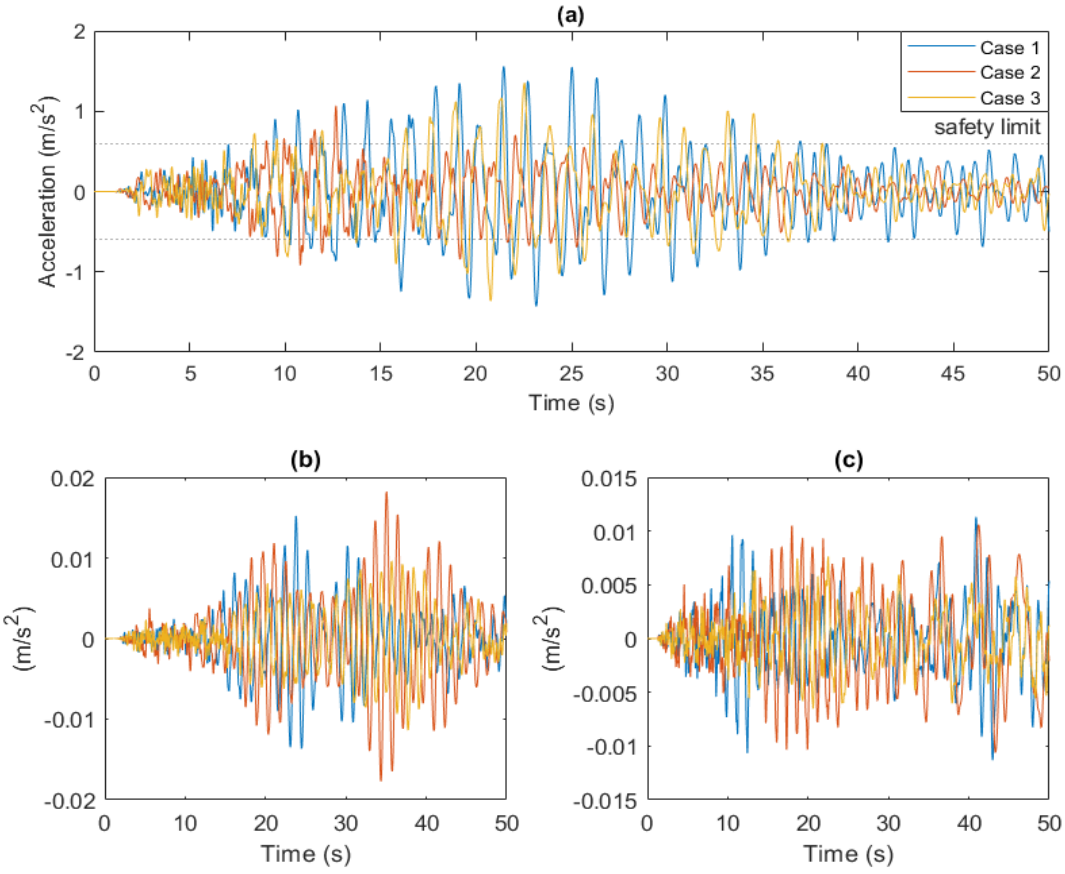

Figure 35 - Nodal accelerations for (a) node 1, (b) node 2 and (c) node 3

The maximum vertical acceleration for mid-bridge and north end (continuous part) is approximately 0.02 m/s^2, which is far below the maximum value of 0.5 m/s^2. However, in the cable-stayed part, the bridge response exceeds the maximum value where the acceleration reaches a value of 1.6 m/s^2 (~0.16g). This is much larger than the values from the continuous floating part of the bridge. This result may be because the cable-stayed span is much larger and induces more motion due to the longer spans, i.e. almost 4 times longer. The two dotted lines in Figure 35 (a) indicates the safety limits of acceleration. It can be seen that the acceleration is too high between 8 and 36 seconds. Before and after, the accelerations are below the limit.

To better see the global response of the bridge, peak accelerations along the bridge length are plotted in Figure 36 (a)-(b). That the accelerations in the cable-stayed part differ a lot from the floating part is very clear in the figures. The floating low bridge has almost neglectable acceleration due to seismic excitation. After about 800 m, the floating high bridge has an acceleration of 0.26 m/s^2 which is 52% of the requirement for acceleration. This might be too high since vibrations due to wind and wave loads are not considered.

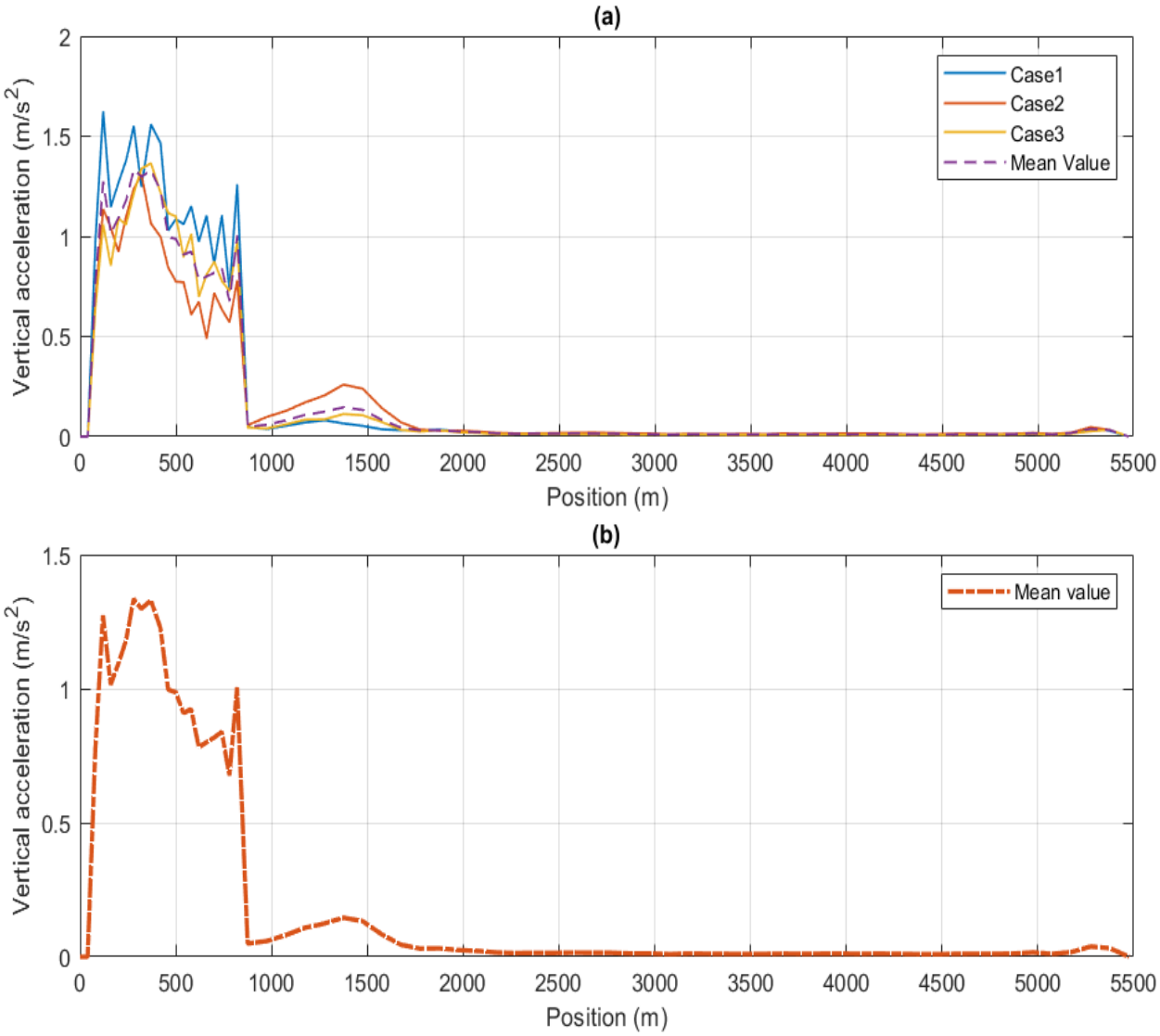

Figure 36 - Peak acceleration along the bridge length (a) all load cases (b) mean value

6.4.2. Displacements

Figure 37 (a)-(c) shows the displacement in the horizontal, transverse, and vertical direction. The accelerations at the cable-stayed part are high from the previous subchapter, but the deformations are small in size.

The floating part of the bridge has an elastic response in both horizontal and vertical directions. The vertical direction has small or very little response in the floating part compared with the cable-stayed response. This can also be compared with the vertical acceleration in Figure 36. The overall maximum displacement of the bridge deck in the floating part is small, i.e. 27 mm in the transverse direction. Furthermore, vertical displacement provides the greatest response for the three directions in the cable-stayed part which can be seen from the displacement plots. The maximum displacement for all directions has a location at the end of the cable-stayed section with a magnitude of 54.6 mm. This section of the bridge has the most flexible part due to the large spans, which induces more motion and deformations than for the floating part.

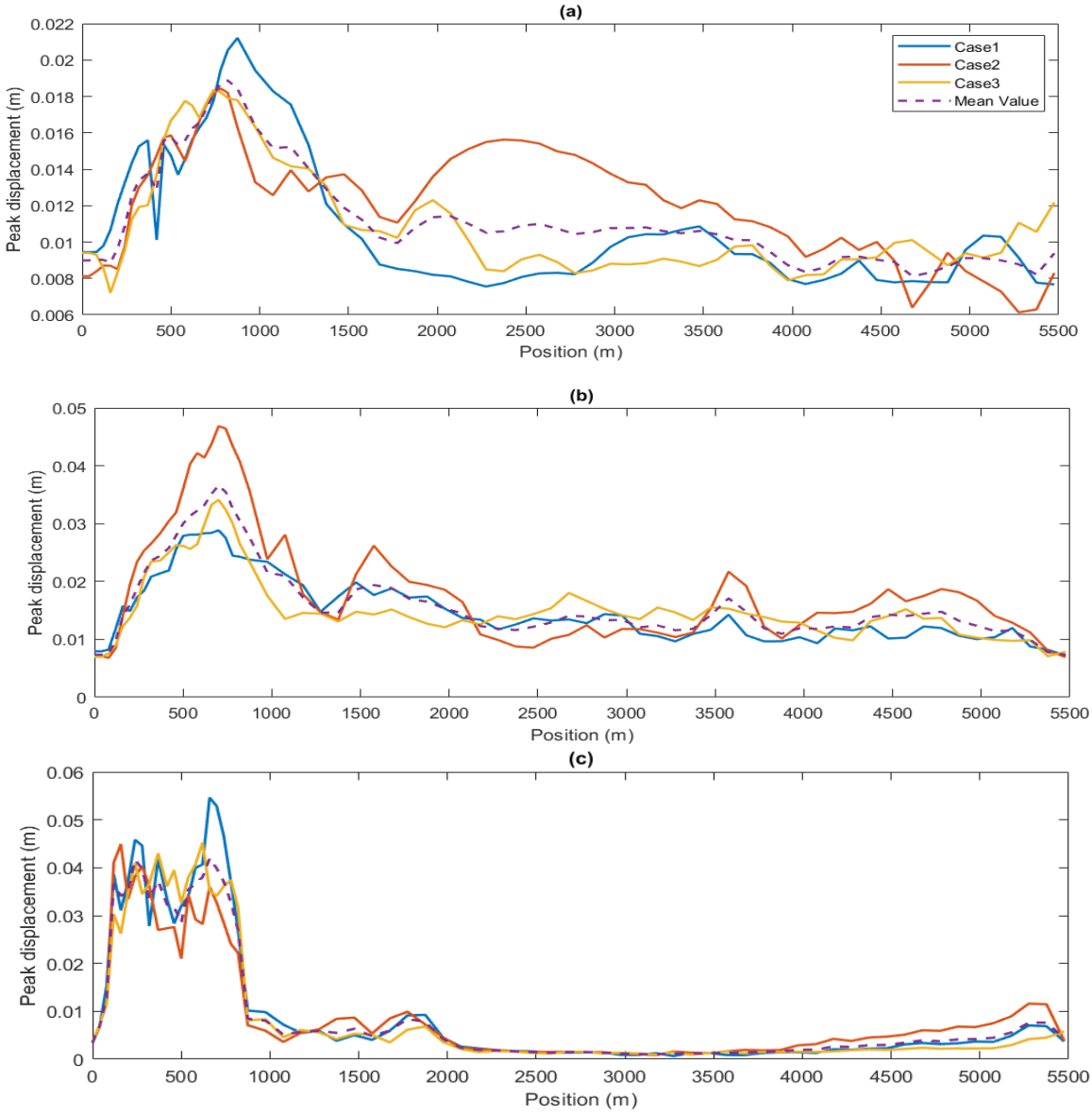

Figure 37 - Displacements along the bridge length (a) Horizontal (b) Transverse and (c) Vertical direction

From the figures, it is clear that the overall displacements are very small for the ground motions made for PGA of 0.08g. Vertical displacement criteria according to N400 (Statens Vegvesen, 2009) and (Statens Vegvesen, 2017c) are L/350 and 1.5 m, respectively. By comparing the results with these values, displacements in all three directions are neglectable for seismic loads. The maximum vertical displacement is 0.0546 m. It should also be noted that the displacements plotted in the figures are peak values at each girder, i.e. the displacements do not occur at the same time in the analysis.

From the results, responses of the floating bridge are bigger near the cable-stayed end than for the north end. This is due to the motions from the cable-stayed part, which is more flexible and generates more motion to the girder. By making a stronger solution here, the response in the floating part close to the cable-stayed section will also decrease. It should also be mentioned that the bridge girder in the north end is 140 m long, which is 40 m longer than the other spans on the floating bridge, and will result in a bit higher response than for the rest of the continuous part. By making this part smaller or stronger, the motion will decrease.

It is therefore safe to assume that structural damages due to displacement are unlikely to happen for seismic action of 0.08g.

6.5. Sensitivity Study

A sensitivity study to see if the displacement will increase drastically and if plastic deformations will occur are simulated. The results from the previous sections is for displacement and accelerations of PGA = 0.83 m/s^2 (about 0.08g). The sensitivity study will scale the displacement input up to 5 and 10 times the size to simulate the scenarios for 0.4g and 0.8g, respectively. The maximum and minimum values for the three seismic cases are used in this section to compare the different scenarios if extreme values will occur.

6.5.1. Forces and Stresses in the Stay-cables

Forces and stresses in the stay-cables are compared with the effect of 0.08g. Since the seismic input for ground motions consists of random vibrations, the response of the bridge will act similarly. Therefore, the minimum and maximum values for forces are used to illustrate the variation of force for the different load scenarios. The values for 0.08g are discussed in Chapter 6.2 but are included in Table 35 and Table 36 to compare with the higher seismic scenarios. It can be seen that in the case of 0.8g, the variation of force for the shortest cable is big, i.e. bigger than the maximum tension force. This indicates that the force in the cable goes over to compression during the analysis, marked in Table 35. Since the cables are very slender structures, this compression force is not good and may cause plastic deformation of the shortest cable.

Shortest cable	Max and min Force [MN]	Variation Force
0.08g	4.975	0.828
	4.147	
0.4g	6.306	4.162
	2.143	
0.8g	8.193	8.384
	-0.192	

Table 35 - Maximum, minimum and variation of force for the shortest cable

Longest cable	Max and min Force [MN]	Variation force
0.08g	6.503	0.401
	6.102	
0.4g	7.261	1.997
	5.264	
0.8g	8.201	3.979
	4.222	

Table 36 - Maximum, minimum and variation of force for the longest cable

Strengthening of the shortest cables is necessary if the bridge is going to be designed for an earthquake of PGA=0.8g. The scenario with 0.4g will keep the stay-cables in tension during the earthquake event for all cables.

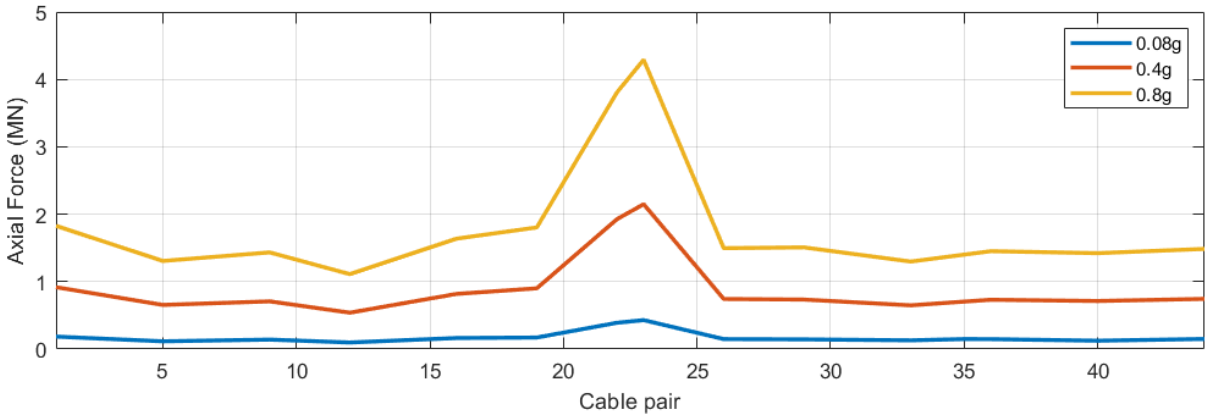

Figure 38 - Axial force along the cable-pairs for 0.08g, 0.4g, and 0.8g only

Figure 38 shows the comparison between the maximum forces along with the cable pair for the three load scenarios, considering only seismic loading. The total maximum axial force in the cables for 0.4g and 0.8g is 6.70 MN and 8.84 MN, respectively. The contribution from the seismic load is then up to 33% for 0.4g and 49% for 0.8g of the total load, when the seismic load is 2.15 MN and 4.29 MN, respectively. Table 37 gives the different values for the maximum seismic load on the stay-cables for each loading scenario.

Max cable force	1	9	16	22	23	29	36	44
0.08g	0.191	0.138	0.158	0.388	0.429	0.144	0.150	0.153
0.4g	0.918	0.707	0.818	1.925	2.149	0.734	0.731	0.744
0.8g	1.827	1.434	1.638	3.806	4.291	1.508	1.452	1.486

Table 37 - Maximum axial force along cable-pairs for 0.08g, 0.4g, and 0.8g only

The overall maximum cable stress for stronger earthquakes appears in cable-pair 23, i.e. one of the shortest cables. This can be seen in Figure 39, and an illustration to see the changes of stress along the length for scenarios of 0.4g and 0.8g are given in Figure 40 (a) and (b). The maximum stress in the cable is 957 MPa and 1263.6 MPa for total load and 307.2 MPa and 613.4 MPa for seismic load alone. If a seismic scenario with 0.8g will occur, the maximum utilization of the yield strength will 70.2% for the capacity of 1800 MPa and 79% for a capacity of 1600 MPa. This is a high utilization and might cause yielding of the cables when subjected to other environmental loads as well.

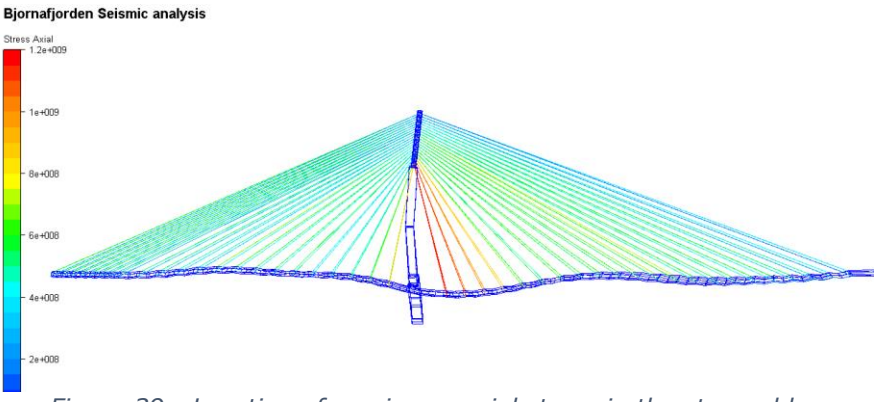

Figure 39 - Location of maximum axial stress in the stay-cables

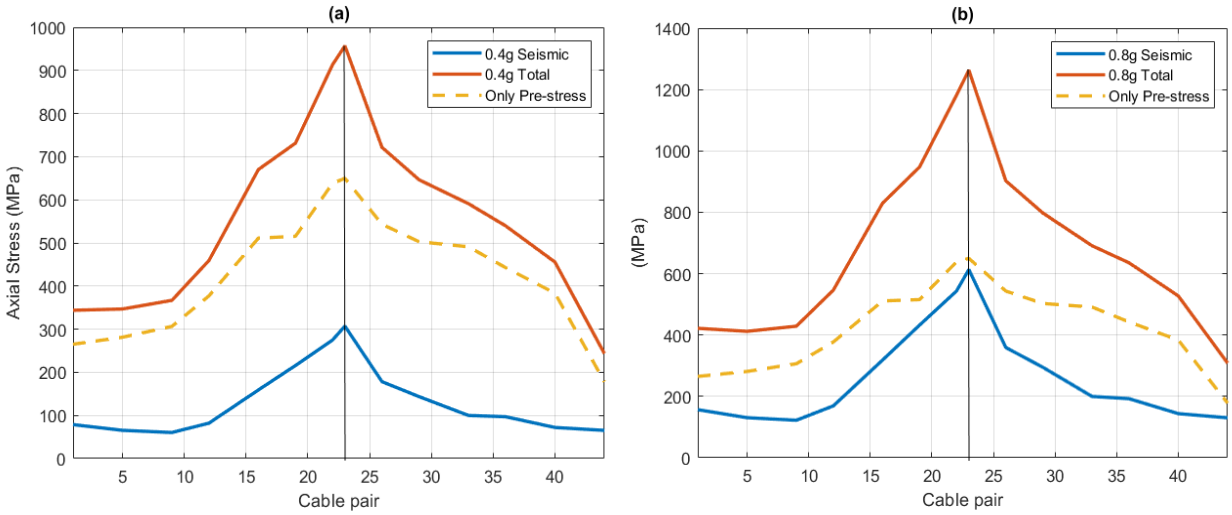

Figure 40 - Maximum axial stress on the east side of cable-pairs for (a) 0.4g and (b) 0.8g

Due to a similar seismic effect on the west and east cable-pairs for the scenario of 0.08g (Figure 29), only forces and stresses on the eastern side will be used for 0.4g and 0.8g, respectively. The total maximum stress for the scenario with 0.08g appears in cable pair 35 on the west side with a magnitude of 750 MPa. This will not be the case for 0.4g and 0.8g since the seismic effect will contribute most to stresses in the shortest cables, which can be seen in Figure 40. This will give the overall maximum stress in cable 23. By comparing the figures, the maximum stress for 0.8g is about twice of that for 0.4g.

The seismic cable-stress alone contributes to 32.1% and 48.6% of the total stress, for case 0.4g and 0.8g. From Figure 30, the seismic load had almost no contribution to the total stress in the cables, i.e. 8.2%. For PGA>0.8g, the seismic effect will be close to dominating the total load in the cables, which can also be seen in Figure 40 (b), where seismic and pre-stress are almost equal at cable-pair 23.

6.5.2. Bridge Girder Response

The axial load, strong axis moment, and weak axis moment are plotted for all three scenarios along the bridge length. These responses are useful to see the total response for the whole bridge. The responses are peak values with the correct sign.

6.5.2.1. Axial Force

Total axial girder forces for scenarios with 0.4g and 0.8g are illustrated in Figure 41 (a) and are compared with the mean value of the three cases for 0.08g. Here, load case 1 for 0.4g and 0.8g are used due to the highest peak responses for the case of 0.08g and limited time. Figure 41 (b) shows the effect seismic load alone has on the bridge girder.

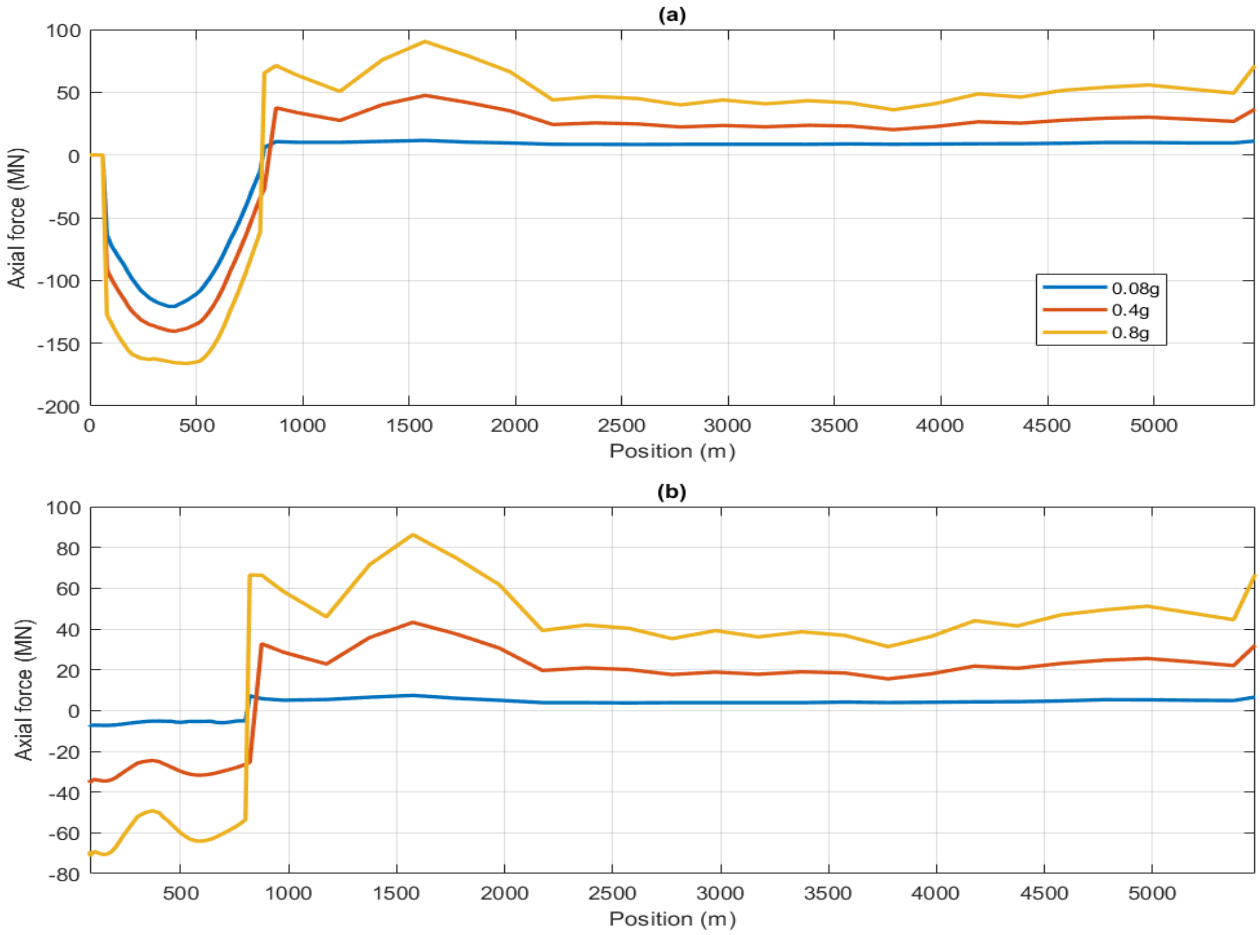

Figure 41 - Axial force in bridge deck for (a) pre-stress and seismic (b) seismic effect only

It can be seen that the bridge responds the same at the start of the bridge but gets a much higher value at the cable-stayed midpoint. The maximum axial force is 166 MN in compression, which causes utilization up to 40% for 0.8g scenario of the buckling capacity. This utilization is accepted since the self-weight and seismic load is included in this utilization. For seismic load only, the maximum axial force is 86.3 MN and gives utilization of 20.6%. This indicates that the seismic effect dominates the axial load in the girder for 0.8g in the floating part. The axial forces will not cause buckling of the girder when seismic excitations up to 0.8g are applied to the bridge. With a girder cross-section of 1.43 m^2, the maximum axial stress in the girder becomes 116.1 MPa for 0.8g. This gives utilization of 27.6% of the yield strength of 420 MPa, which is low.

6.5.2.2. Strong Axis Moment

The maximum moment about the strong axis is 2530 MNm which constitutes a utilization of 82.4% of the moment capacity about the bridge strong axis. This utilization is too high. The bridge deck has less than 20% of the capacity left to resist other environmental loads. This utilization yields for the south side of the bridge, i.e the first 200 m. In this section, the pre-stress load is dominating.

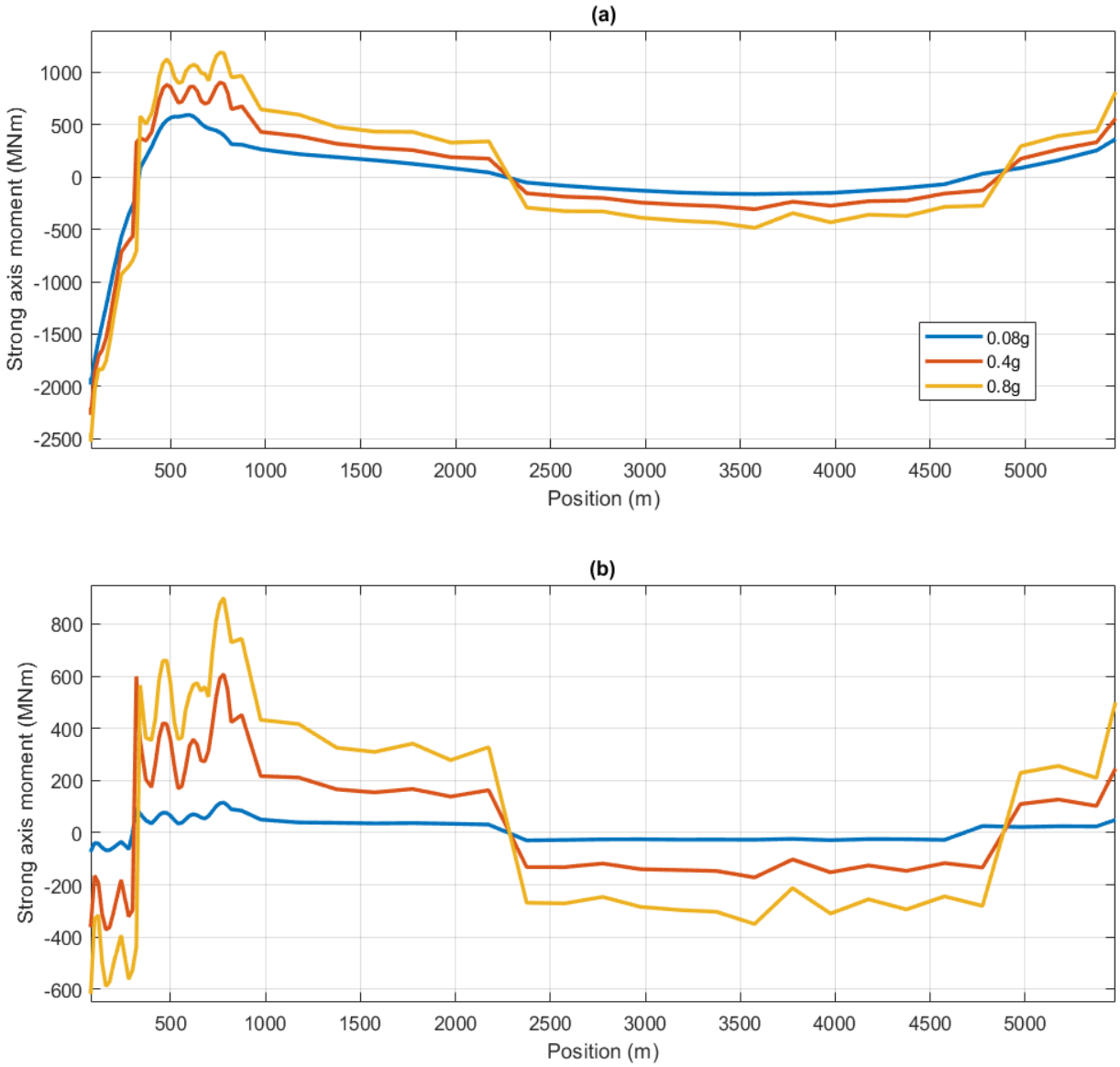

Figure 42 - Strong axis moment for (a) pre-stress and seismic load (b) Seismic load only

To check the contribution from the seismic load, the pre-stress is removed. At the south end, the seismic load contributes to 24% of the total moment. When only the seismic effect is considered, the maximum moment occurs at the end of the cable-stayed part, i.e. after 780m. The total moment is then 900 MNm, which gives a seismic utilization of 29.3% of the strong axis capacity. This utilization is a bit high, but are considered acceptable due to the smaller contribution of pre-stress at this location. The total utilization at end of the cable-stayed part is 38.8%. This is considered acceptable without effect from other environmental loads.

Within the continuous part of the bridge, the strong axis bending moment reaches a maximum of 500 MNm at the north abutment for 0.8g.

6.5.2.3. Weak Axis Bending Moment

The seismic effect on the bridge contributes nearly 40% of the total weak axis moment by comparing Figure 43 (a) and (b). When self-weight are excluded from the moment, the peak value of 430 MNm at 800 m disappear, which can be seen in Figure 43 (a). The peaks for seismic load appears in the floating high bridge and the north abutment due to self-weight. The floating low bridge has almost a constant response along the length indicating that it is not very sensitive for earthquakes, but the response gets bigger in the continuous part for higher earthquakes. In the case of 0.08g, the response is very low. 0.8g gives high responses in the floating high bridge, north abutment, and cable-stayed part. This gives utilizations up to 43.6% of the girder capacity about the weak axis when the maximum moment is 249.7 MN, located in the north. This utilization is high since the self-weight already have utilized 96% of the capacity, see Figure 33 (a). In total, the maximum utilization is 119%, which will cause buckling of the bridge girder.

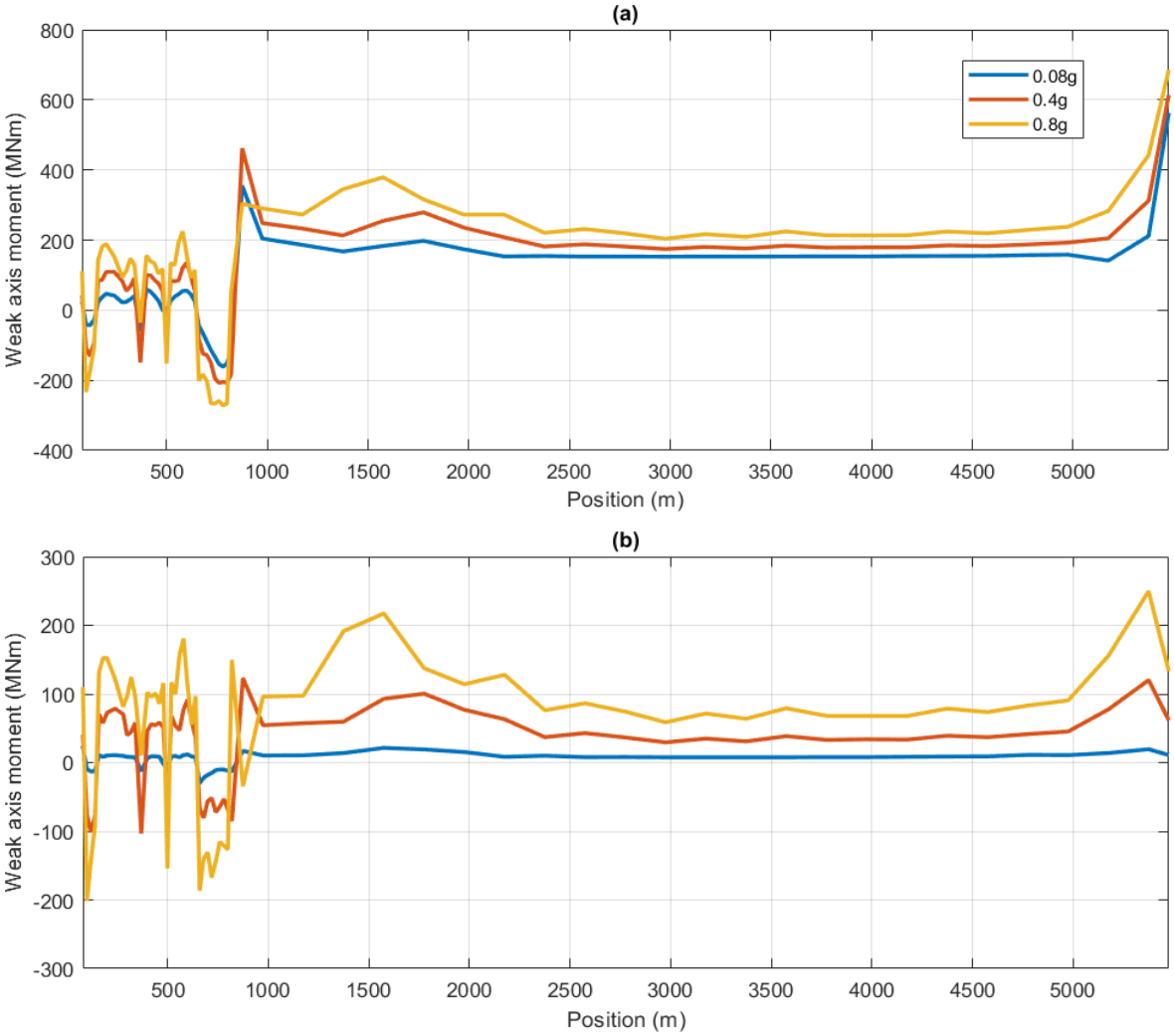

Figure 43 - Weak axis moment for (a) Seismic and pre-stress load (b) Seismic load only

In general, the utilization of 43.6% for 0.8g is a bit high due to the seismic effect only. 0.4g gives a maximum utilization of up to 22%, which is considered acceptable.

6.5.3. Motions Along the Bridge Girder

6.5.3.1. Accelerations

The vertical accelerations at nodes 2 and 3 are still below the safety limit of 0.5 m/s^2 for all seismic scenarios, shown in Figure 44 (b)-(c). The vertical acceleration response in the cable-stayed part is illustrated in Figure 44 (a), where the acceleration is extremely high relative to the safety limit, i.e. 14.97 m/s^2. Here, drastic measures need to be made to reduce the high acceleration.

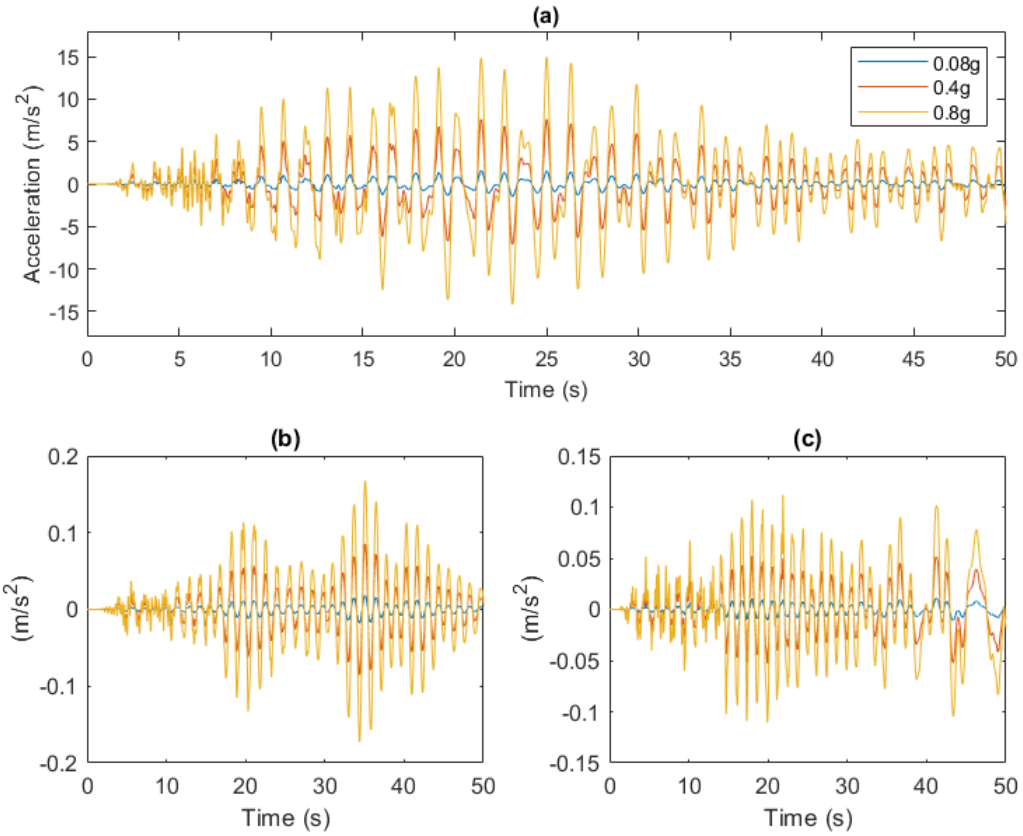

Figure 44 - Vertical acceleration for (a) Cable-stayed part (b) Middle Bridge (c) North Bridge End

6.5.3.2. Displacements

From the analysis with 0.08g, the distribution of displacement over the bridge length gives 3 maximum points at the three different directions. These three points have been checked against the seismic scenario for 0.4g and 0.8g to see if any big differences occur, given in Table 38. The values for displacement increase nearly linear with the increase of seismic load for the different scenarios. Vertical direction gave 0.0546 m as a maximum displacement for 0.08g and 0.5336 m for 0.8g. This is almost 10 times the size of 0.08g. These displacements are small in size for all directions and scenarios, which will not affect the safety of the bridge structure.

Max Displacement	Horizontal [m]	Transverse [m]	Vertical [m]
0.08g	0.0212	0.0449	0.0546
0.4g	0.1065	0.2332	0.2706
0.8g	0.2150	0.4642	0.5336

Table 38 - Displacements of bridge deck for 0.08, 0.4g and 0.8g

Chapter 7

7. Discussion

7.1. Seismic Scenario of 0.08g

The different cases of seismic loading on the bridge have been simulated. Responses of stay-cables and the bridge girder are conducted as well as the motions of the bridge girder for seismic load in three different load cases. Table 39 gives the values for the maximum or critical responses and motions for the scenario with PGA = 0.08g. From the results, the forces and stresses in the stay-cables are small of size for all cases compared with the capacity. The utilization for stay-cables is checked against the yield strength of 1600 MPa to be on the conservative side. As long as the force is in tension, and the stress is below the capacity, the cables are considered safe.

The utilization ratio under variable seismic load is not specified for stay-cables, so decisions need to be made based on utilization ratios for other impact loads. For the stay cables, the utilization requirements for the permanent load are 56% according to Eurocode. Floating bridges, which also are subjected to environmental loads, should use a lower utilization ratio for permanent loads. In phase 1 for the project, COWI suggested a utilization ratio of 28%. For this model, the maximum utilization for the axial load is higher than 28% for permanent load only. Calculations for the longest cable gave utilization of 30-35% of the yield strength, which is considered acceptable since the seismic load is included. However, the overall maximum stress of 750 MPa gives utilizations up to 47% which is high compared to the suggestions from COWI. Adjustments of the stay-cable cross-section might be a solution to reduce the utilization of the cables with the highest utilization. The utilization for axial force, strong axis moment, and weak axis moment in the bridge girder for the seismic load of 0.08g can be seen in Table 39 and is 1.77%, 3.76%, and 5.2%, respectively. These utilization values are acceptable without considering any other external and environmental loads on the structure.

Critical/Maximum responses	0.08g	Capacity/Criterion	Utilization
Axial force (stay-cable)	0.43 MN	Tension	OK
Axial stress (stay-cable)	61.4 MPa	1600 MPa	3.84%
Axial force (bridge girder)	7.42 MN	418 MNm	1.77%
Strong axis bending moment	115.5 MNm	3069 MNm	3.76%
Weak axis bending moment	29.9 MNm	575 MNm	5.2%
Vertical acceleration	1.6 m/s^2	< 0.5 m/s^2	320%
Vertical displacement	0.0546 m	< L/350 or 1.5 m	3.64%
Horizontal displacement	0.0212 m	-	OK
Transverse displacement	0.0449 m	-	OK

Table 39 - Maximum bridge response for the seismic load of 0.08g

The seismic load induces large accelerations in the cable-stayed girder which is far above the safety limit of 0.5 m/s^2, i.e. up to 1.6 m/s^2. Limitations of the vertical vibrations need to be fixed in the cable-stayed part to reduce the acceleration and to ensure safe traffic. To do this, a special design of the cable-stayed part needs to be

considered, in form of a damping system discussed in Section 5.2 in (Yanyan Sha, Amdahl, Jørgen, Aalberg, Aleksander, & Yu, Zhaolong, 2018).

Displacements in the bridge are very small of size compared with the criterion from N400 (Statens Vegvesen, 2009) and bridge design (Statens Vegvesen, 2017c). Displacements in all three directions are considered acceptable during the numerical analysis with PGA = 0.08g.

For all cases, the cable-stayed part gets most affected by the seismic load in the dynamic analysis, and this section of the bridge will be the first part to be subjected to buckling or collapse. The continuous part of the bridge has almost a neglectable response due to seismic excitation alone.

7.2. Seismic Scenario of 0.4g and 0.8g

Table 40 shows the results for the scenario of 0.4g and 0.8g. The result compared with 0.08g gives a nearly linear increase in the responses. The forces in the cables for 0.4g gives values and variation in tension, which are good. The utilization for 0.4g due to axial stress in the cables is low due to seismic load and is considered acceptable. However, for 0.8g, the axial force in the cables goes over to compression during the earthquake, which is not good due to slender cables, which are weak in compression.

For the forces in the bridge girder, the scenario for 0.4g gives acceptable utilization due to the only seismic effect. 0.8g does not give very high utilizations for girder forces, but due to the high contribution of pre-stress to the moments, this utilization is too high. Pre-stress and seismic load together will cause buckling of the girder weak axis with total utilization of 119%.

The values for girder accelerations get extremely high for both scenarios of seismic load, 0.4g, and 0.8g. This is not acceptable due to the safe traffic requirement of 0.5 m/s^2, and drastic changes must be made to the design before the requirements are met. Displacements for both cases are relatively small compared to the size of the bridge and the requirements obtained for vertical displacements in N400. (Statens Vegvesen, 2009)

Critical/Maximum responses	0.4g	0.8g	Capacity/ Criterion	Utilization 0.4g	Utilization 0.8g
Axial force (stay-cable)	2.15 MN	-0.192 MN	TENSION	TENSION	COMPRESSION
Axial stress (stay-cable)	307.2 MPa	613.4 MPa	1600 MPa	19.2%	38.4%
Axial force (bridge girder)	43.3 MN	86.3 MN	418 MNm	10.4%	20.6%
Strong axis bending moment	607.6 MNm	900.2 MNm	3069 MNm	19.7%	29.3%
Weak axis bending moment	123.2 MNm	249.7 MNm	575 MNm	21.4%	43.4%
Vertical acceleration	7.63 m/s^2	14.97 m/s^2	< 0.5 m/s^2	152.6%	299.4%
Vertical displacement	0.2706 m	0.5336 m	<L/350 or 1.5m	18.5%	36.5%
Horizontal displacement	0.1065 m	0.2150 m	-	-	-
Transverse displacement	0.2332 m	0.4642 m	-	-	-

Table 40 - Maximum bridge response for seismic loads of 0.4g and 0.8g

In real life, other environmental loads will be included on the floating bridge which will cause higher total utilization. Wind and wave loads are two important environmental loads that floating bridges are exposed to. These loads need to be considered.

Chapter 8

8. Concluding Remarks

This analysis is done to investigate how floating bridges behave during and after an earthquake event. Within this study, an end-anchored curved floating bridge is investigated, affected by seismic excitations. USFOS is used to conduct a time-domain analysis of a floating bridge and to gather the results. Artificial ground motions are calculated by use of Eurocode 8 and are obtained by Dr. Kaiming Bi, including spatial variations (3 different cases with 3 ground motions). This yielded a wide range of results and the following conclusions can be made based on the results from this numerical analysis:

- It is found that the floating part of the bridge is not significantly affected by seismic ground motions of 0.08g.
- All forces in the cables and girders are below a utilization of 6% of the used capacities for 0.08g. Axial stress in the cables utilizes up to 4% of the yield strength of 1600 MPa, which is low.
- Displacements in horizontal, transverse, and vertical directions are small and considered neglectable for a seismic case of 0.08g.
- Seismic excitation on the bridge induces large vertical accelerations in the cable-stayed part for all cases due to large spans and improvements to the girder design must be made, in form of a vibration reducer. The floating part of the bridge has small accelerations for all cases, i.e. far below the criterion used.
- Responses for a scenario of 0.4g are considered as acceptable, except for the accelerations in the cable-stayed part.
- Responses for a scenario of 0.8g gives relatively high responses and will affect the bridge in such a way that improvements of the current bridge design will be necessary for some of the results.

The seismic loadings on the bridge are only applied to the connections with the ground where the bridge has fixed boundary conditions. These locations give extra stiffness to the bridge motion and the floating bridge will then not get significantly affected.

The probability of an earthquake of 0.4g and 0.8g is small in Norway. Thus, accounting for these large ground motions are not necessary for the design of the Bjørnafjorden bridge.

Further study of the responses and motions in the bridge needs to be made to ensure that the bridge to be fully reliable to earthquakes.

Chapter 9

9. Recommendations for Future Work

To have a powerful computer due to this kind of simulations on a huge structure is necessary. Due to the complexity of the structure, many things and effects have been neglected.

Responses of the bridge tower and pontoons, including more detailed responses of the girder and cables would be interesting to investigate. Including mooring lines to the pontoons to see if the responses would decrease and to assess different bridge towers for the cable-stayed part would be interesting. Changes of the bridge girder properties and cross-sections to investigate if the motions and responses would decrease.

The only external load that has been included in this simulation is the seismic load. Traffic load and other external loads should also be accounted for in practice. Wave, wind, and current has been investigated in other earlier theses and are important to include in the bridge. A dynamic analysis including wave loads would be interesting since the seismic excitations can generate tsunami waves. Interaction between tsunami waves and earthquakes.

This has been a fun thesis to write since I had no clue about what the result would be. During the analysis, there have been ups and downs due to difficulties with the program and unexpected values of the response.

Bibliography

AASHTO. (2009). Guide Specifications for LRFD Seismic Bridge Design. In. Washington D.C: American Association of State Highway and Transportation Officials.

Michael J Abrahams. (2007). *Seismic Design of Floating Bridges* (A11). Retrieved from National Academies of Sciences, Engineering, and Medicine: https://trid.trb.org/view/839629

Norconsult AS. (2017a). *K7 Bjørnafjorden End-anchored floating bridge: Appendix A – Drawings binder* [Unpublished; obtained from Assosiated Professor Yanyan Sha].

Norconsult AS. (2017b). *K7 Bjørnafjorden End-anchored floating bridge; Appendix J – Ultimate resistance of bridge girder*. [Unpublished; obtained from Assosiated Professor Yanyan Sha].

Norconsult AS. (2017c). *K7 Bjørnafjorden End-anchored floating bridge - Summary report*. Statens Vegvesen. [Unpublished; obtained from Assosiated Professor Yanyan Sha].

Kaiming Bi, & Hong Hao. (2012). Modelling and simulation of spatially varying earthquake ground motions at sites with varying conditions. *Probabilistic Engineering Mechanics, 29*, 92-104. doi:10.1016/j.probengmech.2011.09.002

Wai-Fah Chen, & Lian Duan. (2014). *Seismic Design*. In W.-F. Chen & L. Duan (Eds.), *Bridge Engineering Handbook* (Second Edition ed., pp. 722).

Robert D. Cook, David S. Malkus, Michael E. Plesha, & Robert J. Witt. (2002). *Concepts and Applications of Finite Element Analysis* (fourth edition ed.): John Wiley & Sons, INC.

O. M. Faltinsen. (1990). Wave loads on offshore structures. *Annual Review of Fluid Mechanics; (USA), 22*, 35-56. doi:10.1146/annurev.fl.22.010190.000343

Xiuyun Gao, & Yitan Jiang. (2014). Seismic response Analysis to Half Floating System of Cable-stayed bridge. *Vol.619*, 81-90. doi:10.4028/www.scientific.net/KEM.619.81

Junbo Jia. (2012). Seismic Analysis for Offshore Industry: Promoting State of the Practice towards State of the Art. 438-447. Retrieved from www.isope.org

M. Myint Lwin. (2000). Floating Bridges. 24.

V. Abbasian M. Hossein. (2012). Studying the Seismic Behavior of a Kind of Floating Bridges by Using Finite Element Analysis

J. Mirzapour, M. Shahmardani, & S. Tariverdilo. (2017). Seismic response of submerged floating tunnel under support excitation. *Ships and Offshore Structures, 12*(3), 404-411. doi:10.1080/17445302.2016.1171591

Standard Norge. (2008). *Eurokode : Grunnlag for prosjektering av konstruksjoner* (Vol. NS-EN 1990:2002+NA:2008). Lysaker: Standard Norge.

NORSAR. (2020). Seismologi. Retrieved from https://www.jordskjelv.no/om-jordskjelv/seismologi/

Ida Fagerli Osvoll. (2018). *Analysis and Design of Bjørnefjorden Floating Cable-Stayed Bridge subjected to Large Ship Collisions and Extreme Environmental Loads.* (Master). Norwegian University of Science and Technology, Trondheim.

Mohammed Saeed Seif, & Yoshiyuki Inoue. (1998). Dynamic analysis of floating bridges. In *Marine Structures 11* (pp. 29-46).

Seismic waves. Retrieved from https://www.bgs.ac.uk/discoveringGeology/hazards/earthquakes/seismicWaves.html

Yanyan Sha, Jørgen Amdahl, Aleksander Aalberg, & Zhaolong Yu. (2018). Numerical investigations of the dynamic response of a floating bridge under environmental loadings. *Ships and Offshore Structures, 13*(sup1), 113-126. doi:10.1080/17445302.2018.1426818

European Standard. (2004). Eurocode 8: Design of structures for earthquake resistance Part 1 : General rules, seismic actions and rules for buildings. In (Vol. EN 1998-1:2004): European Standard.

European Standard. (2005). Eurocode 8: Design of structures for earthquake resistance – Part 2: Bridges. In (Vol. EN 1998-2:2005+A2:2011): European Standard.

NORSOK standard. (2007). Actions and action effects. In (Vol. N-003, pp. 60). Norway: Standards Norway.

Einar N. Strømmen. (2012). *Structural Dynamics* (Vol. 2). Trondheim, Norway: Springer

USFOS. (1999a). Running USFOS. In *User's Manual* (pp. 8). Retrieved from https://www.usfos.no/manuals/index.html

USFOS. (1999b). Modelling. In *User's manual* (pp. 28): USFOS.

USFOS. (2020). Product info: USFOS. Retrieved from https://www.usfos.no/

Statens Vegvesen. (2009). Bruprosjektering, N400. In: Vegdirektoratet.

Statens Vegvesen. (2017a). The E39 Coastal Highway Route. Retrieved from https://www.vegvesen.no/en/roads/Roads+and+bridges/Road+projects/e39coastalhighwayroute

Statens Vegvesen. (2017b). A floating bridge is the chosen concept- for crossing Bjørnafjorden. Retrieved from https://www.vegvesen.no/en/roads/Roads+and+bridges/Road+projects/e39coastalhighwayroute/news/a-floating-bridge-is-the-chosen-concept-for-crossing-bjornafjorden

Statens Vegvesen. (2017c). Design Basis Bjørnafjorden Rev C, Side- and end anchored floating bridge. 50.

Statens Vegvesen. (2017d). Design basis MetOcean. 18.

Statens Vegvesen. (2017e). Design Basis for Geotechnical Design. 21.

Statens Vegvesen. (2018, 27.09.2018). The E39 Coastal Highway Route: Animation. Retrieved from https://www.vegvesen.no/en/roads/Roads+and+bridges/Road+projects/e39coastalhighwayroute/film

Eiichi Watanabe, Tadaaki Maruyama, Hiroshi Tanaka, & Sumio Takeda. (2000). Design and construction of a floating swing bridge in Osaka. In *Marine Structures* (Vol. 13, pp. 437-458). ELSEVIER: Elsevier Science Ltd. .

Eiichi Watanabe. (2003). Floating Bridges: Past and Present. *13:2*, 128-132. doi:10.2749/101686603777964810

Eiichi Watanabe, & Tomoaki Utsunomiya. (2003). Analysis and Design of Floating Bridges (5), 127-144. doi:10.1002/pse.151

Appendix A

Cable pair number	Cross-sect. area $[mm^2]$	Diameter $[mm]$	Eff.Young's modulus $[GPa]$	Poiss. ratio	Thermal exp. coeff. $[1/°C]$	Temp. western cable $[°C]$	Temp. eastern cable $[°C]$
1	11656	121.8	177.54	0.3	1.20e-05	-229.5	-91.8
2	11245	119.7	178.37	0.3	1.20e-05	-228.3	-91.3
3	10824	117.4	179.18	0.3	1.20e-05	-227.2	-90.9
4	10405	115.1	179.98	0.3	1.20e-05	-226.1	-90.4
5	10001	112.8	180.76	0.3	1.20e-05	-225.1	-90.0
6	8625	104.8	181.53	0.3	1.20e-05	-224.1	-89.6
7	8241	102.4	182.28	0.3	1.20e-05	-200.8	-80.3
8	7859	100.0	183.02	0.3	1.20e-05	-199.9	-79.9
9	11719	122.2	184.43	0.3	1.20e-05	-198.3	-79.3
10	7294	96.4	185.77	0.3	1.20e-05	-196.8	-78.7
11	6928	93.9	187.03	0.3	1.20e-05	-195.3	-78.1
12	6569	91.5	188.21	0.3	1.20e-05	-194.0	-77.6
13	6210	88.9	189.31	0.3	1.20e-05	-300.0	-120.0
14	5844	86.3	190.31	0.3	1.20e-05	-298.3	-119.3
15	5493	83.6	191.23	0.3	1.20e-05	-296.7	-118.7
16	5142	80.9	192.05	0.3	1.20e-05	-295.4	-118.1
17	4807	78.2	192.78	0.3	1.20e-05	-294.2	-117.7
18	4479	75.5	193.40	0.3	1.20e-05	-209.4	-83.8
19	4173	72.9	193.92	0.3	1.20e-05	-208.8	-83.5
20	3899	70.5	194.35	0.3	1.20e-05	-208.3	-83.3
21	3670	68.4	194.66	0.3	1.20e-05	-207.9	-83.2
22	7004	94.4	194.88	0.3	1.20e-05	-207.7	-83.1
23	6996	94.4	194.88	0.3	1.20e-05	-290.8	-116.3
24	3670	68.4	194.66	0.3	1.20e-05	-291.1	-116.5
25	3899	70.5	194.35	0.3	1.20e-05	-291.6	-116.7
26	4166	72.8	193.92	0.3	1.20e-05	-292.3	-116.9
27	4463	75.4	193.40	0.3	1.20e-05	-209.4	-83.8
28	4784	78.0	192.77	0.3	1.20e-05	-210.1	-84.1
29	5112	80.7	192.05	0.3	1.20e-05	-295.4	-118.2
30	5447	83.3	191.23	0.3	1.20e-05	-296.7	-118.7
31	5798	85.9	190.31	0.3	1.20e-05	-298.3	-119.3
32	6149	88.5	189.31	0.3	1.20e-05	-300.0	-120.0
33	6493	90.9	188.21	0.3	1.20e-05	-301.8	-120.7
34	6836	93.3	187.03	0.3	1.20e-05	-303.9	-121.6
35	7187	95.7	185.77	0.3	1.20e-05	-306.1	-122.4
36	7538	98.0	184.43	0.3	1.20e-05	-220.3	-88.1
37	7889	100.2	183.02	0.3	1.20e-05	-222.1	-88.9
38	8225	102.3	181.53	0.3	1.20e-05	-224.1	-89.6
39	8576	104.5	179.98	0.3	1.20e-05	-226.1	-90.5
40	9888	112.2	178.37	0.3	1.20e-05	-228.3	-91.3
41	10269	114.3	176.69	0.3	1.20e-05	-230.6	-92.2
42	10651	116.5	174.97	0.3	1.20e-05	-233.0	-93.2
43	11017	118.4	173.19	0.3	1.20e-05	-235.6	-94.2
44	11398	120.5	171.37	0.3	1.20e-05	-238.3	-95.3

Table 41 - Stay-cable properties (Ida Fagerli Osvoll, 2018)